Università Politecnica delle Marche

Facoltà di Scienze

Dottorato di Ricerca in Protezione Civile e Ambientale

XIV Ciclo

Biogenic habitat distribution and effect on coastal erosion phenomena relating to coastal peculiarities

Tesi di dottorato di:

Ubaldo Pantaleo

Tutor:

Prof.ssa Stefania Puce

Co-Tutors :

Prof. Giovanni Besio

Prof. Carlo Cerrano

Anno accademico 2015/2016

INDEX

ABSTRACT

Structural complexity of underwater environments is closely correlated to biodiversity. Especially in the coastal zone the seabed is characterized by elements able to increase the terrain rugosity such as boulders and other abiotic features, artificial structures and sessile living organisms. With increasing of seabed complexity the interaction between environment and the organisms that inhabit increases as well. The consequence is an increase of biodiversity with increasing of complex elements that characterize the seascape.

Concurrently seascape complexity and roughness may also have influence on abiotic factors characterizing the underwater environment such as sediment transport, wave energy dissipation, flow resistance, light irradiance and so on. Thus the presence of highly rough features in coastal areas and in relatively shallow waters can have important effect on the hydrodynamics and sedimentary process.

To date the importance of several coastal ecosystems is largely recognized not only for economic, aesthetic and recreational values but also for their contribution in increasing biodiversity and in coastal protection. In particular biogenic habitats, here defined as natural features built by living organisms, are able to change the original environment via their own physical structure increasing the seabed complexity and leading to an increase of soil elevation. Until now most of the research work concerning these structures has been focused on the ecological role or targeted to the taxonomic study of the characteristic and associated species and to the study of intra- inter-specific relationships. Abiotic and physical processes (e.g. sediment dynamics and hydrodynamics) were rarely included in the past research works. The accurate definition of the complexity and roughness and the quantification of structural metrics are crucial to fully understand both the relationships between environment and biota, and the effects of different structures (natural or artificial) on wave propagation, currents and sedimentological aspects in coastal zone. Also there is a huge gap between studies carried out in tropical and subtropical environments and temperate ones focused on wave attenuation and coastal protection functions provided by biogenic habitats.

Here, using data gathered at two locations in two different Italian regions, we document the changes in wave propagation energy toward the coast due to dissipation effect generated by several habitats with different complexity and roughness. Results of this study confirm the importance of biogenic habitats in wave attenuation and demonstrate the coastal protection function of the coralligenous bank type. Moreover, for the first time the contribution provided by the coralligenous to wave dissipation is estimated on seabed with different slope characteristics.

1 INTRODUCTION

The effect of climate change are already being felt, especially in many coastal areas (Spalding et al., 2014) where sea level rise, increase of natural extreme events and different human activities take great importance raising the vulnerability of coastal communities and structures.

The modern age has created profound changes in environmental ethics since the humankind, escaping from the control of natural cycles, began to impose their own needs to nature. These changes occur both locally and globally, for natural or anthropogenic reasons. Scientific and technical progress have only intensified these changes and accelerated the rate of occurrence of natural processes.

In the last thirty years, coastal zone has experienced a significant increase of impacts mainly due to the combined action of increasing human pressure on the coast and climate change effects. The unsustainable coastal development is causing the degradation of ecosystems recognized as critical for the ecological and economic role they play. The coastal zone and the seascapes are altered by pollution, mining and resources exploitation (e.g. destructive illegal fishing and/or overfishing) and infrastructures development. All these activities are clearly behind changes in structure and functioning of natural systems. Where human pressures remain unchanged or faintly grow, consequences of climate change (e.g. sea level change, extreme events increasing) are leading to an increase of erosional phenomena and degradation of affected ecosystems. Such figures rapidly translate into heavy growth of economic and social vulnerability of coastal communities (Spalding et al., 2014). Understanding the whole role of natural systems in mitigating destructive effects of extreme events, thus affecting the vulnerability of coastal populations is a pre-requisite for identifying the possible and immediate actions to be taken.

Recently, several authors focused on those natural systems able to absorb the energy released by extreme events and/or mitigate their post-impact effects. These biogenic structures consist of living organisms able to modify soil elevation and thus the characteristics of the substrate on which they grow by acting as a barrier against wave action and actively contributing to coastline protection.

Although various studies have been carried out regarding some habitats as coral reefs, seagrass meadows or coastal vegetation, there is a lack of information about other habitats (e.g. Mediterranean coralligenous assemblage), until now studied from the ecological or taxonomic point of view. Even the studies regarding the combined effect of the presence of different habitats are equally rare.

Application of hydrodynamic model could be a useful tool to address these topics through an untraditional approach.

1.1 Climate changes

The global average surface temperature (the average of near surface air temperature over land, and sea surface temperature) has increased since 1861 (IPCC, 2001) along with the anthropogenic emissions of CO_2 to the atmosphere (in 2008, 27% higher than in 1990) (Le Quéré et al., 2009). Recent works indicate that the increase in temperature in the 20th century is likely to have been the largest of any century during past 1,000 years (Mann et al., 1998; IPCC, 2001). Over the past 25 years temperatures have increased at a rate of 0.19°C per decade, in very good agreement with predictions based on greenhouse gas increases. Even over the past ten years, despite a decrease in solar forcing, the trend continues to be one of warming (Allison et al., 2009).

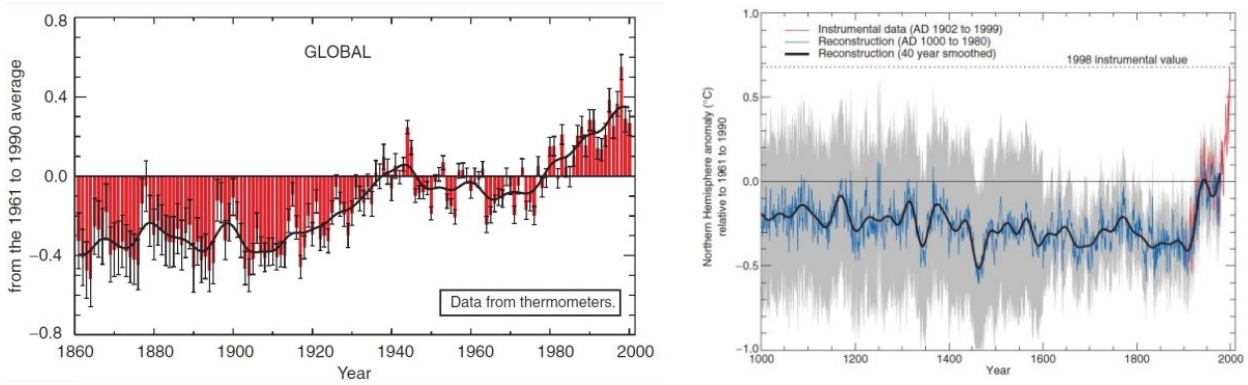

Fig. 1.1 - Combined annual land-surface air and sea surface temperature anomalies (°C) 1861 to 2000 (left) and millennial Northern Hemisphere (NH) temperature reconstruction (right; blue – tree rings, corals, ice cores, and historical records) and instrumental data (red) from AD 1000 to 1999. Smoother version of NH series (black), and two standard error limits (gray shaded) are shown. (From IPCC, 2001).

One of the main effects of the increase of global temperature and human-induced warming is the melting of ice sheets, glacier and ice-caps. Recently, the mass balance of ice sheets became a topic of considerable importance in the context of global warming. Several observations prove that ice sheets are losing mass at an increasing rate (Rignot et al., 2011; Wingham et al., 2009; Allison et al., 2009). The global ice melting is also among the main causes of global mean sea level rise. If totally melted, Greenland and West Antarctica would raise sea level by approximately 7 and 3-5 m, respectively (Canezave & Llovel, 2010); while the glaciers' contribution to sea level rise has been estimated to be at 0.77 ±22 mm $year^{-1}$ over 1993-2003 (Lemke et al., 2007). Under ongoing changes consistent with current warming trends, a mass loss of up to ~55 cm sea level rise is expected by 2100 (Pfeffer et al., 2008).

Thermal expansion of sea water in response to the ocean warming due to the increase of global temperature is also one of the main causes of sea level change (Canezave & Llovel, 2010). Several authors studied the evolution of the ocean thermal expansion during the last decades and highlighted its contribution to the sea level rise (Church et al., 2004; Levitus et al. 2009; Ishii & Kimoto, 2009). The results of their research, although different, show that the mean thermal expansion trend over 1955-2001 range between 0.3 ±0.01 and 0.5 ±0.08 mm $year^{-1}$ (Levitus et al. 2009; Ishii & Kimoto 2009; Dominique et al. 2008; Canezave & Llovel, 2010).

The last two effects of global warming are the main concomitant causes of sea level rise. Domingues et al. (2008) estimated that, for the period 1961-2003, thermal expansion contributed ~40% to the observed sea level rise, while the shrinking glaciers and ice sheets ~60%. Another important factor is the coastal subsidence for natural or anthropogenic reasons. In the past millennia land subsidence was dominated by tectonic setting and earthquakes or gravitational collapse episodes of a growth fault or natural compaction and dewatering of the ground sediment (Woppelmann et al., 2013). This process has been accelerated by subsurface fluid-pressure declines caused by pumping of groundwater or hydrocarbons. The exploitation of subsurface fluids can lead to aquifer-system compaction and consequence land subsidence (Ingebritsen & Galloway, 2014).

Sea level rise over the coming centuries as an inevitable consequence of global warming is probably the most dangerous consequence of climate change. During the last 20 years many models has been developed to simulate past, present and future sea level rise trend. The conventional approach has been to model the major components such as ocean thermal expansion, additional freshwater into ocean basins due to land ice loss and water exchange with terrestrial reservoirs (Pardaens et al., 2011). Conceptually the best way to estimate future changes in sea level would be physical models of all the water storage reservoirs on the planet and their behavior under a changing climate (Jevrejeva et al., 2012). However, take into account all variables is a very complex task and requires a huge research effort, since at present the behavior of all the involved processes is not yet fully understood. Thus another approach is to simulate observed sea level using physical models of reduced complexity. These semi-empirical models connect global sea level rise to global mean surface temperature (Rahmstorf, 2007; Grinsted et al., 2010) or radiative forcing (Jevrejeva et al., 2009-2010-2012). Projections by semi-empirical models are based on the assumption that sea level rise will respond as a linear system, so that future response is analogous to the past (Jevrejeva et al., 2012). This may be a limitation if, in the future, non-linear physical processes come into play. Another issue is due to the lack of spatial variability that allows us to process reliable predictions only on a regional scale. In fact, satellite altimetry reveals strong regional variability in sea level trends and several studies has shown that non-uniform ocean warming (Lombard et al., 2009; figure 1.2), hence non-uniform thermal expansion, is most responsible of the observed spatial trend patterns in sea level (Canezave & Llovel 2010; Lombard et al. 2005).

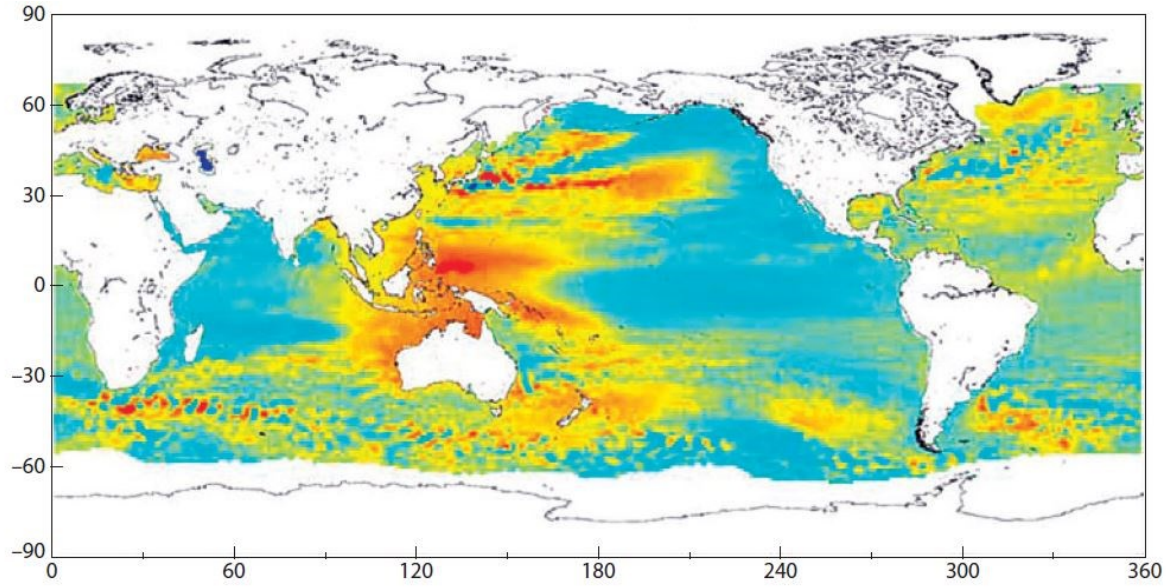

Figure 1.2 – Spatial patterns in sea level trends over 1993-2001 observed by satellite altimetry (from Lombard et al., 2009).

However, the latest semi-empirical models reproduce climate system modelled sea level behavior at scales from centennial to multi-annual (Jevrejeva et al., 2012).

Several recent works, aimed at assessing the past, present and future trend of sea level rise, report similar results, although different spatial and time scales have been used (Canezave & Llovel 2010; Rahmstorf 2007; Grinsted et al., 2010). Figures 1.3 and 1.4 show the evolution of the global mean sea level between 1800-2100 and 1900-2300 respectively.

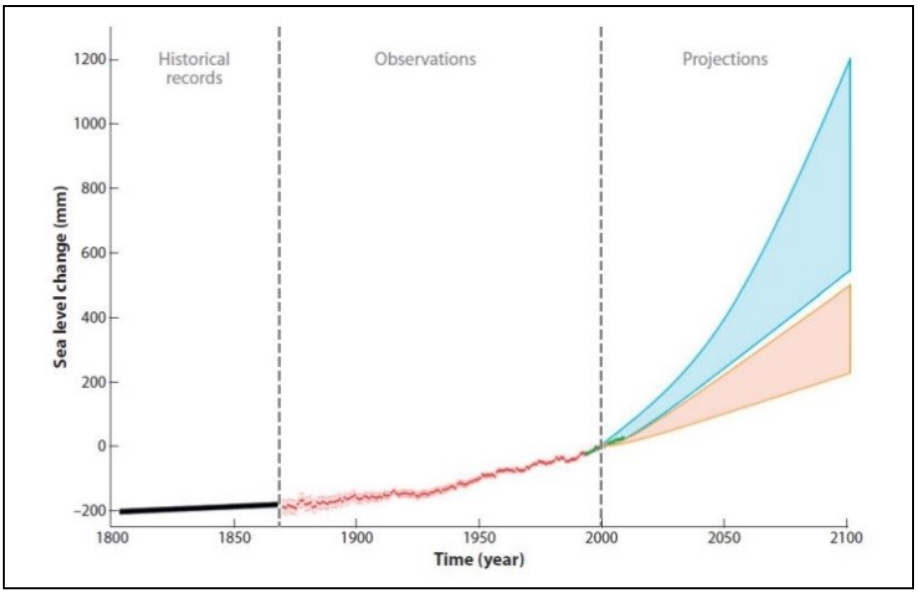

Figure 1.3 – Evolution of global mean sea level between 1800 and 2100 based on the observations for the nineteenth and twentieth century and model projections (from IPCC 2007 and Rahmstorf 2007) for the twenty-

first century (from Cazenave & Llovel, 2010). Pink shaded region includes projections from coupled climate models (IPCC AR4, 2007). Light blue shaded region includes projections from Rahmstorf (2007).

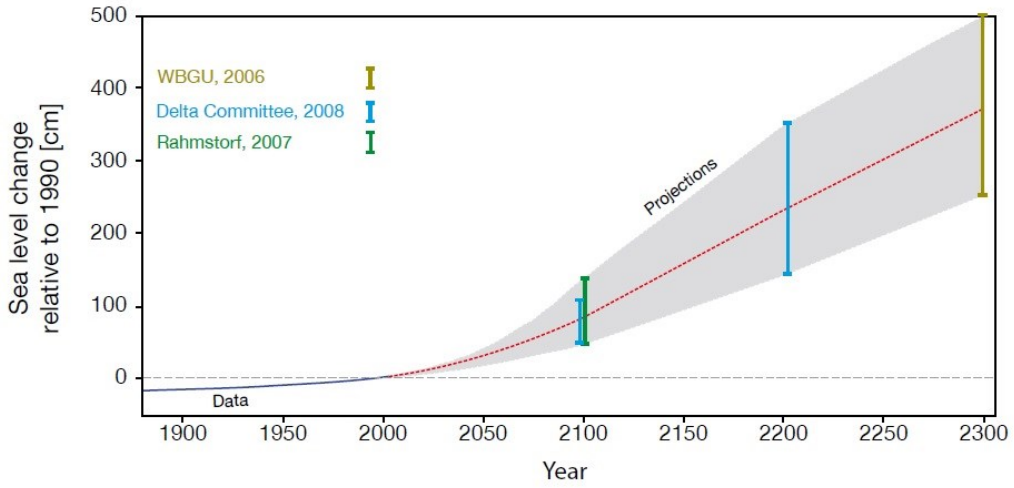

Figure 1.4 - Estimates of future sea level rise (from Allison et al., 2009). Historical data from Church and White (2006). Future projections are from Rahmstorf (2007) and WBGU (2006), while those projections represented here as 'Delta Committee' are from Vellinga et al.,(2008).

Many changes in extremes had been observed since 1970s as part of the warming of the climate system (Allison et al., 2009). Past works concluded that significant changes in temperature and precipitation extremes have occurred in the whole planet during 20th century (Sillmann & Roechner, 2008; Alexander et al., 2007; Collins et al., 2000). Recent studies have shown significant increase of occurrences of hot extremes and decreases in occurrences of cool extremes over the past decades (Allison et al., 2009; Alexander & Arblaster, 2009; Sillmann & Roeckner, 2008). In many mild- and high-latitude areas, the total annual amount of precipitations significantly increased for the contribution of extreme rainfall. Probably, there has been from 2% to 4% increase in the frequency of heavy precipitation events over the latter half of the 20th century (IPCC, 2001). An example is given by the United State where, in the last 30 year, the area with more days with extreme rainfall is greatly increased (Gleason et al., 2008; Fig. 1.5).

Thus the largest increase of precipitation extremes can be found in the eastern part of North-America and West coast of Canada, but high values can be found also in the northern part of Eurasia (Sillmann & Roeckner, 2008).

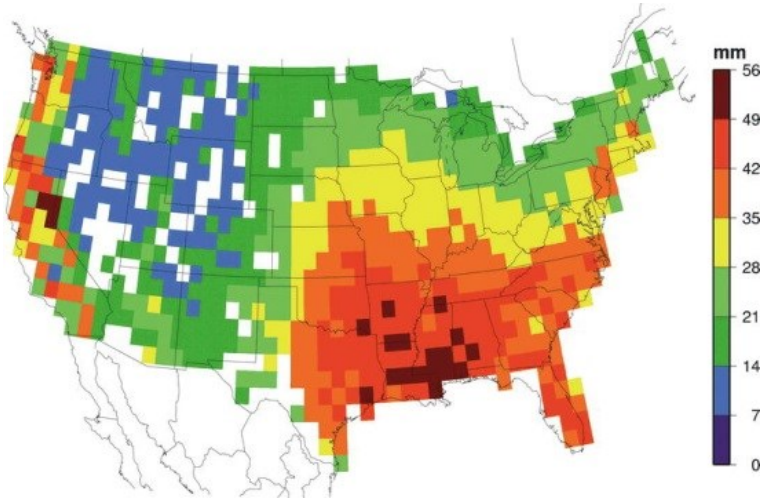

Figure 1.5 - Ninetieth percentile values of daily precipitation for each 1° × 1° grid cell from 1910 to 2003 using a 65% completeness threshold to improve spatial coverage in the western United States (Gleason et al. 2008).

Recent studies suggest an increase in frequency and intensity of tropical cyclones (hurricanes and typhoons) since 1970s, strongly correlated with the rise in tropical sea surface temperature (Webster et al., 2005; Elsner et al., 2008; Hoyos et al., 2006). Bender et al. (2010) argued a doubling of the frequency of category 4 and 5 storms by the end of the 21th century, mainly in the Western Atlantic (north of 20°N). For Europe, Rockel and Woth (2007) estimated an increase of up 20% of the number of storm peak events in the Central Europe over the 21th century. Furthermore, there is some evidence that the winter wind storm over Northwestern Europe have increased over the past 60 years, with a peak in the 1990s (Hov et al., 2013).

1.2 Coastal intense natural events and tsunami

In the context of extreme events, special attention will be devoted to those phenomena affecting coastal system. Storms, storm surges, extreme waves, coastal flooding and tsunami events put the safety of the coastal population and the integrity of the coastal zone at risk (Soukissian et al., 2010). Within the wide category of natural extreme events interesting coastal regions, it's important to distinguish between the forces involved in the different events.

Coastal flooding is one of the most devastating phenomena affecting the world's coasts and can be originated by both storms or extreme waves and tsunamis.

During storms, ocean waves can become significantly higher than normal due to a combination of several factors such as tide, winds, atmospheric pressure and coastal features. Winds blowing in an onshore direction press water toward the coast, overtopping natural and manmade flood protection structures and pushing ocean water inland. Extreme flooding can be caused when storm surge coincides with normal high tide.

Storm surge events affect many coastal areas in the world especially where the coast lies just above or even below the mean sea level. The risk of coastal flooding due to storm surges is rather limited in Mediterranean Sea because the typical tidal range is significantly smaller compared to oceanic coasts. As mentioned by Schmidt-Thomè & Kallio (2006), in Europe storm surges occur mainly in the Northern regions and have caused devastating effects until 1960's. Although the North Sea shorelines is mainly exposed to this hazard, the approximate probability of having storm surges exists in Mediterranean Basin especially in the Northern Tyrrhenian Sea and in the Northern Adriatic Sea (fig. 1.6).

Coastal flooding can be generated even by Tsunamis. These events are triggered mainly by earthquakes, volcanic eruptions, underwater and onshore landslides when large blocks detached from the main substrate falling into water and generating abnormal waves. Tsunamis are characterized by extremely large wavelengths and, in deep ocean, the waves can reach speeds exceeding 900 km per hour. They cannot be felt in the open sea but, in shallower water the wave's velocity diminishes to around 100 km per hour and the height of the waves rapidly grows flooding wide areas and causing catastrophic effects on the coastline. The interest in tsunami events grew especially after 2004 event occurred in the Indian Ocean which caused more than 200.000 fatalities. Since then several studies to estimate both the vulnerability of coastal areas to these hazards and their probability of occurrence have been carried out in order to create and enhance a local and/or regional tsunami warning system to mitigate the risk.

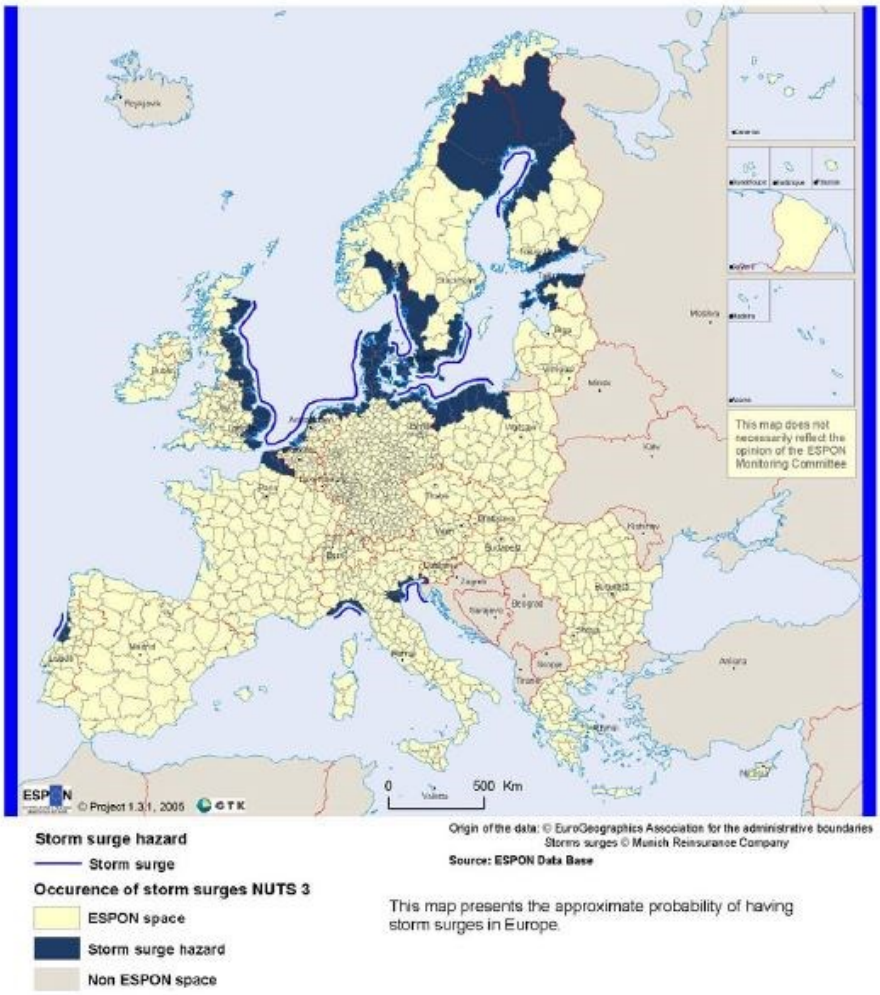

Figure 1.6 – Storm surges probability in Europe (from Schmidt-Thomè & Kallio, 2006).

Within tropical latitudes various works prove the effectiveness of natural barriers such as coral reefs and mangroves against catastrophic effects of tsunamis. In Mediterranean Basin there is a complete lack of knowledge about this topic despite many studies provide documentary evidences of the occurrence of several catastrophic tsunamis in the past 2500 years and prove a high probability of occurrence of these events in the future. The most well-known occurred in the Messina Strait in 1908 and in the Southern Aegean Sea in Greece in 1956 (Papadopoulos and Fokaefs, 2005). Other events occurred in 365 A.D. and in 1303 A.D. caused by earthquakes in the Hellenic Arc (Sorensen et al., 2012). Furthermore at least 96 tsunamis were documented in the Eastern Mediterranean during the last 36 centuries (Altinok and Ersoy, 2000). Probabilistic tsunami hazard assessment can provide important information about areas affected by tsunami risk (fig. 1.7 from Schmidt-Thomè).

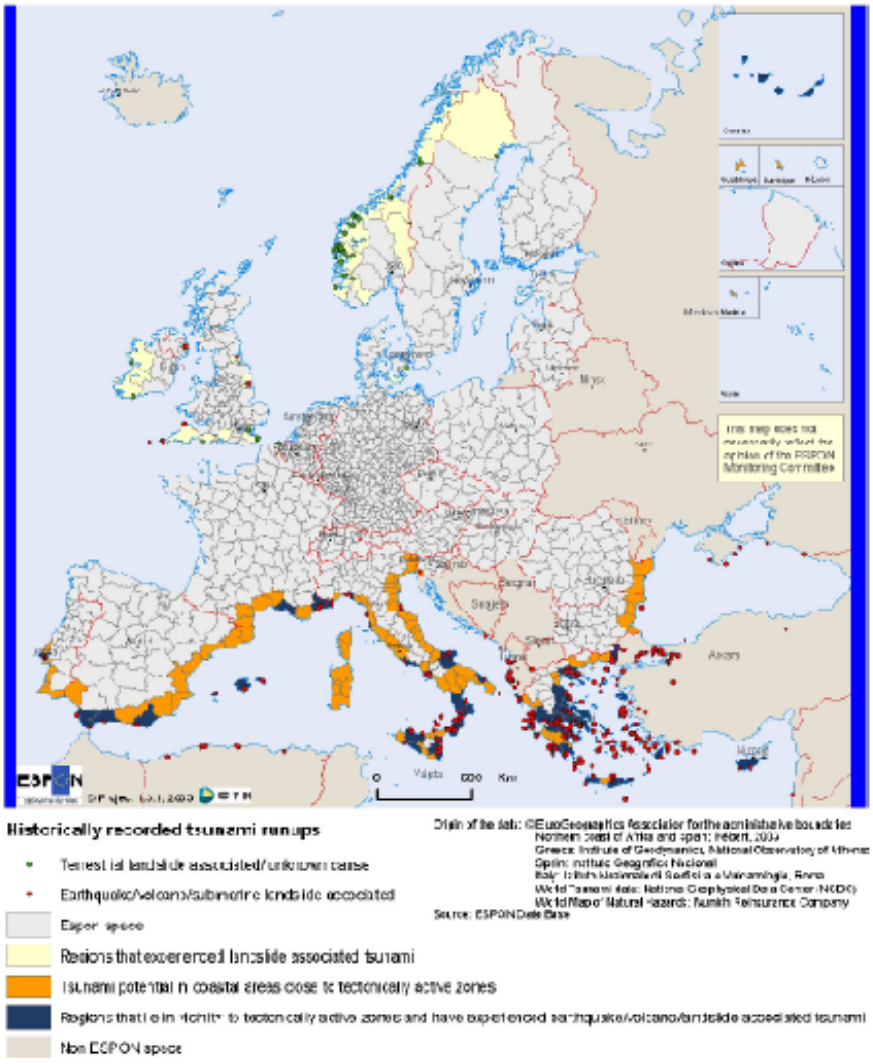

Figure 1.7 – Historically recorded tsunami runups (from Schmidt-Thomé, 2006).

Another important element to be taken into account is the occurrence of extreme waves. The increased frequency of these events causes troubles not only for coastal erosion and shoreline retrieve but also to defense structures, artifacts and safety of coastal populations. Extreme waves can be defined as those waves that are 2.2 to 2.4 times higher than the significant wave height (Faulkner ,2001), although someone considers extreme wave any unusually large wave. Mediterranean Basin is often characterized by strong winds causing rough seas with the formation of local low pressure zones surrounded by raging currents that reach and exceed 100 km/h. When the wind comes up with certain intensity and persists for several days, the coasts directly faced to the trajectory of wind forcing can be attacked by waves. These actions could damage the structures

against they break. The whole Mediterranean Basin is prone to similar phenomena which, added to any existing swell and long fetch wind waves, can critically increase the maximum wave heights.

In the past years, Mediterranean Sea has experienced many severe storms able to generate waves several meters high. There are many examples that may be mentioned: unforgettable is the sea storm occurred in the Ligurian Sea on February 1955 that devastated the Port of Genoa destroying the breakwaters and sinking several boats; on 6 December 2000, always in the Ligurian Sea, a sea storm mercilessly hit harbors and beaches flooding wide areas in several coastal locations. During the event, the port of Rapallo could not withstand the wave impact. But the worst sea storm in the last 30 years date back to 2008 and its epicenter was located between Voltri and Camogli (Genoa, Liguria). The violence of waves up to 8 meters caused huge loss in terms of boats, defense structures and artifacts. Worthy of mention is the extreme event that hit the French Riviera (Cote d'Azur) in May 2010 which led to a surge effect near the port of Cannes. Recently (December 2014) an event similar to those previously described has struck the Algerian coasts. The activation of strong winds coming from north and north-northwest, between the Balearic Sea, Sea of Corsica and Sardinian Sea, caused a rapid increase of the waves in all these basins. Due to the long fetch, the waves reached the Algerian coast with a height over 5 meters.

Many examples causing extensive damages and difficulties to local people can be found also in Adriatic Sea, Ionian Sea and Southern Tyrrhenian. Although in Mediterranean the tidal range is relatively low, these particular sea states, when combined with sea-level rise or storm surges, can cause flooding resulting to land loss and shoreline retrieve. Furthermore, the sea storms along with the large wind waves, being phenomena that occur at high frequency, are mainly responsible for reshaping coastal strip.

1.3 Vulnerability to coastal hazards

In the recent years, the advancement of knowledge on the effects of climate change and their mitigation and adaptation has become a challenge for future research. Researchers are placing great interest on coastal zone where the most sensitive impacts of extreme events are felt. In this context of particular importance is sea level rise. Also increase of storm frequency and intensity plays an important role, but even where these decrease or remain unchanged it is likely that the wave impacts will intensify due to the growth of sea level (Spalding et al., 2014). The main impacts on coastal zone include the inundation of low-lying lands and flooding in occurrence of storm events, increased coastal erosion phenomena, wet-land loss and groundwater salinization. Climate change and coastal hazards are already impacting coastal communities causing extensive damages to people, buildings and other artifacts. Just think about Indian Ocean Tsunami in 2004 or storm surge that hit Philippines in 2013 or the risk faced by Maldives in tropical latitudes. For mid- and high-latitude the risks are lower but still high. Examples are periodic storm tides in the North Sea or the biggest storm surge occurred in Liguria in the last 30 years (30 October 2008).

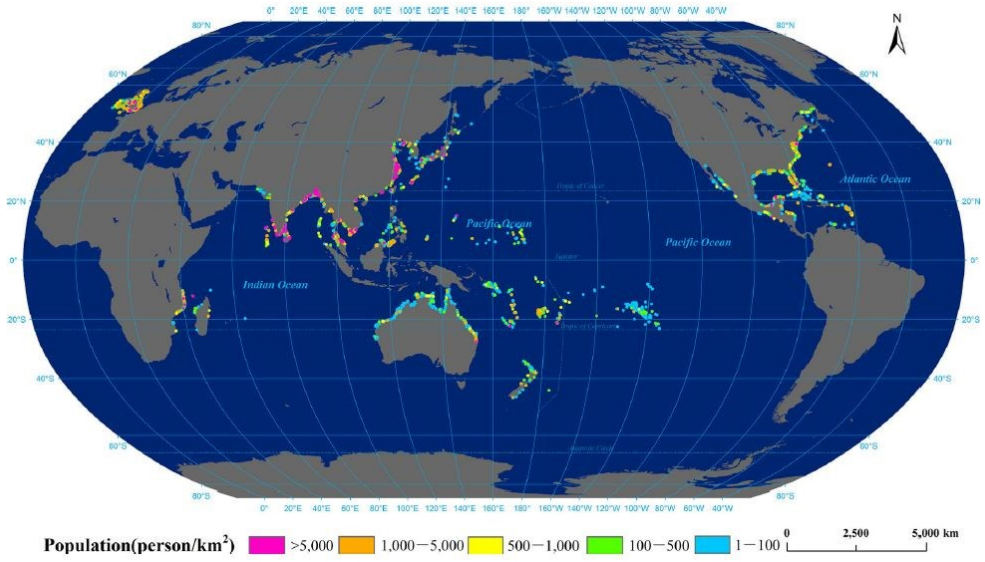

Figure 1.8 – Expected demographic risk of storm surge impact of the world (from Fang et al., 2014).

Another aspect to be considered is the global coastal population trend. In the mid-2013 the world population was of 7.2 billion but it is projected to reach 8.1 billion in 2025, and to exceed 10 billion by 2100 (UN, 2013; figure 1.9).

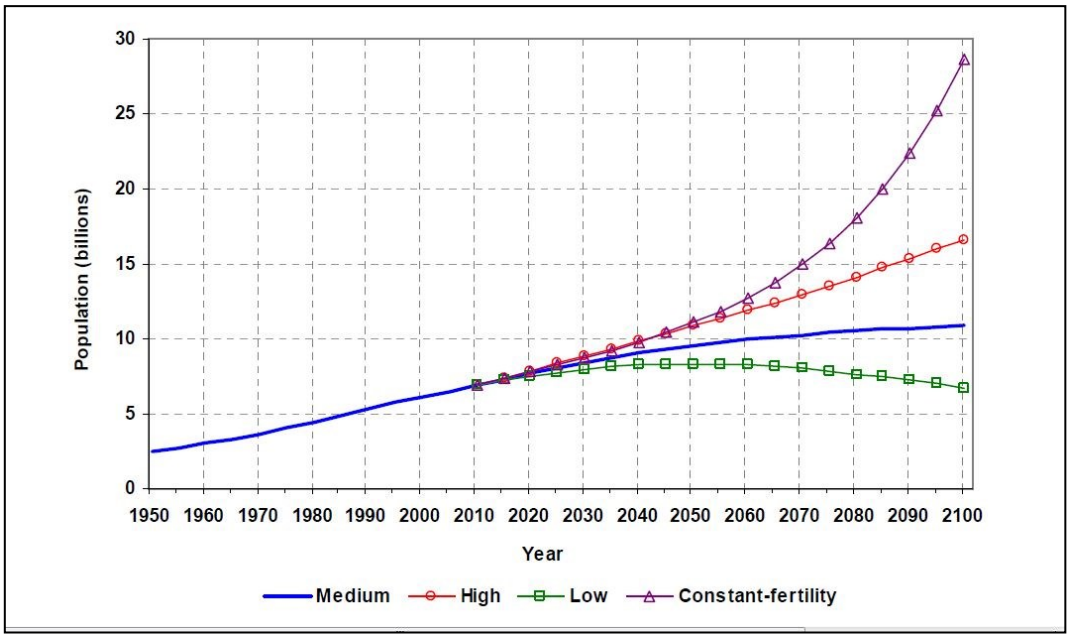

Fig. 1.9 – World population trend, 1950-2100, according to different projections and variants (UN, 2013).

Eight of the ten largest cities in the world are located at the coast and 44% of the humanity lives within 150 km of the coast on just 10% of the earth's land surface (Reed, 2010). Already in 1998, over the half of the world's population inhabited within 200 km of a coastline (Hinrichsen, 1999; Creel, 2003; Reed, 2010).

Figure 1.10 – World by night can give an idea of coastal population.

The reason is to be found in the limitless economic opportunities and in the better quality of life offered by sea-coast system. Although living and working on the coast provides indisputable benefits, inevitably increased population density brings pollution, overexploitation of resources and

habitat degradation, decreasing or altering functions and value of coastal zone ecosystem services. Habitats and landscapes are altered and/or destroyed to accommodate growing population, decreasing the natural capability to provide resources and coastal protection. Human pressure on the environment, change of natural conditions and coastal habitat degradation, as a result of unsustainable development, lead to a heavy increase (amplification) in economic and social vulnerability to coastal hazard and climate change (Spalding et al., 2014).

For coastal communities, an urgent need for action on mitigation and adaptation to coastal hazards and sea level rise is globally recognized.

1.4 The role of ecosystems in coastal protection

Traditionally protection of coastal areas is achieved through engineering "hard" solutions (such as seawalls, breakwaters or dikes), overlooking the innate function of natural systems to absorb any impacts and to react to the major changes taking place. This approach, although often effective, can be costly both to build and to maintain (Bosello et al. 2012). Furthermore, hard structures could have negative and unforeseen effects on environmental conditions and ecosystems, even irreversible (Borsje et al., 2010). Sometimes the problems of coastal erosion and/or damage can be exacerbated and/or moved to adjacent areas by the introduction of these structures (Stancheva et al., 2011; Brown et al., 2011; Spalding et al., 2013). Another aspect to be considered is that the traditional engineering solutions are static and don't respond to the natural evolution of the coastal system in perspective of future sea level rise and increasing natural hazards (Borsje et al., 2011).

Only in the last two decades researchers focused on coastal ecosystems and their role in coastal protection. In particular there is a growing literature that studies ecosystem engineers in relation to their capability to create and enhance biogenic habitat. Jones et al. (1994) defined the ecosystem engineers like "organisms that directly or indirectly modulate the availability of resources (other than themselves) to other species, by causing physical state changes in biotic or abiotic materials. In so doing they modify, maintain and/or create habitats". This definition suggests that almost all

living organisms could be considered a sort of engineer species. Thus, in this paper underwater biogenic features will be considered as natural structures leading to an increase of soil elevation built by living organisms called "Autogenic engineers", namely organisms that change the environment via their own physical structure, i.e. their living and dead tissues (Jones et al. 1994). As they grow and become larger, their living and dead tissues create massive structure where other organisms can live on or in. Biogenic construction, considering their size and physical form, can be considered natural barriers against the wave action and could be able both to absorb the energy released during extreme events and/or mitigate the post-impact effects, and by increasing soil elevation could keep up with long –term trend in sea level rise.

To date, the importance of several coastal ecosystems is largely recognized not only for economic, aesthetic and recreational values but also for their contribution in coastal protection (UNEP, 2011), reducing vulnerability of coastal communities to natural hazards and climate change. The intrinsic characteristics of biogenic structures amplify the effectiveness in countering the effects of climate change.

Martin et al., in the document "Manual of marine and coastal datasets of biodiversity importance" edited by UNEP in 2014, included within the general category of main worldwide biogenic habitat as warm-water coral reefs, cold-water corals, coralligenous and maërl (Mediterranean), mangrove forests, seagrass meadows, saltmarshes. However, this is a list of biogenic habitat considered interesting from the point of view of biodiversity. Others well known biogenic habitats include kelp forests, bryozoan fields and shellfish beds. The functions provided by these habitats are diverse, and can include the increase of biodiversity, complexity and productivity, bentho-pelagic coupling, nutrient recycling, the provision of shelter and food, CO_2 regulation, sediment trapping, protection from erosion, and even the creation of geological features over longer time scales (Morrison et al., 2014).

Until now, most of the research work regarding these structures has been focused on the ecological role or targeted to the taxonomic study of the characteristic and associated species and of inter-

intra-specific relationships. Bostrom et al. (2011) reviewed the progress made in the emerging field of coastal seascape ecology, applying the landscape ecology approach in several coastal sub-tidal and intertidal biogenic habitats. They mainly focused on the effect of spatial patterning for individual focal habitats, organism-seascape relationships, animal movements and connectivity between different biogenic habitats. Abiotic and physical processes (e.g. sediment dynamics and hydrodynamics) were rarely included in the past research works. Despite the growing interest in the issue of coastal erosion relating to climate change, relatively few papers have been published concerning how biogenic habitats affect the wave propagation process and sediment transport process, and how these natural barriers can reduce the energy of incident waves on the coast, thereby better defining their role in coastal protection. Koch et al. (2009) discussed several aspects regarding the function of wave attenuation provided by biogenic habitats such as mangroves, seagrasses, marshes and coral reefs, highlighting temporal and spatial variability in ecosystem services. Recent studies also tried to quantify the economic value of services provided in terms of coastal protection in order to include these values into socio-economic analyses (Barbier et al., 2008; Koch et al., 2009; Guannel et al., 2011).

The most of the research effort about the changes in wave propagation and sediment transport induced by biogenic habitats is focused on coral reefs (e.g. Massel & Brinkman, 2001; Lowe et al., 2005; Kunkel et al., 2006; Ferrario et al., 2014; Harris & Vila-Concejo, 2006; Quiroga & Cheung, 2013;), seagrasses (e.g. Asano et al., 1988; Van Keulen & Borowitzka, 2003; Bradley and Houser, 2009; Paul & Amos, 2011; Granata et al., 2001), mangroves (Alongi, 2008; Tusinski, 2012; Dahdouh-Guebas et al. 2005) and salt marshes (Moller et al., 1999; Moller & Spencer, 2002; Moller, 2006; Moller et al., 2014). Several other papers describe the evolution of the waves over mobile beds (Grant & Madsen, 1982; Elgar & Raubenheimer, 2008; Hurther & Chassagneux, 2013; Harris & Grilli, 2014) and/or ripple beds (Fredsøe et al., 1999; Wilberg & Harris, 1994; Mathisen & Madsen, 1996; Marin, 2004) and/or artificial structures such as breakwaters (Kofoed, 2002; Geeraerts et al., 2009; Grilli et al., 2003). Few studies have been carried out on shellfish beds

(Leeuwen et al., 2010; Meyer et al. 1997; Piazza et al., 2005) and kelp forests (Jackson, 1984; Elwany et al., 1995; Rosman et al., 2007; Utter & Denny, 1996).

Many of these issues have been addressed for tropical and subtropical marine environments, while the amount of papers decreases if we shift the focus on temperate and cold-temperate seas. Focusing on Mediterranean basin, the only available studies are concerning the seagrass meadow *Posidonia oceanica* (Gacia & Duarte,2001; Hendriks et al., 2008; Infantes et al. 2012; Prinos et al., 2010; Koftis et al., 2013; Elginoz et al., 2011; Folkard, 2005). Generally scientific research focused on cold-water corals, bryozoans and/or coralligenous assemblage are rare or not-existent.

The evaluation of the wave attenuation benefits provided by bioconstructed structures to coastal communities can lead both to a complete understanding of multiple ecosystem services and a quantification of economic value of coastal protection function thus can be used to justify conservation decisions into coastal planning.

1.5 Coastal hydrodynamic modelling

One of the main tools currently used to analyze the coastal hydrodynamics processes and investigate changes in wave propagation is the hydrodynamic modeling (physical models, process-based numerical models, hybrid and/or composite models) because of its capacity to simulate the main phenomena in coastal zone. These models are based on representation of physical processes and usually include forcing by winds, waves or currents, dissipation factors occurring during wave transformation process, and a response in terms of sediment transport and/or shoreline evolution. Traditionally, hydraulic studies have been carried out with physical model and laboratory experiments. Through their implementation, the phenomena are faithfully reproduced at reduced scale. Nowadays, with the rapid development of computational technology, numerical models are increasingly being used in place of physical models. These models rely on mathematical description of complex turbulent processes and boundary conditions (Sutherland & Barfuss, 2012). The success

of numerical models is due both to the versatility and the cheapness of this technique. In effect, physical models have the weakness to suffer from scale effect, while being able to reproduce complex nonlinear physical phenomena (Sutherland & Barfuss, 2012). Furthermore, numerical models can provide an equally adequate representation of many physical phenomena and can be run with many configurations and options depending on the purpose which must be achieved (Sutherland & Barfuss, 2012). Thus numerical models can be used for studying of a flurry of hydrodynamic processes and for different spatial and temporal scale by applying proper filtering techniques. Composite modelling tries to integrate physical and numerical models combining their strengths to solve complex problems. In hydraulic studies it is a rather young subject and relatively few papers have been published only in the last years.

In the context of coastal hydrodynamics, the research is mainly focused on coral reefs (e.g. Nelson, 1997; Kunkel et al., 2006; Ferrario et al., 2013; Quiroga & Cheung, 2013; Lowe et al., 2005; Massel & Brinkman, 2001), mobile beds (e.g. Elgar & Raubenheimer, 2008; Harris and Vila-Concejo, 2006; Harris & Grilli, 2014; Hurther & Chassagneux, 2013), vegetated seafloors (Ghisalberti & Nepf, 2002; Bouma et al., 2005; Mendez et al., 2009; Myrhaug et al., 2009; Chen & Zhao, 2012; Infantes et al., 2012; Mendez & Losada, 2013; Zhao & Chen, 2014) and artificial or other hard structures (Grilli et al., 2003; Zhuang & Lee, 1996; Kofoed, 2002; Geeraerts et al., 2009), or has the purpose of merely studying the wave transformation processes, taking into account only the morphological characteristics of the seabed and omitting hydraulic ones. Furthermore, most of these works assess the dissipation effect due to the turbulence associated with breaking waves rather than the energy dissipation due to bottom friction. The latter can be a relevant term even in relatively deep water where the presence of natural structures that rise from the seabed greatly increases the hydraulic roughness value, and consequently the wave friction factor and the drag coefficient on the bottom. The bed stress is an important parameter for the calculation of wave friction factor and it is dependent on the orbital velocity at the bed and the effective or equivalent roughness height k_w (Raudkivi 1988). Since roughness height remains quite

difficult to estimate (Camenen et al., 2006) and although in the literature several existing relationships for equivalent roughness under different flow conditions have been investigated, many researchers directly measure the shear stress in situ by employing acoustic sensors deployed near the bed. Only a few works highlight the utility of using the bottom roughness for better calculating the friction factor and the drag coefficient (e.g. Infantes et al. 2012; Lowe et al. 2005). If studies of the roughness have been carried out for different habitats such as sandy bottoms, coral reefs and vegetated seafloors (e.g. seagrass meadows, kelp forest), a gap exists for other biogenic habitats (e.g. coralligenous assemblage, cold-water corals or shellfish beds).

Application of numerical models coupled with other emerging techniques such as optical and acoustic, also by means a reliable assessment of the hydraulic roughness of different seascapes can lead to a more accurate prediction of surface waves on seabed with different textures and, consequently, to a definition of coastal erosion phenomena and the risks associated with them. The representation of the results in GIS (Geographic Information System) environment and integration with different types of datasets can be an excellent decision making tool for coastal zone managers.

1.6 ICZM Protocol, Action Plan in Mediterranean Sea and Disaster Risk Reduction initiatives in Europe

During the recent decades, coastal risk management and reduction have been promoted in a systematic way through several national and international programs in the context of Integrated Coastal Zone Management (ICZM) and Disaster Risk Reduction Program. ICZM has a key role to play to deliver in the coastal zone, providing the bridging between land and sea. More precisely, ICZM *"would contribute to ensure coherence between policies, plans and programs, and the effective nesting and implementation of plans and programs at different scales of intervention. Working at different scales and across administrative and sectorial boundaries remains a formidable challenge, but is central to achieving integration. The overall result should be greater*

clarity, certainty and predictability of policy and decision-making. This will facilitate the sustainable development of maritime economies and enhance the livelihoods of coastal communities". (An evaluation of Integrated Coastal Zone Management (ICZM) in Europe; Communication from the Commission, COM (2007) 308). In the document of adoption of the Action Plan for the implementation of the ICZM Protocol for the Mediterranean, which defines the timeframe of the actions to be taken between 1st January 2012 and 31 December 2019, among the key issues that limit the full and effective implementation of the Protocol in Mediterranean Sea emerges the need to fully integrate into the ICZM process future risks and uncertainties, particularly those related to climate change and natural disaster such as flood, earthquakes, storms and tsunamis. In this framework European Community recognizes the role of integrated coastal zone management and ecosystem-approach in addressing the challenges of climate change and natural disaster, and promotes a sustainable coastal management and development, supporting socio-economic development, biodiversity and ecosystem services. A series of research initiatives and funded projects at European level have been undertaken in order to avoid the negative impacts of climate change on marine areas and coastal zones and to achieve the integrated management of this strip. Many projects focused on climate change adaptation in coastal areas and on blue and green infrastructures have been funded in the recent years. RESMAR strategic project, CoastAdapt and ECOSHAPE are only some of several projects funded by EU.

In the framework of Disaster Risk Reduction (DRR) systematic efforts are made in order to analyze and manage the causal factors of disasters, prepare the communities to hazard events and improve warning systems and planning. Notable initiative is the European Commission Humanitarian aid and Civil Protection department Disaster Preparedness Program (DIPECHO) launched in 1996. Ever since DIPECHO is funding projects in the main disaster-prone regions of the world. DIPECHO projects are carried out by European-based aid agencies and UN agencies in close cooperation with local authorities and NGOs. The objective is to reduce the impact of natural disasters by strengthening local physical and human resources in high risk areas. At the same time it

raises awareness among decision-makers for the need to integrate disaster risk reduction into longer term development policies. The program covers activities in the fields of awareness-raising, community training and capacity building, provision of equipment, local early warning systems, emergency planning and small-scale damage limitation works for demonstration purposes. Directorate General of ECHO (DG ECHO) also supported the establishment of the Tsunami Information Centre for the North-Eastern Atlantic, Mediterranean and connected seas (NEAMTIC) with the specific objective to make citizens aware of the risks associated to coastal areas (tsunami, storm surges, strong swells) in order to develop affordable measures for disaster prevention and preparedness, including mitigation through integrated coastal zone management.

These are just some of the initiative launched worldwide trying to harmonize intergovernmental and transnational actions on risk reduction topic.

1.7 Aims and structure of the thesis

From the above paragraphs, it appears clear that there is a gap between studies carried out in tropical and subtropical environments and temperate ones focused on wave attenuation and coastal protection functions provided by biogenic habitats. But above all, there is a huge gap between hydrodynamic studies focused on some habitat as coral reefs, sandy or mobile beds, mangroves or vegetated seafloor, than others such as coralligenous assemblages, shellfish beds or cold-water corals nonetheless important for both distribution and extent and ecosystem services provided.

Here, we aim to partially fill these gaps focusing on Mediterranean underwater bioconstructed ecosystems and in particular on coralligenous formations.

The reasons of our choice are to be found in wide distribution, in the great extent and in the inherent characteristics of this Mediterranean habitat. Therefore we consider it necessary to devote the first part of the research work to the description of different coralligenous formations existing in

Mediterranean and of the main research efforts aimed at a better definition of the distribution, extent and conservation status of this seascape.

Thus we documented the effects induced on wave propagation by different underwater habitats and biogenic structures capable to increase the complexity of the seabed asking different main questions:

1) Could different habitat types, giving different roughness values to the seabed, differently influence wave propagation process?

2) Are biogenic habitats such as coralligenous formations more effective than other coastal habitats in attenuating wave energy and how much?

3) How can these habitats reduce the energy of incident waves on coastal strip and what are the involved hydraulic mechanisms?

4) How much can their presence and integrity affect the mitigation effect?

5) Can this information be integrated in coastal zone management plans and how?!

Once the general aspects, the features and the processes associated with concretions have been defined, the basics of coastal hydrodynamics and the parameters used into process-based numerical models for calculating wave propagation from deep water to surf zone will be described. The discussion will focus mainly on the most recent advances regarding the development of simulation models and on the description of the main dissipative forces involved during the wave transformation process (wave breaking and bottom friction) and relative energy dissipation functions. Thus the equations and the assumptions, as well as the approximations employed for the numerical models, will be defined.

Successively, the two case studies will be presented. The environmental setting and the wave regimes of these areas will be described within each regional context and the underwater seascapes will be characterized more in detail.

Within each area, several information from different sources was used and several methods for data gathering were employed. The sources of the information will be specified and the methods will be described in the section 4 “Materials and Methods”, primarily highlighting the innovation aspects of the methodologies (e.g. roughness assessment of seabed with photogrammetric techniques).

Then the process-based numerical models will be performed with the dual aim of highlighting the combined effect of several habitats on wave propagation and of estimating the effectiveness of each habitat in dissipating waves’ energy via bottom friction.

Finally, the emerging results from numerical models will be interpreted, processed and integrated within geographic information systems to date available, trying to better explain the possible relationship between the vulnerability conditions of the different coastal zones during several wave conditions (from strong to extreme events) and the presence of biogenic habitats.

2 CORALLIGENOUS ASSEMBLAGES: BACKGROUND

Provide a single definition of coralligenous assemblages in an arduous task as those are not made up of just one but by a group of communities that are the result of a dynamic equilibrium between bio-builders (i.e. rhodophytes, scleractinians, serpulids, bryozoans, etc.) and bio-borers (mainly represented by *Porifera* family *Clionaidae*) (Sarà, 1973; Cerrano et al., 2001), and could be considered as underwater seascape.

The coralligenous is a formation referring to secondary hard bottoms resulted by the biogenic carbonate accumulation and the biota inhabiting them (Sarà, 1969) and it plays a key-role recognized at European level (92/43/CE Habitat Directive 1992, habitat code 1170-14: Reefs, coralligenous assemblage) (Cerrano et al., 2014). The organization of these habitats in different layers (basal, middle and upper layers) confers great structural and functional complexity and contributes to enhance the three-dimensionality of the seabed.

In general, within this manuscript, we will consider the coralligenous as a hard bottom of biogenic origin mainly produced by the accumulation of calcareous encrusting algae growing in dim light conditions (Ballesteros et al., 2006). Among the underwater biogenic formations, coralligenous is undoubtedly one of the most important and complex in Mediterranean Basin in terms of ecological role, biodiversity, production and extent. In particular, besides being a biodiversity "hot-spot" hosting around 20% of the Mediterranean species (Ballesteros et al., 2006), coralligenous assemblages are also considered of great relevance for fisheries activities and CO_2 regulation, as well as representing a strong attraction for diving tourism. Generally coralligenous develops in littoral system from 10 to 120m of depth, in both circalittoral and infralittoral zone, on rocky shores and on detritic beds (Perès & Picàrd, 1952) in relatively steady conditions of temperature, currents and salinity, and in low-light condition (between 0.5% and 3% of surface irradiance) (Garrabou & Ballesteros, 2000). Ages obtained by radiocarbon dating of coralligenous blocks, situated at depth between 10 and 60m in the North-western Mediterranean, range from 600 to 8000 years BP (Sartoretto et al., 1996). Canal & Ballesteros (1997) estimated the carbonate production of

phytobenthos thriving in relatively shallow waters between 100 and 465g $CaCO_3$ m^{-2} yr^{-1}, whereas the animal carbonate production amount to around 660g $CaCO_3$ m^{-2} yr^{-1} (Ballesteros, 2006). The accumulation rate of coralligenous constructions has been estimated to be between 0.006 and 0.83mm yr^{-1}, as a consequence the thickness of concretion layer has been estimated variable between 20-25 cm and 3-4 m (Ballesteros, 2006).

According to several authors and on the basis of the research carried out along the Italian coasts, it is possible to distinguish between two main typologies:

1) Coralligenous biocenosis forming rims developed in the outer part of marine caves and on vertical cliff. The thickness of the rims ranges from 20-25 cm to more than 2 m and increases from shallow to deep waters (Laborel, 1987). Sometimes the concretions can lead to develop structures similar to terraces with the above side well-lighted and the sciaphilic lower one ;
2) Coralligenous concretions forming banks develop as flat buildups with variable thickness (from 0.5m to 3-4m) on either rocky substratum or biodetritic beds. They are mainly built over more or less horizontal substrates, and they have a very cavernous structure (Ballesteros, 2006). Perès & Picàrd (1952) hypothesized that they developed from coalescence of rhodoliths or maerl belong with organogenic sand and gravel (*coralligène de plateau*). Branched or massive species like gorgonians, bryozoans and/or sponges cling on these buildups develop a rich associated fauna that leads to a highly complex biocenosis. These banks are sometimes surrounded by sedimentary bottoms and/or associated to marine angiosperms. Typically, the progressive action of calcareous organisms leads to overlap consecutive calcareous layers producing a sort of discontinuous armor, mostly very hard and rough, on an originally mobile bed (Sarà, 1968). Sometimes isolated rocky outcrops surrounded by coastal mud can lead to similar features.

Therefore the complexity of this mosaic of communities involves a vulnerability to different threats. The main causes of disturbance that affect coralligenous are related to both human activities and climate change:

- Mechanical damage due to fishing activities, anchoring and diving tourism is probably the most destructive impact affecting coralligenous assemblages. The action of trawling gear can lead to the detachment and death of erect species. Furthermore the performance of trawling and other gears increases turbidity and sedimentation rate affecting negatively algal growth and suspension feeding. Finally lost gears can smother and/or break sessile benthic species among which some long-lived organisms. Anchoring and diving tourism are also severe impacts on coralligenous communities, breaking the fragile organisms and concretions.
- Consequences of climate change are ocean acidification and global warming. Recent studies prove that the extinction risk of some typical species living in coralligenous, such as red coral (*Corallium rubrum*), is enhanced by ocean acidification (Cerrano et al., 2013). In the last 20 years, mass mortality events of suspension feeders are probably related to the current global warming trend (Cerrano et al., 2000).
- Pollution (waste water discharge, nutrient inputs, aquaculture, changes in land uses and coastal infrastructure construction, eutrophication), increasing water turbidity and altering sediment load, involves an increase of bioerosion rate, an inhibition of coralline algal growth, a decrease of species richness and an increase in abundance of highly tolerant species. Blooms of mucilaginous and filamentous algae affect negatively coralligenous communities and they seem to be caused by eutrophication.
- Several lessepsian species are seriously threatening coralligenous assemblages. In particular some algal species such as *Womerseyella setacea*, *Caulerpa racemosa* and *Caulerpa*

taxifolia are invasive species able to grow also in deep waters where coralligenous thrives, thus inhibiting growth of the main bioconstructors and altering communities' composition.

Although there is an overall knowledge concerning coralligenous buildups, one of the major gaps is the lack of cartographical data related to their distribution and extent at smaller scale (UNEP-MAP-RAC/SPA, 2008). Most of the research studies have been carried out in the north-western of Mediterranean Sea, in the eastern Adriatic Sea and around Apulian coasts. Only a few studies derive from research carried out in the Aegean-Levantine sub-region and there is an absolute lack of information about coralligenous in the southern and in the eastern part of Mediterranean Basin (Agnesi et al., 2008). The absence of data in many areas and the fragmentary nature of the available data are probably due to the lack of standardized protocols for mapping, characterization and monitoring of assemblages because of difficult accessibility of coralligenous habitat and high heterogeneity of the hosted communities. The depth where coralligenous buildups thrive is often a constraining factor in terms of practicality during diving operations due to diver safety issues. This means that most of the studies carried out on coralligenous formations are confined to the first 50 m of the water column (fig. 2.1).

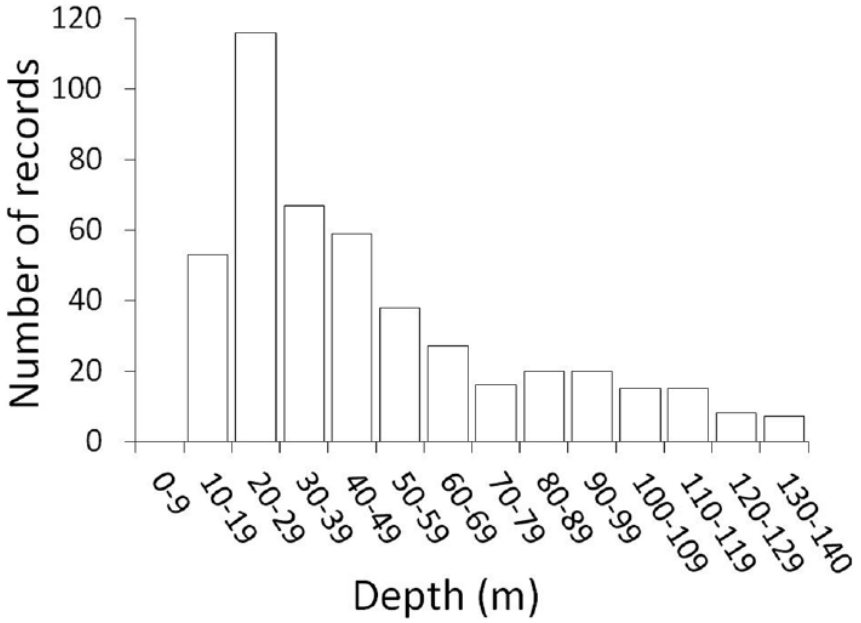

Figure 2.1 - *In situ* depths for coralligenous assemblages and maerl beds (from Martin et al., 2014).

Research works involving scientific divers at depths greater than 50 m are still few (i.e. Cerrano et al., 2014). Rapid development of remote sensing techniques has opened new perspective in mapping coralligenous biodiversity, condition and extent at different scales (Zapata et al., 2013). Recently acoustic sensors, remote-operated vehicles and optical methods are widely used for collecting data without impact on the seabed. These facilities allow post-processing of gathered data reducing the time-consumption of field activities but increasing the costs of the investigations. While using these techniques is now easier to achieve an extensive data collection, it is also true that the quality and the details of the data acquired *in situ* by scientific divers are not matched by remote sensing methodologies. Thus the purposes of the surveys and the scale of detail to reach become key-elements to be defined before choosing the methods to be used and starting the investigations.

Numerous initiatives, formulated during the last decade, have highlighted the importance of identifying coralligenous and other bio-concretions distribution throughout the whole Mediterranean Sea. In the document prepared for the Regional Activity Centre for Specially protected Areas (RAC/SPA) in 2009, Agnesi et al. carried out a Mediterranean bibliographic census in order to build a specific GIS database containing all available cartographic data on coralligenous habitats and other bioconcretions in the Mediterranean. They analyzed 524 scientific documents published until the end of October 2008 to produce 25 Data Sheets of the calcareous concretions' distribution within the whole Basin (i.e. fig. 2.2).

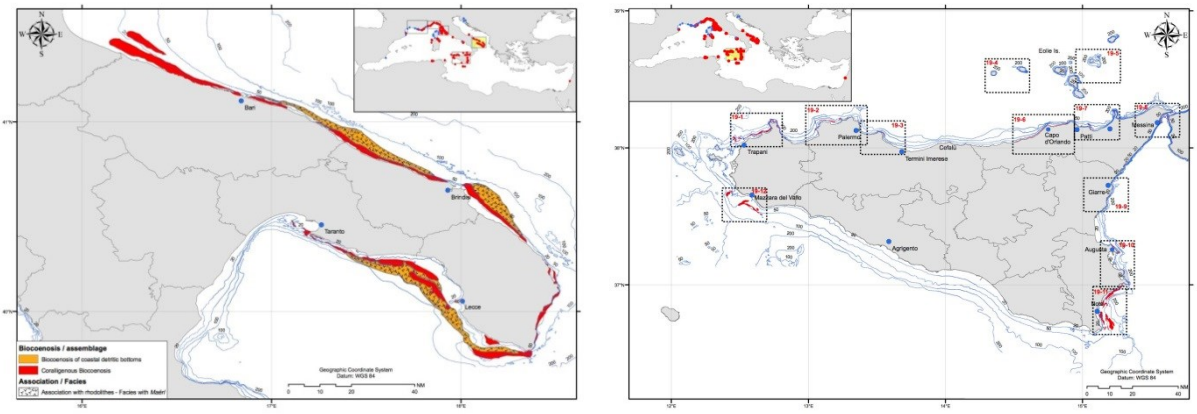

Figure 2.2 – Examples of data sheets of concretions' distribution from Agnesi et al. (2009).

In the 2014, an additional contribution came from the work of Martin et al. (2014). They have updated the distribution map of coralligenous assemblages for the entire Mediterranean collating heterogeneous datasets from a total of 17 countries. The coralligenous outcrops dataset was composed of 4,293 points, 12 lines and 23,632 polygons for a total surface area of 2,263.4 km^2 (points and lines were not considered) and they estimated that datasets provided information for approximately 30% of the Mediterranean coasts between 10 and 140 m of depth. The resulting small-scale map is shown here below (fig. 2.3).

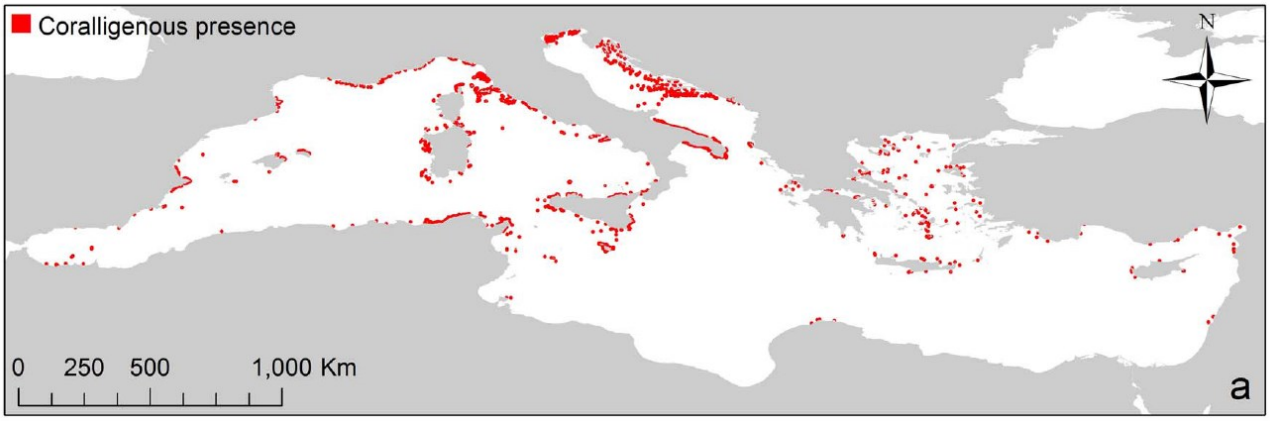

Figure 2.3- Occurrence of coralligenous outcrops across the Mediterranean Sea from the review work of Martin et al. 2014.

It can be noted that the scientific information is unevenly distributed and the major research effort has taken place especially in the western part of the basin. The map provides an overview of the distribution of this habitat along the Mediterranean coasts but does not take into account the difference between the two main typologies of coralligenous: banks and rims. However, the available spatial data indicate that these formations widely occur in the whole Mediterranean Sea.

The emerging trend of the recent years is the integration of available dataset with distribution modelling techniques. Distribution modelling tools for predicting the distribution from a set of records and environmental predictors provide a useful way to synthesize the information from scattered samples into rationale maps (Reiss et al., 2014). Moreover predictive modelling is also useful to identify most suitable areas for coralligenous habitat presence and to address preliminary

surveys especially in deep environments. Recent research studies focused on bio-constructions distribution predictive modelling in Mediterranean Sea (i.e. Zapata et al. 2014, Martin et al. 2014). Martin et al. (2014), into his recent work, have produced the first continuous distribution map of coralligenous assemblages across the entire Mediterranean Sea through predictive modelling techniques based on environmental predictors. The map below shows the probability of occurrence of coralligenous outcrops across the whole Mediterranean Basin (fig. 2.4).

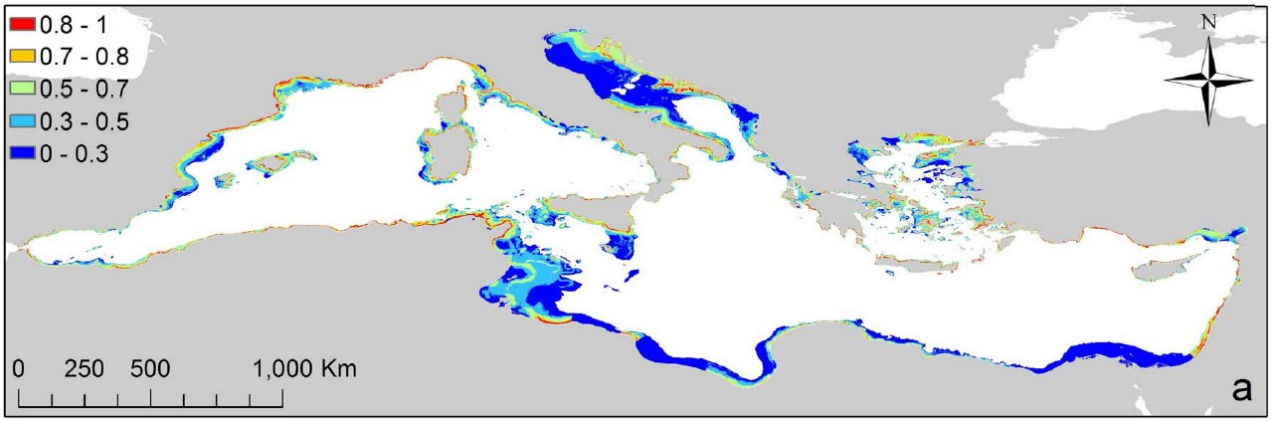

Figure 2.4 - Occurrence probability map for coralligenous assemblages throughout the Mediterranean Sea (from Martin et al., 2014).

They used six variables to model the occurrence of coralligenous outcrops: bathymetry, slope of the seafloor, nutrient input, euphotic depth, phosphate concentration and sea surface current. They also found that the main three predictors were bathymetry, slope and nutrient input contributing for 84.1% to the model (respectively 37.4%, 31.9% and 14.8%). The predicted areas were consistent with the already available information and the model suggested unexplored areas where focus future research studies.

3 COASTAL HYDRODYNAMICS AND PROCESS-BASED NUMERICAL MODELLING: THE BASICS

Many hydrodynamic processes that occur in the coastal region are examined by modeling techniques being able to reproduce the main phenomena involved in the wave propagation toward the coastline. Wave modeling attempts to depict the sea state and predict the evolution of waves using numerical techniques. Numerical models are useful to obtain solutions within the continuous spatio-temporal domain. These are discretization methods by which it is possible to obtain a reliable and approximated solution in a finite number of points (space) and instants (time). As already mentioned in the paragraph 1.5, today numerical models are increasingly being used in place of traditional physical models because of their versatility, reliability and cheapness.

The waves are the expression of forces whose action, by acting on the water in the normal and tangential direction, leads to warp the free surface of the water. When wind waves are generated by a long fetch or a distant storm, they usually consist of a wide range of wave frequencies. The wave component with a higher frequency propagates at a slower speed than those with lower wave frequencies. In deep waters, the waves are not affected by the bathymetry. As soon as the depth decreases and reaches a certain value, the wave motion undergoes a change in its propagation. The depth where this phenomenon appears mainly depends on the characteristics of the waves. Upon entering in shallower water, the generated waves are either refracted by the bathymetry or current, or diffracted around abrupt bathymetric features. A portion of wave energy is reflected back to the deep sea (Liu & Losada, 2002). During their shoreward propagation, waves modify their amplitude and height and loose some of their energy through dissipation near the bottom. The amount of the dissipation is function of both bottom roughness, reducing near-bed velocity, and wave's parameters (amplitude, length, height). Approaching the coastline, the seabed becomes shallower causing an increase in wave amplitude and a decrease in wavelength. Because the wave speed is proportional to the square root of the water depth in very shallow water, wave profile becomes steeper and the front face of the wave moves at a slower speed than the wave crest, leading to the

overturning of the wave crest and hence to wave breaking. Thus the wave energy is dissipated. The turbulence associated with breaking waves is responsible not only for the energy dissipation but also for sediment movement in the surf zone (fig. 3.1).

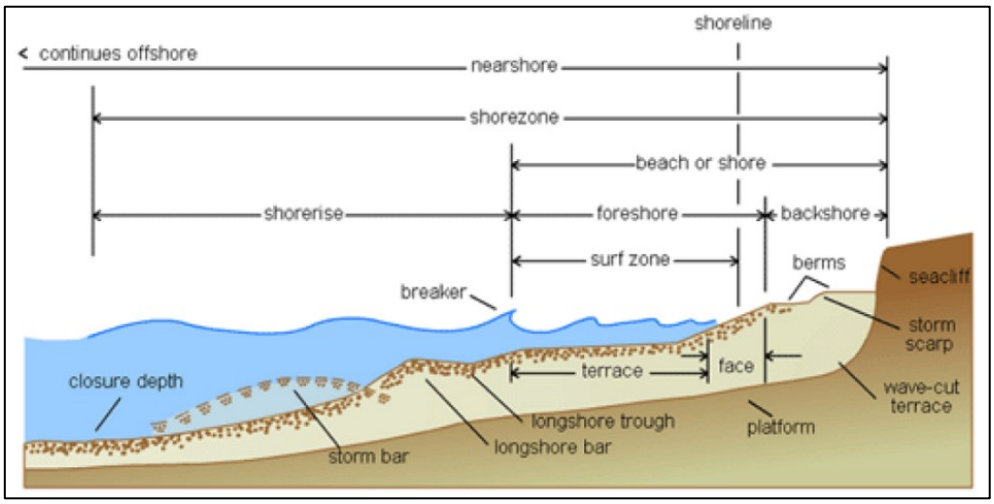

Figure 3.1- Beach profile zonation scheme.

3.1 Wave propagation: hypotheses and parameters

In the discussion about the wave propagation phenomena, the basic assumption is to consider wave as regular and progressive (fig. 3.2). This type of wave reveals both temporal and spatial periodicity.

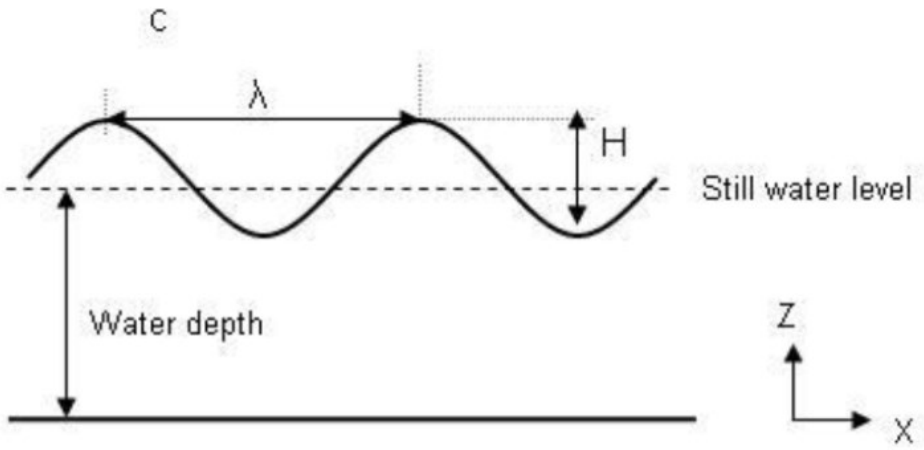

Figure 3.2 - Regular wave representation.

In order to describe it, we will consider an approximation effective for infinitesimal waves using a perturbation method truncated at the first term (first-order approximation).

A regular wave can be mathematically described by a sinusoidal function, and it is characterized by different elements:

- **Wave Crest**: highest point of the wave;
- **Wave Trough**: lowest point of the wave;
- **A**: Wave Amplitude = distance between free surface and undisturbed level (equilibrium point) [m];
- **H**: Wave Height = vertical distance between wave crest and trough [m];
- **L**: Wave Length = horizontal distance between two consecutive crests (or consecutive troughs) [m];
- **T**: Wave Period = the time spent by wave to complete one cycle. The period can be also defined as time (expressed in seconds) required to a crest to travel a distance equal to the wavelenght [s];
- **c**: Velocity of propagation or celerity= $\frac{L}{T}$ [$m\ s^{-1}$];
- **σ**: Angular frequency = $\frac{2\pi}{T}$ [s^{-1}];
- **K**: Wave number = $\frac{2\pi}{L}$ [m^{-1}];
- **Θ**: Wave phase = ($KX-\sigma T$) [*adimensional*]

Sea waves are also known as dispersive waves because σ and K (angular frequency and wave number) are related by the following dispersion equation:

$$\sigma^2 = gK\tanh(Kh)$$

Solving for L (wave length), we find the equation:

$$L = \frac{gT^2}{2\pi}\tan h\left(\frac{2\pi}{L}h\right)$$

Solving this equation for infinite and shallow depths (respectively $Kh \to \infty$ and $Kh \to 0$):

(1) For shallow depths: $Kh \to 0$ $\quad L = \sqrt{ghT}$

(2) For infinite depths: $Kh \to \infty$ $\quad L_0 = \frac{gT^2}{2\pi}$

The consequence of this relation is that L decreases with the depth.

Solving for C we obtain:

(1) For shallow depths:

$$C = \sqrt{gh}$$

(2) For infinite depths:

$$C_0 = \frac{gT}{2\pi}$$

Group velocity is defined as the speed at which a set of waves, characterized by different frequency and amplitude, propagates toward the coast. It is defined by the following relation:

$$C_G = \frac{C}{2}\left[1 + \frac{2kh}{\sin h(2kh)}\right]$$

(1) For shallow depths: $Kh \to 0$ $\qquad c_G = c$

(2) For infinite depths: $Kh \to \infty$ $\qquad c_{G0} = \frac{c}{2}$

Being $C \geq C_G$, each wave travels faster than the group so that, once it arrived in front of the group, the wave disappears within it. The continuous formation of waves in its tail ensures the existence/maintenance of the group. Group velocity represents the velocity of propagation of the wave energy.

3.2 Wave energy

The amount of energy contained in a regular wave is given by the sum of kinetic and potential energy:

$$E_{TOT} = E_c + E_P$$

At the first order of approximation, the potential energy is equal to the kinetic one:

$$E_p = E_c = \frac{1}{16}\rho g H^2$$

Thus:

$$E_{TOT} = E = \frac{1}{8}\rho g H^2$$

Where wave energy is defined as *density* of energy.

The energy flux is an important dimension and it is defined as the wave power crossing the vertical section per unit of width:

$$E_f = Ec_G$$

$$E_f = [M] * [L] * [T^{-3}]$$

3.2.1 Energy processes

The processes of energy transport can be divided in two main classes: conservative phenomena and dissipative phenomena. Conservative phenomena (as shoaling and refraction) are those that preserve the wave energy flux. Dissipative ones (for instance those due to bottom friction and wave breaking) on the contrary lead to a progressive loss of wave energy content.

3.2.1.1 Shoaling

The shoaling is a phenomenon linking depth with wave height. It is based on conservation of energy between two wave orthogonals (figure 3.3). The wave orthogonals are imaginary lines held perpendicular to the wave's front and identifying the direction of the wave motion. Assuming a two-dimensional propagation of regular waves, thus bottom slope moderate and constant, rectilinear and parallel bathymetry, frontal attack of the waves, E_f must remain constant between the two orthogonals, from deep to shallow waters.

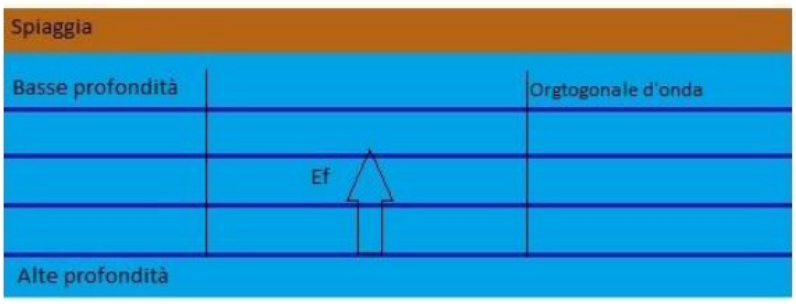

Figure 3.3 - Energy flow between two wave orthogonals.

Hence: $$E_f = Ec_G$$

If the energy flux is constant, thus: $\boldsymbol{E_{f0} = E_f}$

$$\boldsymbol{E_0 c_{G0} = E c_G}$$

By replacing and simplifying: $\boldsymbol{H_0^2 c_{G0} = H^2 c_G}$

$$\boldsymbol{H = K_s H_0}$$

Where K_s represents the coefficient of shoaling and its value is

$$\boldsymbol{K_s = \sqrt{\frac{c_{G0}}{c_G}}}$$

$$\boldsymbol{K_s^2 = \frac{c_{G0}}{c_G} = \frac{c_0}{2}\frac{2}{c}\left(1 + \frac{2kh}{sin\, h(2kh)}\right)^{-1} = \frac{2\cos h^2\,(kh)}{2kh + sin\, h(2kh)}}$$

Thus, K_s is a function of relative depth kh and wave period T.

The trend of K_s is called shoaling curve and its value is represented in the figure 3.4 below for different values of $\boldsymbol{h/L_0}$.

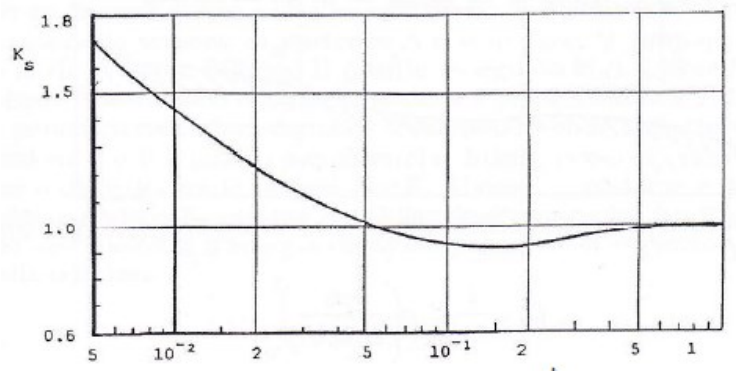

Figure 3.4 - Shoaling coefficient K_s for different value of h/L_0.

Moving toward to the shore, shoaling generates a progressive raising of the wave height, which is affected by the decreasing depth. Wave height increases up to a critical value, after which the wave energy decays producing the wave breaking (fig. 3.5).

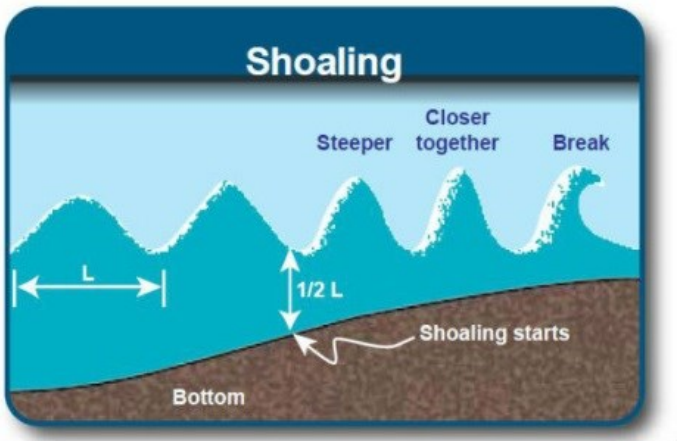

Figure 3.5- Progressing raising of wave height due to the shoaling.

3.2.1.2 Wave refraction-diffraction

Refraction-diffraction phenomenon occurs if the attack of the wave is not frontal and the wave orthogonals form an angle with the axis normal to the bathymetry; in this case we speak of almost two-dimensional propagation. This phenomenon is based on the assumption of conservation of energy flux and it is governed by Snell's Law:

$$\frac{\sin \alpha}{L} = \frac{\sin \alpha_0}{L_0}$$

Where α and α_0 represents the angles between the wave front and respectively local isobath and offshore isobaths; L represents the local wave length and L_0 represents the wave length in deep water ($L<L_0$).

As a consequence, angle α tends to decrease moving towards the shore.

From the definition of celerity of a single wave and remembering that the period T is an invariant of the propagation, we can also describe the relationship as following:

$$c = \frac{L}{T}$$

$$\frac{\sin \alpha}{c} = \frac{\sin \alpha_0}{c_0}$$

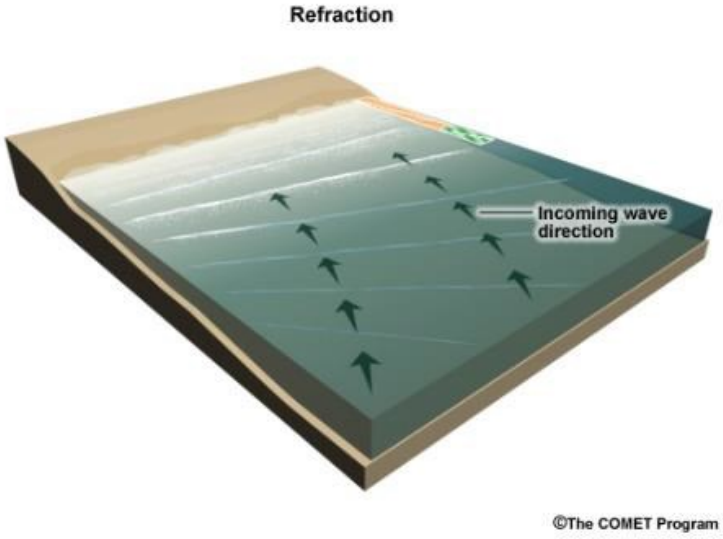

Figure 3.6 – Wave refraction phenomenon representation.

Concerning the conservation of energy flux between two wave's orthogonals, we highlight that, unlike what happens for the shoaling process, a term $\boldsymbol{b}$ describing the distance between two wave's orthogonals appears. Thus we can write:

$$\boldsymbol{E_{f0} b_0 = E_f b}$$

$$\boldsymbol{\rho g \left(\frac{H_0^2}{8}\right) c_{G0} b_0 = \rho g \left(\frac{H^2}{8}\right) c_G b}$$

$$\boldsymbol{H = H_0 \sqrt{\frac{c_{G0}}{c_G}} \sqrt{\frac{b_0}{b}} = H_0 K_s K_R}$$

Where $\boldsymbol{K_s}$ is the coefficient of shoaling, while $\boldsymbol{K_R}$ is the refraction coefficient.

Being $$\boldsymbol{b = a\ \cos(\alpha)}$$

$$\boldsymbol{b_0 = a\ \cos(\alpha_0)}$$

Thus

$$\boldsymbol{\frac{b_0}{b} = \frac{\cancel{a}\ \cos(\alpha_0)}{\cancel{a}\cos(\alpha)}}$$

In case of rectilinear bathymetry, refraction generates a decrease of wave height.

In presence of promontories or coves, where usually isobaths are not parallel to the shore, refraction acts on wave motion: in presence of a promontory waves thicken and grow in height approaching the coast; while in presence of a cove, the opposite happens.

Figure 3.7 – Refraction in presence of coves and/or promontories.

3.2.1.3 The wave breaking

Wave breaking occurs following an excessive increase of the wave height which generates instability; the wave therefore, exceeded its characteristic values, begins to break, decreasing its height and dissipating a large amount of energy.

Several dimensionless formulas exist for relating the height of breaking wave with its wave length. Considering the wave length in deep water $\boldsymbol{L_0}$ and the length of the breaking wave $\boldsymbol{L_f}$=*1.2* $\boldsymbol{L_0}$, the following relationships are described:

- For deep water: $\frac{H_f}{L_f} = \boldsymbol{cost}$
- For intermediate depth: $\frac{H_f}{L_f} = \boldsymbol{f}\left(\frac{h}{L_f}\right)$; $\frac{H_f}{gT^2} = \boldsymbol{f}\left(\frac{h}{gT^2}\right)$
- For shallow water $\frac{H_f}{h} = \boldsymbol{f}\left(\frac{h}{gT^2}\right)$
- For shallow water and significant bottom slope (S_b): $\frac{H_f}{h} = \boldsymbol{f}\left(\frac{h}{gT^2}, \boldsymbol{S_b}\right)$
- For depth tending to zero: $\frac{H_f}{h} = \boldsymbol{cost}$

Many formulas have been proposed to determine the height of breaking wave; here below an example of the most used formulas:

- Infinite water depth (Michell, 1893; Yamada, 1957; Cokelet, 1977):

$$\frac{H_f}{L_f} = 0.142, L_f = \frac{1.2gT^2}{2\pi}$$

- Intermediate depth (Goda, 1974):

$$\frac{H_f}{gT^2} = \left(\frac{0.17}{2\pi}\right)\left\{1 - e^{-\frac{3\pi^2 h}{gT^2}}\right\}$$

- Shallow water depth with nearly horizontal bottom (Scarsi e Stura, 1980):

$$\frac{H_f}{h} = 0.727 - 1.12\left(\frac{h}{gT^2}\right)^{0.5}$$

- Shallow water depth with steeper seabed (slope=S_b):

For S_b<0.05 (Scarsi e Stura, 1980)

$$\frac{H_f}{h} = [0.73 + (13S_b)^2] - [1.12 + (30S_b)^2]\left(\frac{h}{gT^2}\right)^{0.5}$$

for S_b>0.05 (Scarsi e Stura, 1972)

$$\frac{H_f}{h} = \frac{\frac{1.56}{[1 + e^{-19.5Sb}]}}{1 + 43.75[1 + e^{-19.5Sb}]\left(\frac{h}{gT^2}\right)}$$

3.2.1.3.1 Iribarren number

The Iribarren number, also known as the surf similarity parameter, is a dimensionless parameter used to describe breaking wave types on beaches or breakewaters:

$$\xi = \frac{S_b}{\sqrt{\frac{H_f}{L_0}}}$$

We can distinguish three main types of breaking waves:

1. $\xi<0.4$ Spilling breaker: Wave breaking typical of beaches with a very slight slope. The seabed may remain shallow up to hundreds meters from the coast and it is mainly sandy bottom. Waves rise up to assume a pointed shape and are subjected to light and continuous breaking along the surf zone (fig. 3.8).

Figure 3.8 – Spilling breaker.

2. $0.4<\xi<2$ Plunging breaker: the bottom slope is slightly more pronounced compared to the previous case. Even in this situation the waves begin to break far from the shore, but assume greater heights (fig. 3.9).

Figure 3.9 – Plunging breaker.

3. ξ>2 Surging breaker: this is the most violent wave breaking. The seabed rises sharply near the coast and the wave grows rapidly in height, producing a sudden and punctual wave breaking on shore and a violent dissipation of energy (fig. 3.10).

Figure 3.10 – Surging breaker.

3.2.1.4 Bottom friction

During their shoreward propagation, waves modify their amplitude and height and loose some of their energy through dissipation due to bottom friction. The amount of the dissipation is function of both bottom roughness and wave's parameters. The dissipation of wave energy caused by bottom friction becomes smaller in the surf zone (Thornton and Guza 1983), where breaking phenomena are prevalent. During the last years, several authors highlighted the relevance of considering dissipation due to bottom friction. This can be a relevant term even in relatively deep water where the presence of natural structures that rise from the seabed greatly increases the hydraulic roughness value, and consequently the wave friction factor and the drag coefficient (dimensionless quantities used to quantify the resistance of an object in a fluid environment) on the bottom. The bed stress is an important parameter for the calculation of wave friction factor and it is dependent on the orbital velocity at the bed and the effective or equivalent roughness height K_w (Raudkivi, 1988). Since roughness height remains quite difficult to estimate (Camenen et al., 2006) and although in the literature several existing relationships for equivalent roughness under different flow conditions

have been investigated, many researchers directly measure the shear stress *in-situ* by employing acoustic sensors deployed near the seabed. Despite this trend, recent works highlight the utility of using the bottom roughness for better calculating the friction factor and the drag coefficient (e.g. Infantes et al. 2012, Lowe et al. 2005). The main issue is that for those hydrodynamic models that consider dissipation term due to bottom friction, a hydraulic roughness K_w must be specified and it depends on particular characteristics of surveyed sites, besides it could be different also within the same site being made up of a mosaic of several types of sea bottom (i.e. sand, rocks and different habitats). Theoretically, K_w can be calculated indirectly from wave attenuation measurement as a typical approach, but it would be preferable specify hydraulic roughness length based on physical roughness of the seabed (Lowe et al. 2005).

In this research we will present a new method for directly estimating the bottom roughness of the seabed and will show the relationship with the hydraulic roughness which can be easily integrated into hydrodynamic models.

3.2.2 Statistical analysis and Rayleigh distribution

Random waves have heights varying over time (fig. 3.11). The statistical description of the wave heights characteristics of a sea state is essential for studying its evolution. Statistical analysis is performed using the Rayleigh distribution (fig. 3.12), which is characterized by the following probability density function:

$$\boldsymbol{p(H) = \frac{H}{4\sigma_\eta^2} e^{-\frac{H}{8\sigma_\eta^2}}}$$

Where $\boldsymbol{\sigma_\eta^2}$ is the variance of the water heights, instant for instant.

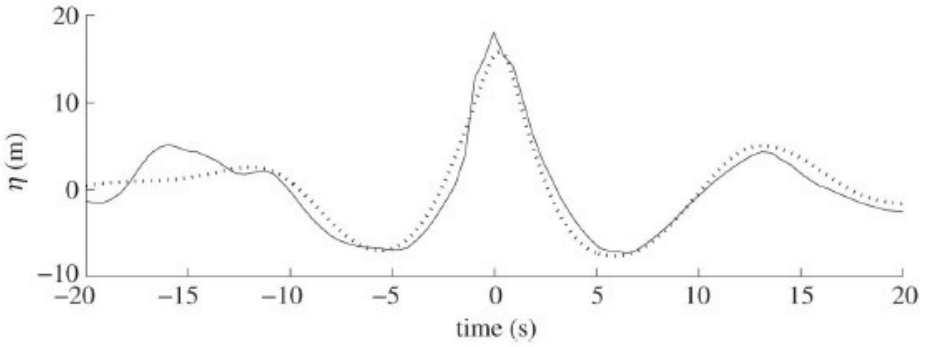

Figure 3.11 – Instantaneous wave height profile over time.

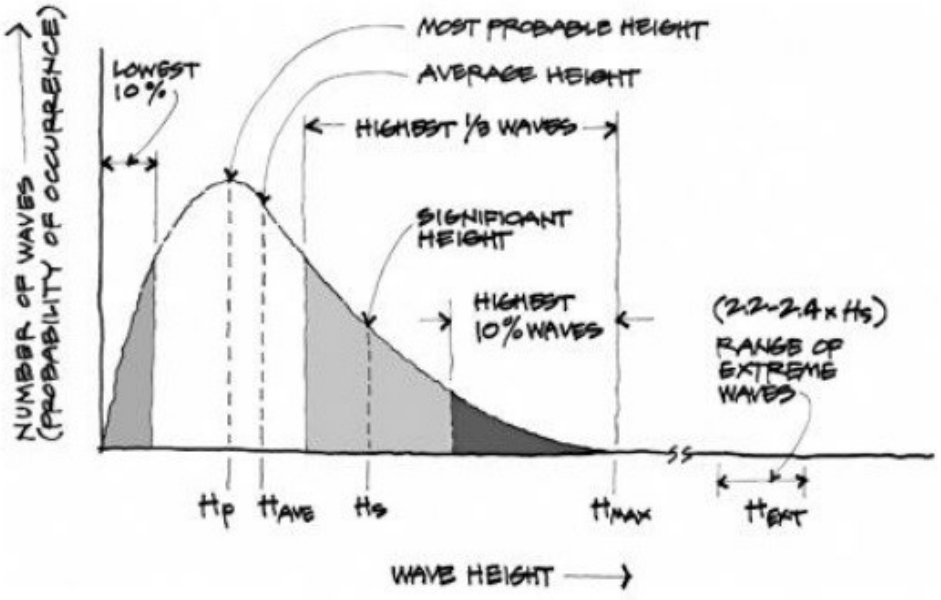

Figure 3.12 – Rayleigh distribution and statistical wave height.

Statistical wave parameters are calculated based on this distribution.

The wave height values most used for the description of a sea state consisting of *N* values of *H* are:

- $\boldsymbol{H_{av}}$: average of the wave heights;
- $\boldsymbol{H_{rms}}$: root mean square of the wave heights

$$\boldsymbol{H_{rms} = \left\{\frac{1}{N}\sum_{1}^{N} H^2\right\}^{0.5}}$$

- $\boldsymbol{H_s}$: significant wave height which is the mean of the highest third of the waves in a time-series of waves representing a certain sea state. It is the most used for random waves;
- $\boldsymbol{H_{1/10}}$: represent the mean of the 10% highest waves.

The statistical parameters are linked to each other by fixed relations; in particular:

$$H_{\frac{1}{3}} = 4\sigma_{\eta}^{2}$$

The term $4\sigma_{\eta}^{2}$ is often referred to Hm_0, where m_0 is defined as the "zero" order momentum and derive from the spectral analysis of a wave. A momentum of **r-order** is defined as:

$$m_r = \int_0^{\infty} f^r S(f) df$$

Where f is the frequency and $S(f)$ is the frequency spectrum of the random wave system (fig. 3.13).

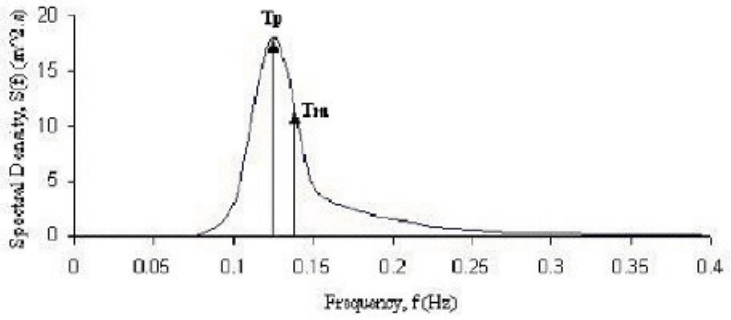

Figure 3.13 – Random wave frequency spectrum.

Thus:

$$H_{\frac{1}{3}} = H_{m0} = 4\sigma_{\eta}$$

$$H_{\frac{1}{3}} = \sqrt{2}H_{rms}$$

These relations allow us to estimate the necessary parameters starting from σ_{η}, which is easily calculable from the experimental data of the instantaneous wave profile $\eta(t)$.

3.3 Parametric wave transformation models

3.3.1 Equation of the conservation of wave energy

The accurate description of wave transformation during the propagation from offshore to shore, such as wave height and energy content, is essential to be able to predict phenomena affecting the coastal zone.

Assuming that linear wave theory is valid and assuming straight and parallel bathymetric contours, the evolution of wave energy flux and wave height from an initial condition, approximate to infinite depth, until the breaking zone may be written as:

$$\frac{\partial(Ec_G \cos\theta)}{\partial x} = -\varepsilon_D = -(\varepsilon_B + \varepsilon_F)$$

Where:

- Ec_G represents the energy flux;
- $E = \frac{1}{8}\rho g H^2$ is the wave energy density;
- $c_G = \sqrt{gh}$ is the group velocity for shallow depth;
- θ is the wave angle relative to shore normal;
- ε_D is the total energy dissipation;
- ε_B is the dissipation due to breaking;
- ε_F is the dissipation due to bottom friction.

The equation describes as the energy content changes along the direction perpendicular to the coast (coordinate x) and as a function of the dissipative term ε_D.

By using the definition of energy:

$$H = \sqrt{\frac{8E}{\rho g}}$$

The solution of the equation of the conservation of wave energy flux allows to estimate wave characteristics from infinite depth section to breaking zone, under certain initial conditions.

The approach used for the analysis of wave propagation is the WEPM (Wave Energy Propagation Model).

The energy conservation equation is solved and developed through the Runge-Kutta fourth-order method.

The numerical model used and the dissipation terms considered will be described and detailed in the following sections.

3.3.2 WEPM model

The WEPM model defines the energy dissipation during wave propagation from offshore to shore, and then analyzes the evolution of the wave during its propagation taking into account refraction and shoaling phenomena. In order to be able to use the WEPM model, it is necessary to know the initial wave conditions in infinite depth, in other words the depth where the wave is not affected by the presence of the seafloor.

The initial information required to use the model are: offshore wave height $\boldsymbol{H_0}$, wave period $\boldsymbol{T}$ and offshore wave angle relative to shore normal $\boldsymbol{\alpha_0}$, and of course the seabed profile along the $\boldsymbol{x}$ direction, from the offshore section to the wave breaking **.**

3.3.3 Runge-Kutta iterative method

In numerical analysis, the Runge-Kutta methods (**RK**) are a family of iterative methods used in temporal discretization for the approximate solutions of ordinary differential equations. They are part of the general family of discrete methods for ordinary differential equations, in other words that class of numerical methods able to approximate the solution of a differential equation in a discrete set of points.

Given a differential equation, this can be discretized as following:

$$\begin{cases} \boldsymbol{y' = f(x, y)} \\ \boldsymbol{y(x_n) = y_n} \end{cases}$$

Where x_n e y_n are known and the interval *h* is defined.

$$\boldsymbol{y_{n+1} = y_n + \frac{h}{6}(k_1 + 2k_2 + 2k_3 + k_4)}$$

$$\boldsymbol{x_{n+1} = x_n + h}$$

The RK method will be more accurate the smaller will be the size of interval *h* considered (fig. 3.14).

The “k” parameters are defined as:

$$k_1 = hf(x_n\,,\, y_n)$$

$$k_2 = hf(x_n + \frac{h}{2}\,,\, y_n + \frac{1}{2}k_1)$$

$$k_3 = hf(x_n + \frac{h}{2}\,,\, y_n + \frac{1}{2}k_2)$$

$$k_4 = hf(x_n + h\,,\, y_n + k_3)$$

These represent four increments respectively based on the slope of beginning, middle and end range.

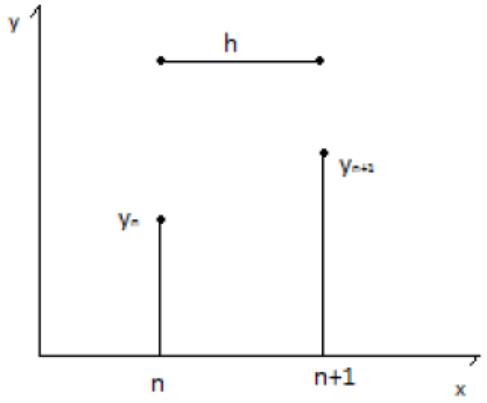

Figure 4.14 – Interval *h* between x_n and x_{n+1}.

To solve the energy conservation equation, knowing the distance $\boldsymbol{x}$ and offshore wave parameters at the initial section, energy of waves and the other parameter can be calculated at the next point, as following:

$$\frac{\partial(Ec_G \cos\theta)}{\partial x} = -\varepsilon_D$$

$$\frac{\partial E}{\partial x} C_G \cos\theta + \frac{\partial C_G}{\partial x} E \cos\theta + \frac{\partial \cos\theta}{\partial x} EC_G = -\varepsilon_D$$

$$\frac{\partial E}{\partial x} = -\frac{\varepsilon_D}{C_G \cos\theta} - \frac{\partial C_G}{\partial x}\frac{E\cos\theta}{C_G\cos\theta} - \frac{\partial \cos\theta}{\partial x}\frac{EC_G}{C_G\cos\theta}$$

$$k_1 = \left[-\frac{\varepsilon_{bi}}{C_{Gi}\cos\theta_i} - \frac{\partial C_G}{\partial x}\bigg|_i \quad \frac{E_i}{C_{Gi}} - \frac{\partial \cos\theta}{\partial x}\bigg|_i \quad \frac{E_i}{\cos\theta_i} \right] dx_i$$

$$k_2 = \left[-\frac{\varepsilon_{b_{i+1/2}}}{C_{G_{i+1/2}}\cos\theta_{i+1/2}} - \frac{\partial C_G}{\partial x}\bigg|_{i+\frac{1}{2}} \quad \frac{E_i + 1/2k_1}{C_{G_{i+1/2}}} - \frac{\partial \cos\theta}{\partial x}\bigg|_{i+\frac{1}{2}} \quad \frac{E_i + 1/2k_1}{\cos\theta_{i+1/2}} \right] dx_i$$

$$k_3 = \left[-\frac{\varepsilon_{b_{i+1/2}}}{C_{G_{i+1/2}}\cos\theta_{i+1/2}} - \frac{\partial C_G}{\partial x}\bigg|_{i+\frac{1}{2}} \quad \frac{E_i + 1/2k_2}{C_{G_{i+1/2}}} - \frac{\partial \cos\theta}{\partial x}\bigg|_{i+\frac{1}{2}} \quad \frac{E_i + 1/2k_2}{\cos\theta_{i+1/2}} \right] dx_i$$

$$k_4 = \left[-\frac{\varepsilon_{b_{i+1}}}{C_{G_{i+1}}\cos\theta_{i+1}} - \frac{\partial C_G}{\partial x}\bigg|_{i+1} \quad \frac{E_i + k_3}{C_{G_{i+1}}} - \frac{\partial \cos\theta}{\partial x}\bigg|_{i+1} \quad \frac{E_i + k_3}{\cos\theta_{i+1}} \right] dx_i$$

The wave energy on the next point is then given by:

$$E_{i+1} = E_i + \frac{1}{6}(k_1 + 2k_2 + 2k_3 + k_4)$$

And the wave height is given by:

$$H_x = \sqrt{\frac{8E_x}{\rho g}}$$

4 MATERIALS AND METHODS

Starting from the hypothesis that biogenic habitats, conferring high levels of complexity to the seabed, are able to increase wave attenuation influencing sediment transport dynamics and reducing coastal erosion, the effects induced by several coastal seascapes on wave propagation have been modeled in two locations with different characteristics: Porto Cesareo with mild-slope seabed and Bogliasco hosting steeper seabed if compared to the previous. Once the environmental setting and the marine climate of the two areas have been defined, the sampling strategies and the data collection procedure will be described. Then the process for building three-dimensional models of the seabed and for estimating physical roughness will be detailed. Several measures of roughness were compared for testing their effectiveness in discriminating different habitats. After selecting the most appropriate measure and converting physical roughness into equivalent hydraulic roughness, a simplified numerical model of wave propagation based on the formulation developed by Thornton and Guza (1983) was implemented in order to highlight the variation in waves' height and energy from offshore toward the shoreline along straight transects. By analyzing data from numerical simulations, the contribution provided by different habitats to wave dissipation will be estimated. Finally, an example of application for calculating wave run-up and for estimating inundation on land under different seabed impact scenarios will be shown.

4.1 Study areas and environmental setting

Based on the bibliographical research and on the general framework on coralligenous distribution set out in the section 2, we chose to focus on two Italian regions: Apulia Region (Southwestern Italy) and Liguria Region (Northwestern Italy). Several works in fact prove the presence of this habitat on horizontal or sub-horizontal bottoms also in relatively shallow waters.

The Apulian coralligenous stretches for hundreds of miles parallel to the coast (fig. 4.1), growing with variable thickness between 1 and 2.5 meters and covering seabed between 4 and 35 m of depth (Sarà, 1971).

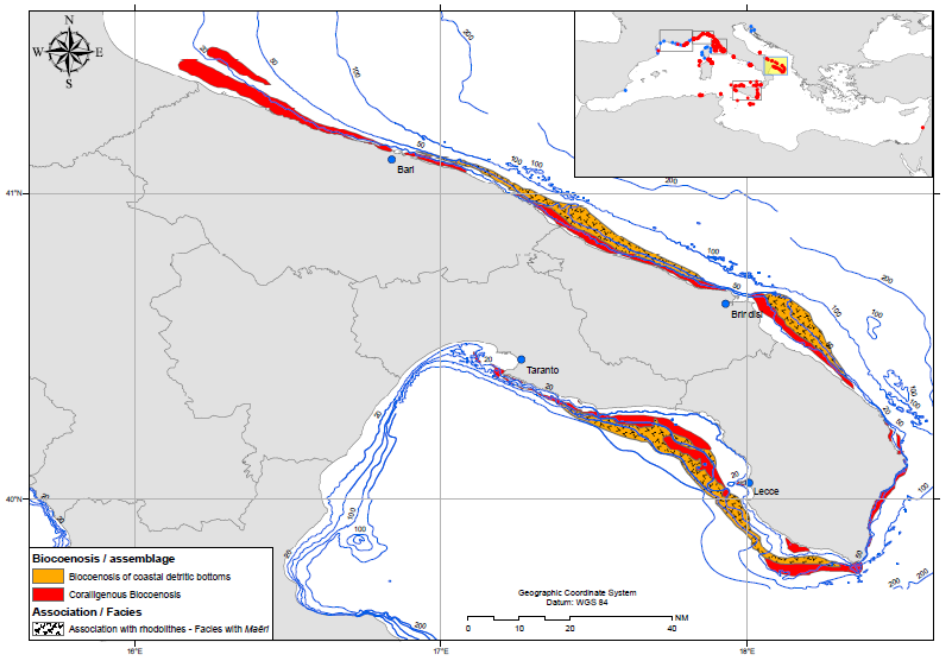

Figure 4.1 – Distribution of coralligenous and coastal detritic bottoms in Apulia Region (from Agnesi et al., 2009).

Infralittoral formation similar to the Apulian coralligenous has been described by Pansini and Pronzato (1973) on Levantine ligurian coasts. These frameworks run parallel to the coast on seafloors much steeper if compared with the apulian seabed.

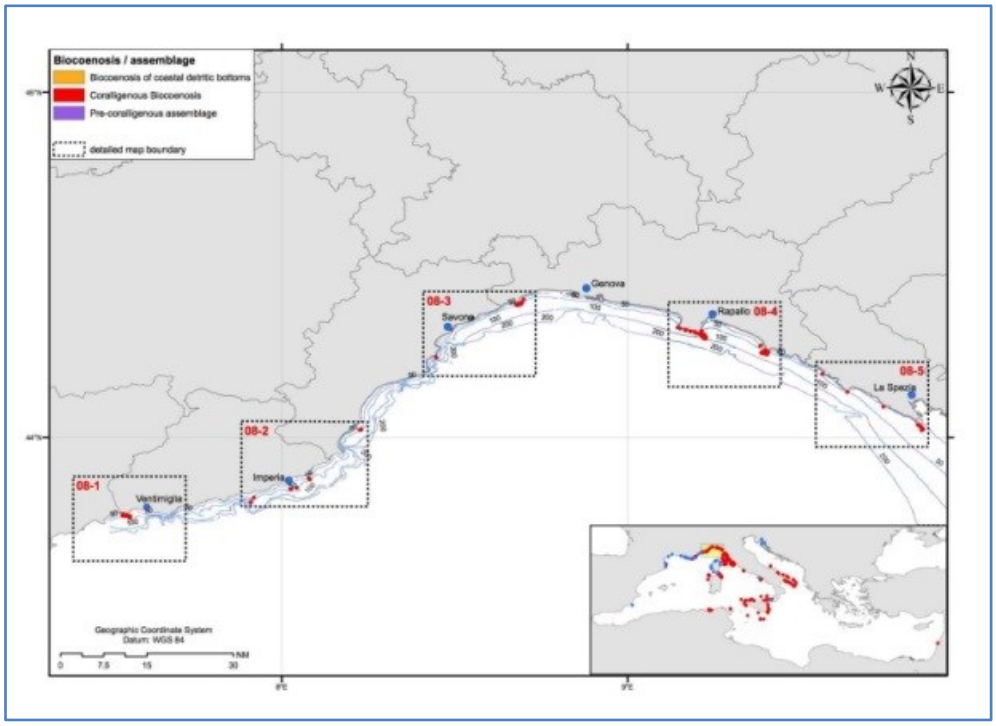

Figure 4.2 – Distribution of coraligenous, pre-coralligenous and detritic bottoms along Ligurian coast (from Agnesi et al., 2009).

Based on chartographic data to date available, we selected two main areas on which focus our research (fig. 4.3): Bogliasco (44°22’34.7’’N, 9°04’05.1’’E) in the province of Genoa, Liguria, and Porto Cesareo (40°15’16.1’’N, 17°52’59.2’’E) in the province of Lecce (Apulia). The seafloors are characterized by similar exposure to the open sea (S-SW) but by different slope.

Figure 4.3 – Geographical localization of case studies: Bogliasco (Liguria Region, Italy) on the left; Porto Cesareo (Apulia Region) on the right side.

4.1.1 Bogliasco – Genoa coastal tract

In Bogliasco, the seabed, being not included within the boundaries of any area subjected to special protection regime, have never been characterized in detail. Although the "Atlas of marine habitats" (2006) updated by Liguria Region in 2009 does not report the presence of coralligenous concretions on the seabed in front of Bogliasco, historical sources (Sarà, 1971 and Pansini & Pronzato, 1971) prove the presence of infralittoral formations developing almost parallel to the coast, with frequent interruptions represented by *Posidonia oceanica* meadows and sandbanks. These outcrops are located about 300 meters seaward from Bogliasco town. In order to better define the presence and the distribution of different habitats, underwater field surveys were planned and performed in September and October 2014. During field activities, 3 cross-shore transects have been carried out up to 22 meters depth by using a Diver Propulsion Vehicle (DPV) Dive-Xtras CUDA650 equipped with GoPro Hero 3+ camera and GPS placed on towed buoy (fig. 4.4).

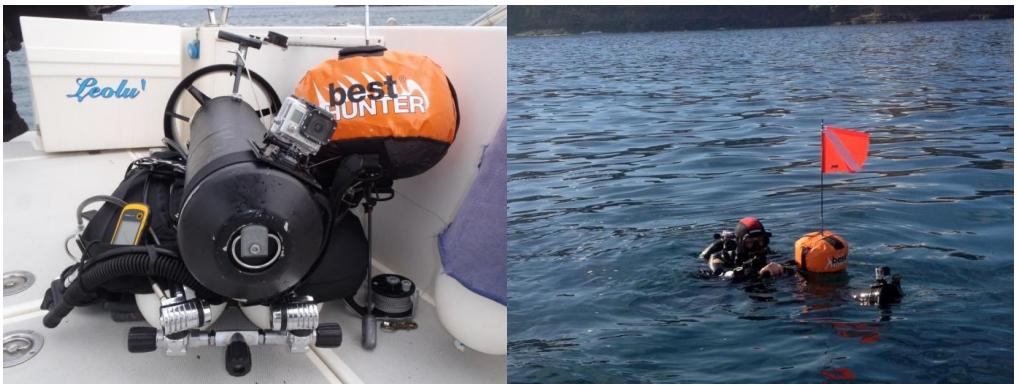

Figure 4.4 – Equipment used underwater field surveys.

Video analysis of geo-referenced transects integrated with bionomic cartography provided by Liguria Region (2009) allowed to outline a more accurate picture of habitat distribution (fig. 4.5).

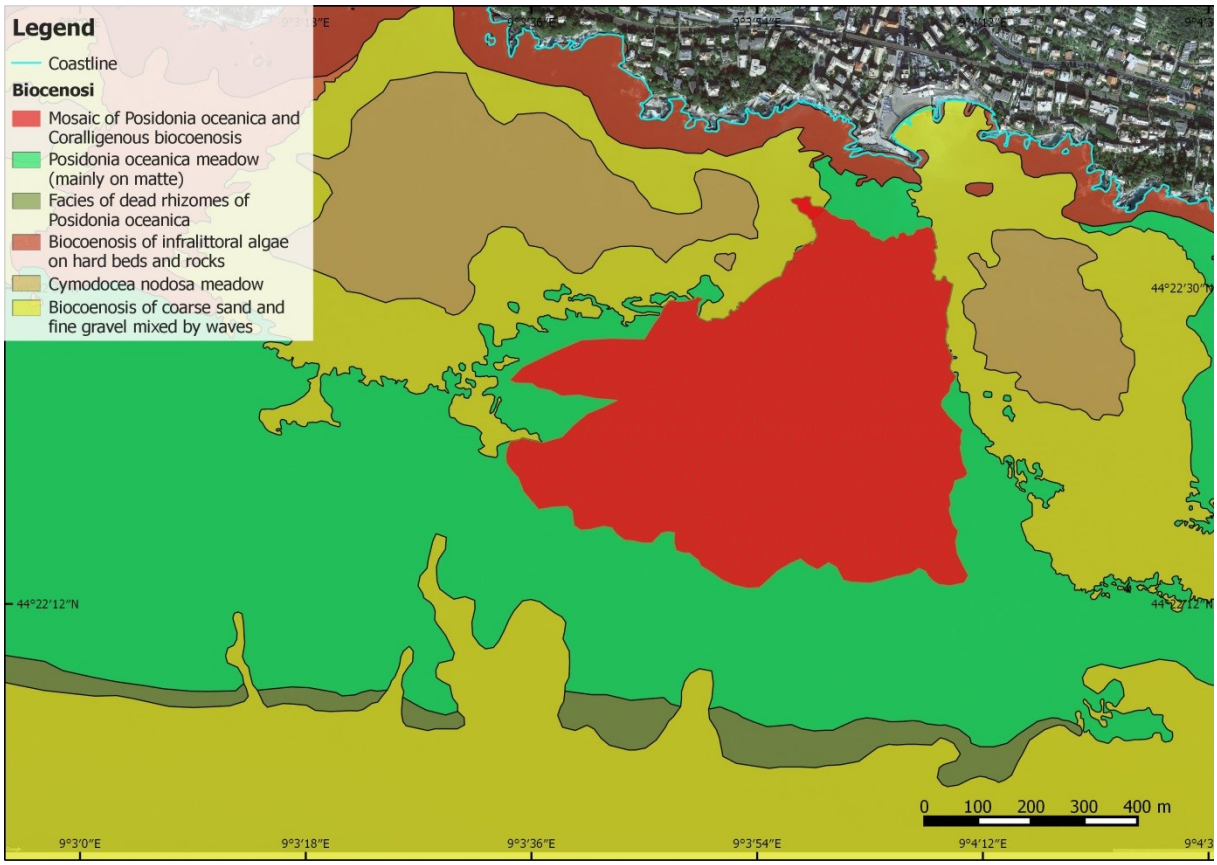

Figure 4.5 – Habitat distribution map of the seabed in the vicinity of Bogliasco.

Starting from the shoreline, the bottom slopes gently toward the sea with a succession of pebbles, sand and then *P. oceanica* meadow. Proceeding towards the open sea, coralligenous concretions take over the *P. oceanica* meadow, but not replacing it completely. Here the coralligenous encloses numerous patches of meadow which, though thinned out, remain present above and at the edge of the sandy basins between the concretions. The coralligenous outcrops, with a clear predominance of algae, have irregular shape with small vertical walls but rich in niches, crevices and ledges. The average height of the blocks is approximately one meter, while the diameter ranges between one meter, for the smallest, to 5-6 meters of the largest formations. As shown in the above habitat distribution map, the site host four main infralittoral benthic marine habitat types (elaborated from the RAC/SPA biotopes nomenclature, Bellan-Santini et al. 2002): *Posidonia oceanica* meadow; Biocenosis of infralittoral algae on hard beds and rocks; Biocenosis of coarse sand and fine gravel mixed by the waves; Coralligenous biocenosis.

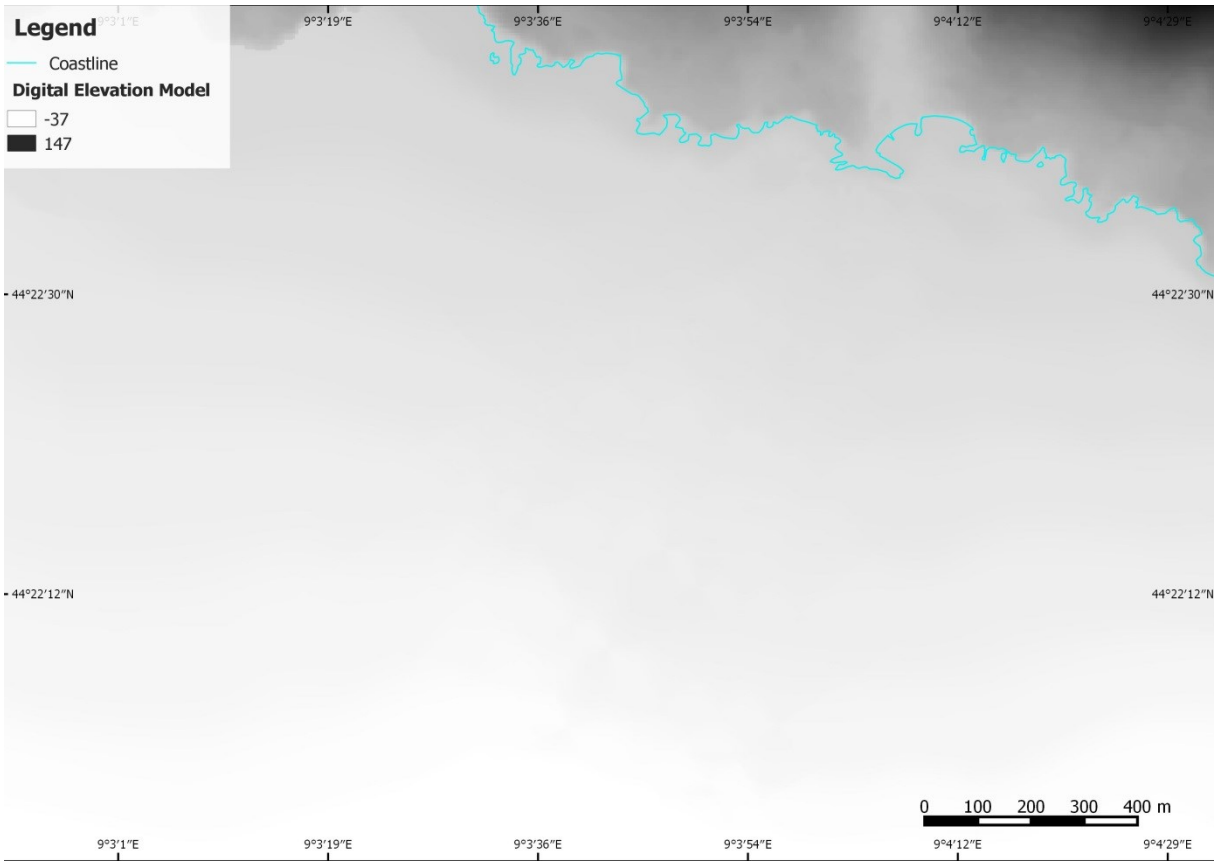

Figure 4.6 – Digital Elevation Model of Bogliasco study area: emerged and submerged territory.

In addition, bathymetric surveys were carried out on May 2015 by using BF Lowrence LMS525 single-beam echo sounder with double sonar frequency (50/200 kHz). After correction and cleaning, the collected data were integrated with bathymetric data already available provided by Liguria Region and interpolated through kriging interpolation method by using the mapping software Surfer 9. Once the DEM of the submerged part has been created, the DEM of the corresponding emerged part provided by Liguria Region has been merged with mosaic tool available in QGis Wien 2.8.2 in order to obtain a whole DEM of the area of interest with 5 m of resolution (fig. 4.6).

4.1.2 Porto Cesareo – Lecce coastal tract

Porto Cesareo represents the mildly sloping seafloor and it's is located within the homonymous Marine Protected Area. Here it was possible to find very detailed and recently updated mapping

(fig. 4.7). Bionomic cartography, the multi-beam bathymetric surveys and LIDAR surveys for the emerged coast were kindly provided by the Marine Protected Area of Porto Cesareo.

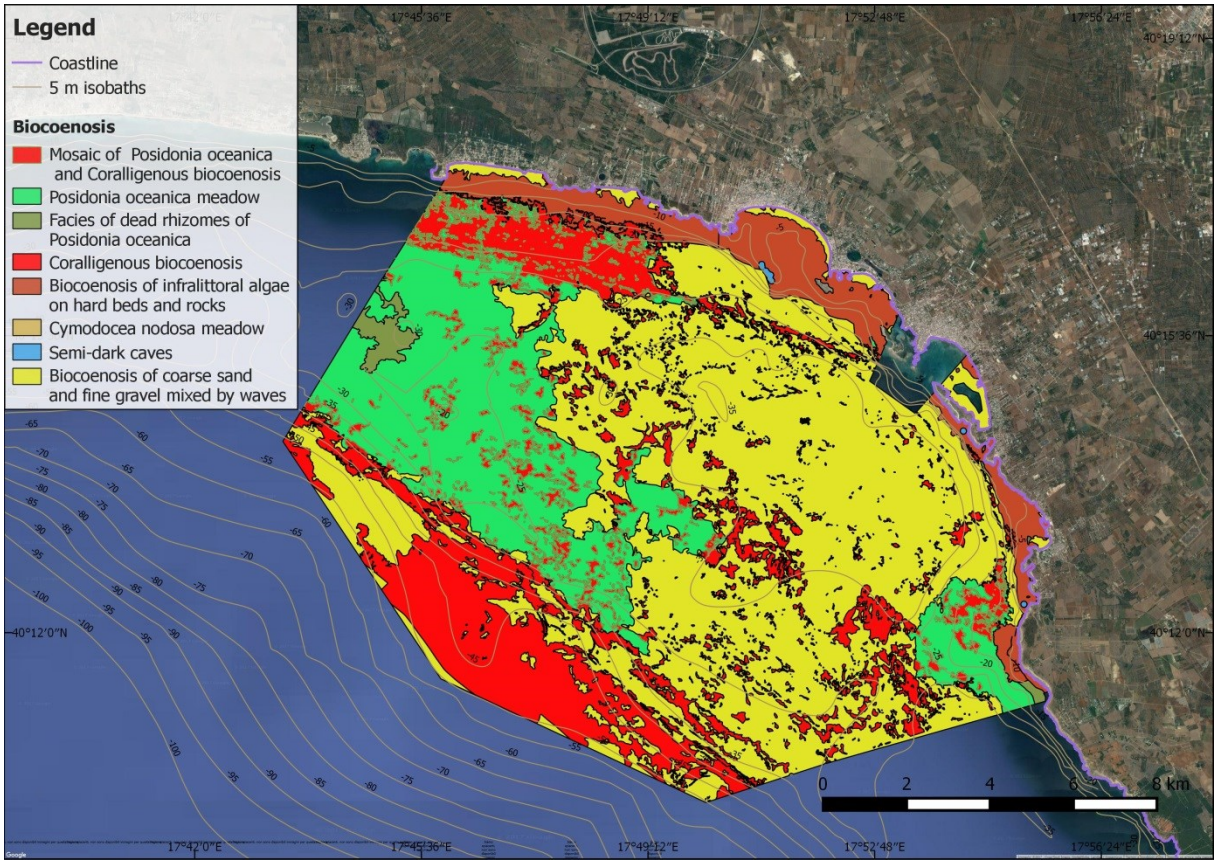

Figure 4.7 – Habitat distribution map of the seabed in front of Porto Cesareo.

The seabed of Porto Cesareo appears as a mosaic of different habitats with a predominance of *P. oceanica* mixed with coralligenous concretions, coralligenous bank type and biocenosis of coarse sand and fine gravel under the influence of bottom currents. Starting from the shore, a narrow zone consisting of coarse sand is soon replaced by the rocky bottom with photophilic infralittoral algae. From 5 meters depth the first concretions (*pre*-coralligenous) appear and, between 12 and 15 meters depth coralligenous "bank" type is fledged developed. In the south-western sector it seems similar to rocky pillows interspersed with sandy patches, while in the eastern sector coralligenous forms a mosaic with *P. oceanica* meadows. So, proceeding off the open sea, between 30 and 45 meters depth, the deepest concretions are observed. These are replaced by coarse sand at greater depths. Also in this case the site hosts four main infralittoral benthic marine habitat types: *Posidonia*

oceanica meadow; biocenosis of infralittoral algae on hard beds and rocks; biocenosis of coarse sand and fine gravel mixed by the waves; coralligenous biocenosis.

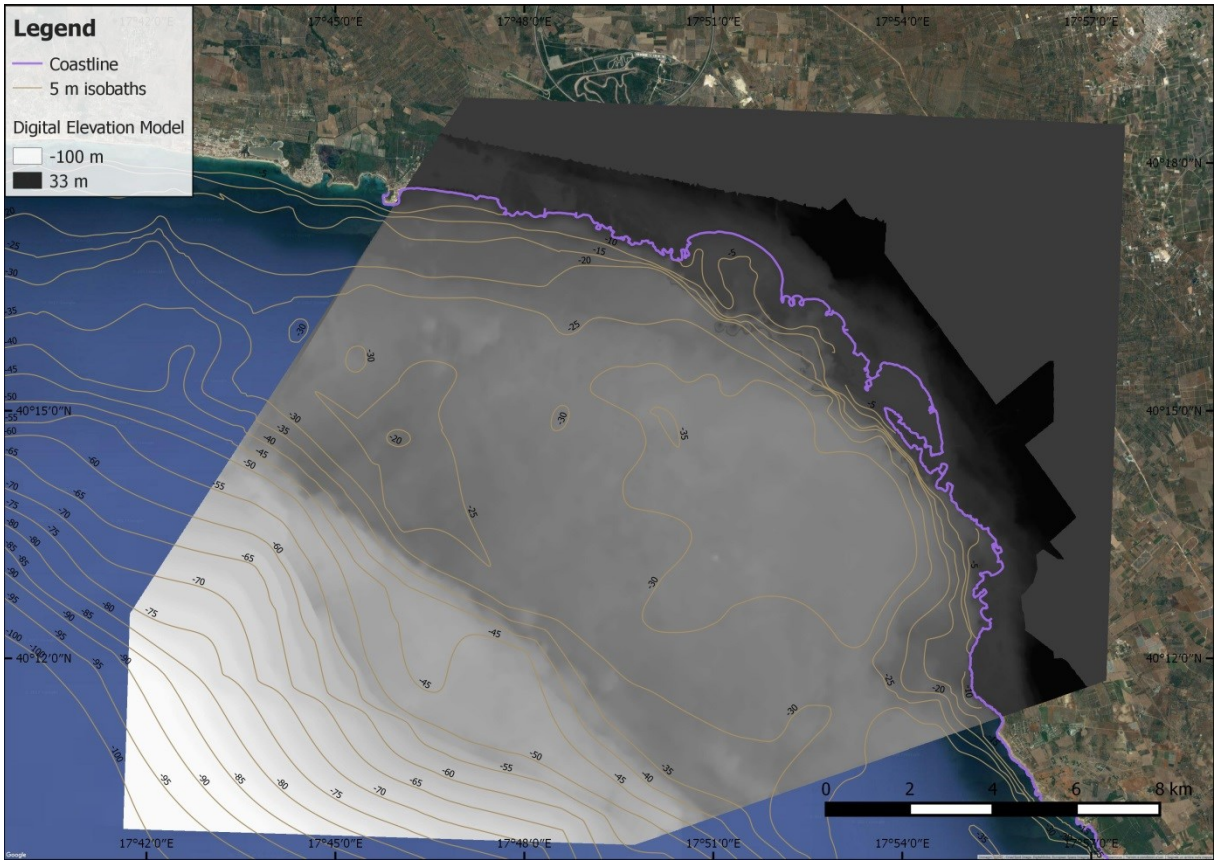

Figure 4.8 – Digital Elevation Model of Porto Cesareo study area obtained by processing and merging multi-beam and LIDAR data.

Multi-beam bathymetric data and LIDAR elevation data were processed and merged into a whole 5m resolution DEM using mosaic tool available QGis Wien 2.8.2 (figure 4.8 above).

4.2 Wave regime and marine climate

Several methods for reconstruction of the marine weather climate and sea storms through both indirect methods (from wind data) and direct methods (from measurements of wave parameters) have been described in the past years. In both cases, long time series of data are needed to give reliability to statistical procedures necessary for the reconstruction of the average wave climate and to forecast extreme events.

The data used for the characterization of the marine weather climate through direct methods were, until a few years ago, quite rare, so that often a reliable time series could not be reconstructed. For nearly two decades, a wave measurement network (National Wave Measurement Network) managed by ISPRA (Istituto Superiore per la Protezione e la Ricerca Ambientale) is operating on the Italian coasts. The buoy data, although not able to characterize the entire Italian coast (for both the shortness of the observation period and for the lacking of geographic coverage), allow interesting analysis of the sea storm reconstruction methods currently in use.

The definition of the wave climate in an area has substantially two objectives; the reconstruction of the mean sea weather climate offshore and the determination of the probability of occurrence of extreme waves. This paper takes into account the latter category being the most dangerous not only for coastal erosion but also for structures, artifacts and safety of coastal population.

In our research we used data provided by Dipartimento di Ingegneria Civile, Chimica e Ambientale (DICCA) of the University of Genoa. The MeteOcean group at DICCA has performed a re-analysis of atmospheric and wave conditions, producing a hindcast database spanning from January 1979 till the end of December 2015 over the domain employed for the atmospheric and wave condition simulations. Meteorological re-analyses have been developed employing NCEP (National Centers for Environmental Prediction) Climate Forecast System Reanalysis CFSR for the period from January 1979 to December 2010 and CFSv2 for the period January 2011 to December 2015.

Wave climate at two locations has been studied by interpolating data obtained from 3rd-generation wave generation model Wavewatch III (Komen et al., 1994; Tolman, 2009) implemented by DICCA. In detail, data were extracted from the re-analysis MeteOcean 1979-2015 database (www.dicca.unige.it/meteocean/hindcast.html).

Results from a specific analysis of significant swell in recent years have been processed for the two considered areas.

4.2.1 Ligurian Sea and Bogliasco area

The Ligurian Sea is enclosed in a coastal arch that, from a geological point of view, can be divided into two parts: the western part of the arch, NE-SW oriented, called “Riviera di Ponente”, and the eastern part called “Riviera di Levante”. When the wind blows from southwest, it originates heavy storms that strike mainly on the Riviera di Levante and on northern coasts of the Tuscany, from Genoa to the Cinque Terre and Versilia. This is the situation that occurs in the case of transit of an Atlantic cyclone: during the passage of the front, winds take on a southwestern component which, with the formation of a low-pressure zone over the Gulf of Genoa, can generate gusts over 100 km/h.

With regard to Riviera di Ponente, given the topography of the coast, the heaviest storms are originated by a continuous and strong sirocco.

The biggest storm in the last 30 years dates back to 30th October 2008 and had its epicenter between Voltri and Camogli towns (Genoa Province). Waves up to eight meters (fig. 4.9) have literally “devoured” the ridge of rocks destroying the seaside and maritime structures. In Bogliasco, the fury of the sea has raised and cracked the concrete structure and boulders of the breakwater with serious damage to the entire coastline.

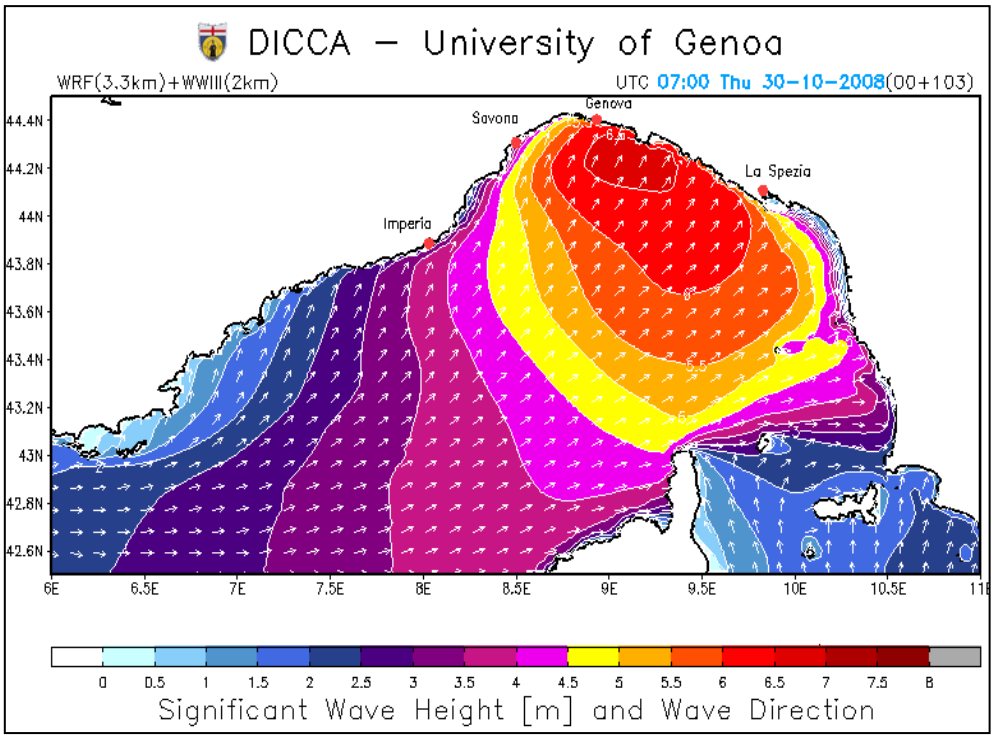

Figure 4.9 – Significant wave height and wave direction in the Tyrrhenian Sea during the sea storm on 30th October 2008.

Data obtained from the database of re-analysis, once interpolated and plotted, show that the wave climate of Bogliasco area is characterized by an almost unimodal regime with clear dominance of sea states from SW (between 200° and 240°N) which, during strong storms, may experience wave height over 5 meters (fig. 4.10). Below we report the results of our study on the marine weather climate in Bogliasco area (fig. 4.10 and 4.11). The dominant direction of the wave motion and the probability of occurrence of different wave heights and periods are clear.

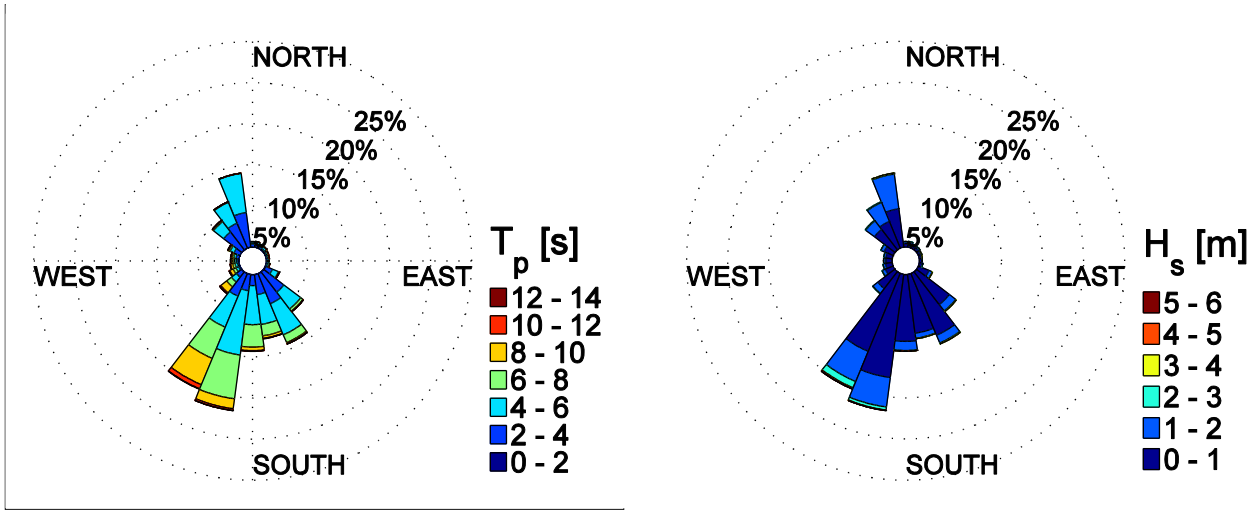

Figure 4.10 – Polar diagrams showing the wave climate in the area of Bogliasco: wave periods T_p (left) and wave heights H_s (right).

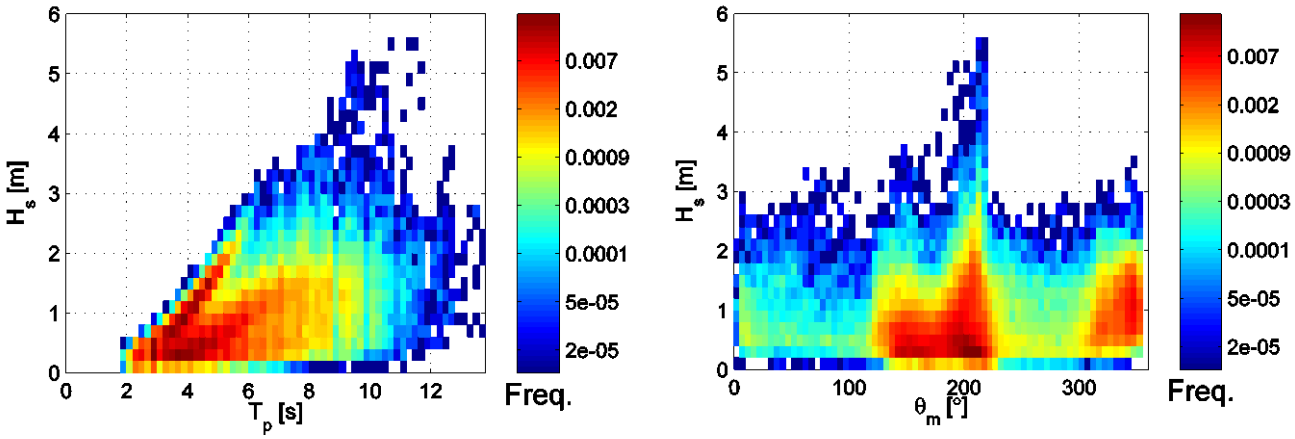

Figure 4.11 – Wave height (H_s) frequency as a function of the wave period (Tp) on the left and as a function of the direction (θ) on the right in the area of Bogliasco.

4.2.2 Ionian Sea and Porto Cesareo area

Regarding the Ionian Sea, the reference buoy is located in front of Taranto, about 60 km from the town of Porto Cesareo, and it has been installed since 2006 off San Vito Cape at a depth of 72 meters. The geographic sector, where the longest fetch lengths are observed, is rather limited. This sector is delimited by Calabria Region in the south, Basilicata in the west, Salento peninsula in the east and Africa's coasts in the south-southeast. The main sector is between 130° and 175°N, with fetch lengths extended up to 1400 km, while the secondary sector is between 180° and 260°N, with very limited fetch length.

In the specific case of Porto Cesareo, by analyzing data, we can see as the maximum frequency is recorded for sea states from S-SE with significant wave heights up to 4-5 meters. In particular, the biggest waves are from 150°N with heights over 5 m and periods over 11 seconds (fig. 4.12 and 4.13). The probability of occurrence, however, is very low and it was not possible to obtain data relating exceptional sea storms for this area.

Below we report the results of our study on the marine weather climate in Porto Cesareo area.

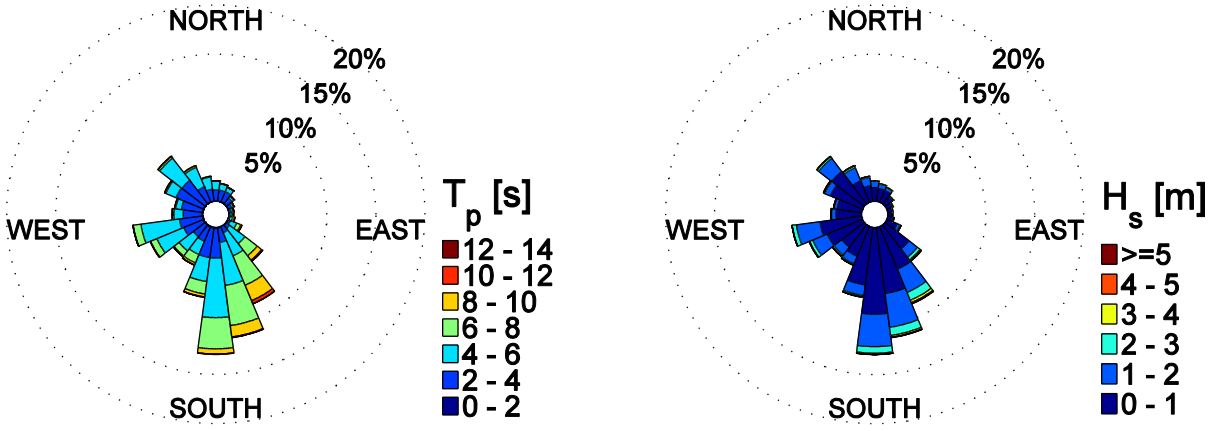

Figure 4.12 – Polar diagrams showing the wave climate in the area of Porto Cesareo: wave periods T_p (left) and wave heights H_s (right).

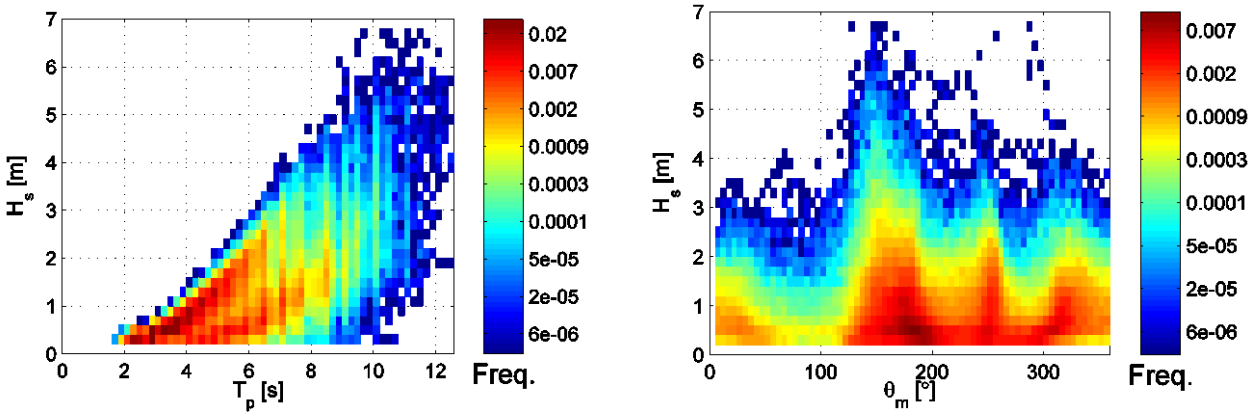

Figure 4.13 – Wave height (H_s) frequency as a function of the wave period (Tp) on the left and as a function of the direction (θ) on the right in the area of Porto Cesareo.

4.3 Estimation of seabed physical roughness

In marine environments, habitat complexity is closely related to species diversity and abundance (Gratwicke & Speight 2005; Hauser et al. 2006). Especially in the coastal zone the seabed may be characterized by many elements able to increase the surface heterogeneity such as boulders and other abiotic features, artificial structures and sessile living organisms. With increasing of seabed heterogeneity, the interaction between environment and the inhabiting organisms increases as well (Crowder et al. 1982; Eriksson et al. 2006). Effectively the high complexity of seafloor entails a great availability of ecological niches for living organisms that are able to further increase the

surface complexity, thus supporting more diversity, abundance and species richness (Graham & Nash 2013, Zeppilli et al., 2016). Concurrently seascape complexity may also have influence on abiotic factors characterizing the underwater environment such as sediment transport, wave energy dissipation, flow resistance, light irradiance (Massel & Brinkman 2001; Neumeier & Ciavola 2004; Hendriks et al. 2008). Consequently, the presence of high roughness elements in coastal areas and in relatively shallow waters can have important effect even on the hydrodynamics and sedimentary process (erosive and/or depositional process).

The accurate definition of the complexity and the quantification of structural metrics are crucial to fully understand both the relationships between environment and biota, and the effects of different structures (natural or artificial) on wave propagation, currents and sedimentological aspects in coastal zone.

There is a close relationship between the concepts of both roughness and complexity, so that surface roughness is widely used as a measure of seascape (and/or terrain) structural complexity.

Today, the measurements of roughness are obtained through a wide range of different surveys techniques and there are many ways to calculate the rugosity with different outcomes and at different spatial scales depending on the field to which the concept is applied. Traditionally, roughness is estimated as the ratio between the length of the contoured surface profile and the linear distance between the end points (chain-tape method, Risk 1972) or as the ratio between the area of the contoured surface and its orthogonal projection onto a plane (Area Based Rugosity Index). In the last decades, several methods and complex techniques have been developed in order to quantify the topographic surface parameters in the field (Carleton & Sammarco 1987; Mc Cormick 2004). These techniques often fail to capture roughness at different spatial scale and resolution because of the limitations imposed by data collection methods and their sampling rate (Friedman et al. 2012). Recent advances in technology are enabling the development of methods more accurate, precise and versatile and are making accessible to the general public equipment before expensive and unwieldy. Furthermore, the improved performance of increasingly powerful computers led to significant

progress in the fields of computer vision, 3D modelling and photogrammetry, allowing to gather, manage and process large amount of data and reducing time- and resources-consumption. The measurement of the physical properties of surfaces in three-dimensional environment is fundamental prerogative for an accurate definition of topographic features. Among the applied techniques for extracting 3D data, photogrammetry is probably the one with greatest benefits in terms of versatility, cost and performance. Moreover, photogrammetry allows the reconstruction of objects and the determination of their characteristics without requiring any physical contact with surrounding environment, so that it can be considered non-destructive and non-invasive methodology.

Several authors highlighted the capabilities of photogrammetric techniques especially in underwater environment where traditional techniques are useless or time/cost-consuming and showed how accurate and reliable results can be achieved through using relatively low-cost equipment (Skarlatos et al., 2012; Drap et al. 2013; Gintert et al., 2012; Schmidt & Rzhanov, 2012; He et al., 2012; Lavy et al., 2015; Friedman et al., 2012).

In this section we describe the methodology used for generating three-dimensional high-resolution models of the seafloor throughout Structure from Motion (SfM) technique. Information included in the generated DEMs can be extracted in different format (.tiff, .xyz, .txt or .asci) and processed with statistical and geospatial software tools for quantifying benthic coverage and rugosity characteristics of different benthic habitats and hard elements of the seabed.

We evaluated an alternative approach to traditional techniques through which obtain a measure of surface roughness useful for different purposes (biological, ecological and engineering) able to summarize characteristics of hard-bottom submerged habitats from 3D seascape models obtained by using photogrammetry and computer graphic techniques. Several measures of roughness were compared for testing their effectiveness in discriminating different habitats. More specifically, we tested the ability of four amplitude parameters of physical roughness to differentiate the coastal habitats in the two study sites exposed at different levels of anthropic pressure: biocenosis of infralittoral algae on hard beds and rocks (IA), biocenosis of coarse sand and fine gravel mixed by

waves (SB), coralligenous biocenosis banks-type (CA). In addition, two Area Based Rugosity Indexes were also calculated and compared with amplitude parameters.

On the basis of our results, we selected the amplitude parameters that better describe the complexity of considered habitats. We underlined that roughness statistical parameters as measure of absolute roughness is not merely a habitat complexity measure, but also allows the accurate evaluation of the spatial properties of the seabed making these results exploitable for several fields of application (geology, engineering, ecology, coastal zone management). We further highlighted as amplitude parameters, being in metric system, can be easily employed for several purposes. Finally, we describe the relationship between physical and hydraulic roughness in order to allow integration of bottom roughness measure also into wave's dissipation models.

4.3.1 Sampling strategies and data collection

Field surveys were carried out at two locations. As already said above, both sites host 4 main infralittoral benthic marine habitat types, according to the RAC/SPA (Regional Activity Centre for Specially Protected Areas) biotopes nomenclature (Bellan-Santini et al., 2002 and 2007): 1) Posidonia oceanica meadow (PO); 2) Biocenosis of infralittoral algae on hard beds and rocks (IA); 3) Biocenosis of coarse sand and fine gravel mixed by the waves (SB); 4) Coralligenous biocenosis (CA). In particular IA and CA exhibit substantial differences within the two locations. While in Bogliasco we did not observe obvious signs of impact on these habitats, the CA and the IA in Porto Cesareo during the past years have long been subject to mechanical impacts due to trawling and fishing of date mussels, and only recently, after the establishment of Marine Protected Area, these habitats show signals of recovery.

For each of these habitats, except for Posidonia oceanica meadow, 3D reconstructions have been realized by means of photogrammetric techniques. Survey locations were chosen randomly within each habitat type. Two scientific divers deployed a measure tape in order to define a quadrat around

the area of interest. This quadrat complies with the slope of the surveyed seabed section. Steel tags were used as Ground Control Points (GCPs). GCPs were placed along the tape at known distance. An additional 50 × 50 cm square plastic frame equipped with 8 markers was placed in a corner of the tape quadrat in order to validate model's accuracy and evaluate the error of the measurement. Then the tape was removed. A GoPro HERO3+ Black Edition, high definition sport camera with 12MP HD CMOS sensor, equipped by RGBlue BM3100G underwater lighting systems (100° irradiation angle, 5000K color temperature, LED 2400 lumen) has been used for imagery acquisition (fig. 4.14).

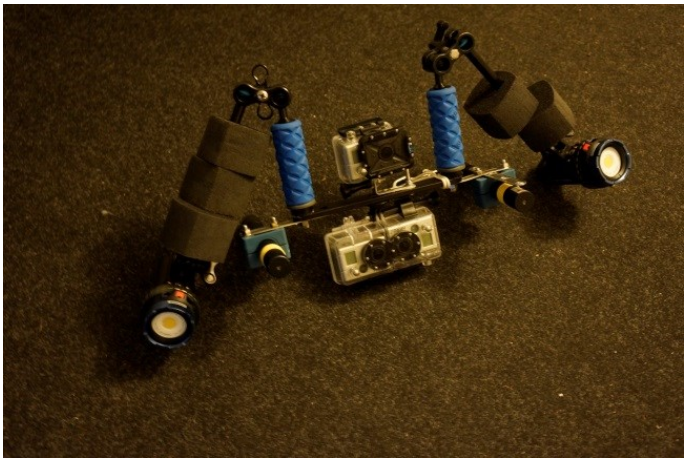

Figure 4.14 – Equipment used for capturing images.

Several research works demonstrate that GoPRO camera was able to capture scenes at good resolution and with little effort (Rende et al. 2015, Teo 2015, Kim et al. 2014, Gintert et al. 2012, Schmidt and Rzhanov 2012.). The bright fixed-focus all-glass lens with reduced distortion and with maximum aperture of f/2.8 allows acquiring sharp and stable images even in low-light condition thanks also to the excellent image stabilization. Field of view (FOV) was set as medium (ca 95° in water) in order to further reduce radial distortion of acquired images. This FOV allows to obtain picture at 7MP resolution. In addition, a calibration chessboard was used before the survey in order to extract camera calibration parameters and correct the distortion due to the lens.

Photo samples of seabed hosting different habitats were collected at different depth depending from their natural distribution range (fig. 4.15 and 4.16): between 14 m and 17 m of depth for CA, between 2 m and 7 m depth for IA, between 2 m and 6 m depth for SB.

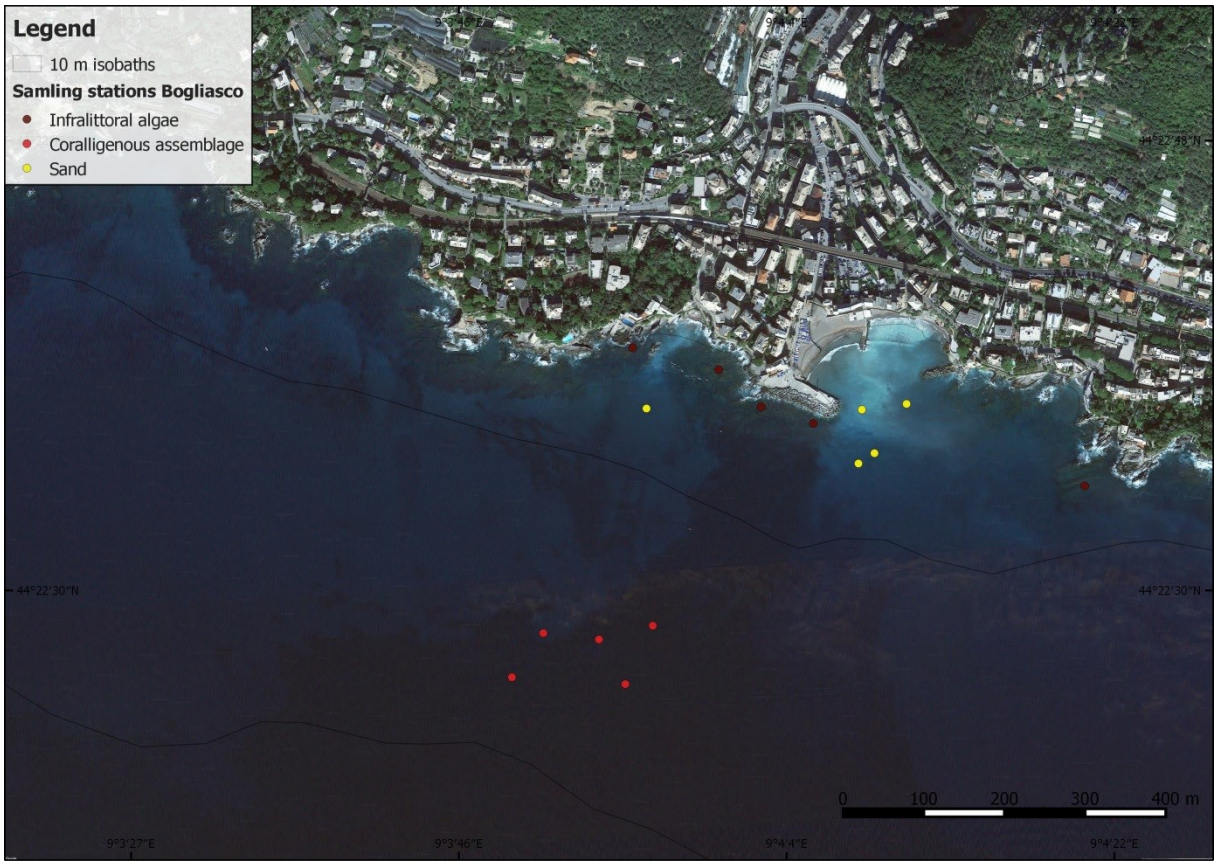

Figure 4.15 – Sampling stations in Bogliasco.

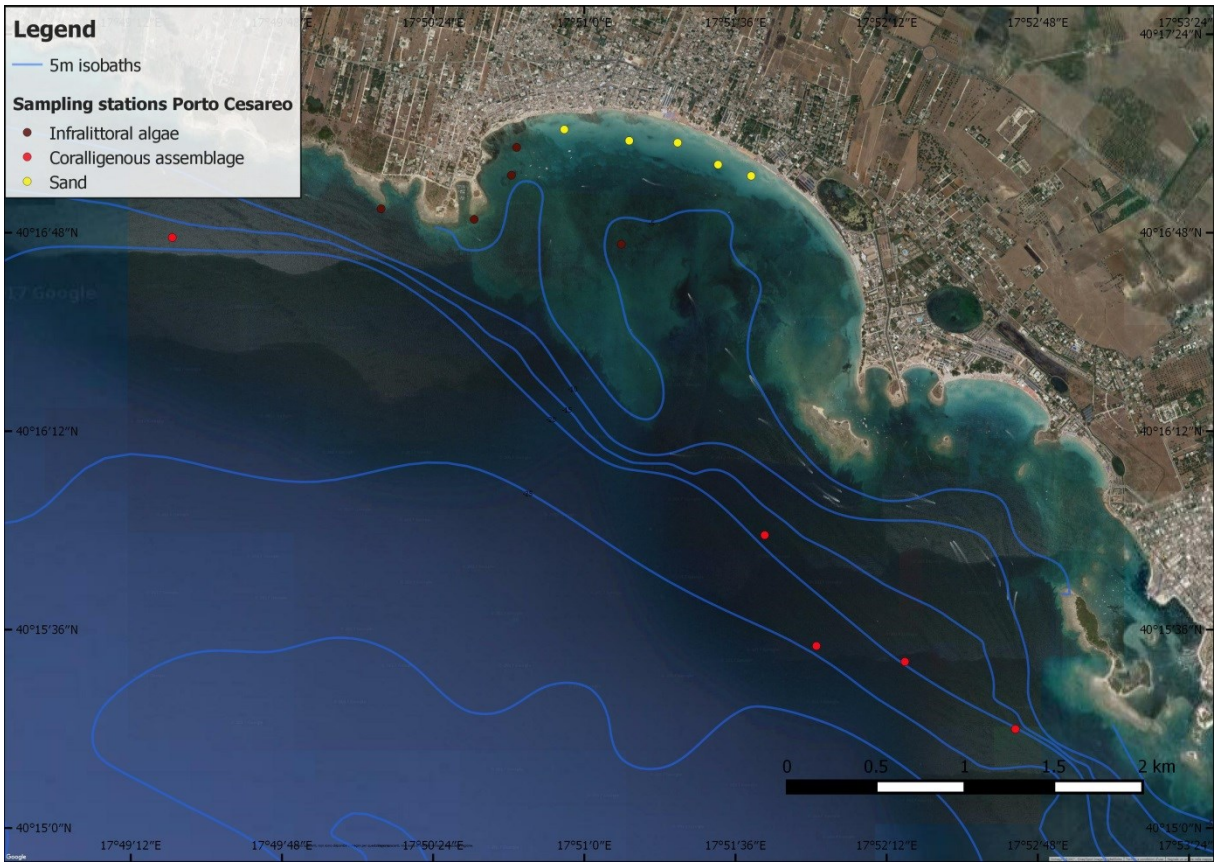

Figure 4.16 – Sampling stations in Porto Cesareo.

The procedure for 3D model generation consists of different phases: 1) camera calibration; 2) image acquisition of surveyed area; 3) 3D model reconstruction; 4) reference the model; 5) export results. Camera calibration is a necessary preliminary step before using camera data (Clarke & Fryer 1998). This process aims to determine intrinsic (internal camera geometric and optical characteristics) and extrinsic (position and orientation of the camera) parameters of the camera. To date many software are able to perform calibration process automatically and directly using the EXIF file (EXchangeable Image file Format) of the images. However, differences exist between underwater and air vision. The changes of media (air-water) entail refraction effect, so that the light ray changes direction leading to a geometrical distortion. Calibration in the field can substantially improve model accuracy. This operation should be carried out at investigated locations by placing and taking pictures of a chessboard of known dimension. Importing the taken photos in any calibration software, the selected camera calibration parameters and distortion coefficients (horizontal and tangential) are defined. The obtained parameters are then imported into the image processing software employed for 3D model reconstruction. We finalized camera calibration process through Agisoft Lens, an automatic lens calibration software capable to estimate the focal length (fx, fy), principal point coordinates (cx, cy) and radial distortion coefficient (K1, K2, K3, P1, P2) using Brown's distortion model.

Once the images useful for camera calibration have been gathered, pictures of the investigated area were acquired every 0.5 seconds (at 0.5 Hz) by swimming with constant speed at approximatively 1-meter distance from the bottom covering the entire area of investigation. The chosen acquisition time-lapse leads to collect images with high overlap, allowing a total coverage of the surfaces and, in addition, the identification of large number of keypoints useful for both photo-alignment process and determination of camera position and orientation.

Field procedure require about 10 minutes for each site allowing to make more than one measurement (variable number) during a single dive depending on the operational depth and the extent of the investigated area.

4.3.2 Three-dimensional model generation

The generation of 3D model was carried out using Agisoft PhotoScan (available from Agisoft LLC., St. Petersburg, Russia) modeling software. It operates with arbitrary images and it is effective both in controlled and uncontrolled conditions (Agisoft, 2014). Also it has an affordable cost and allows us to obtain excellent results through a simple workflow. In addition, it allows exporting multiple file formats compatible with a wide range of software for subsequent analysis. However to date there are several free/open-source software that allow to obtain similar results as mentioned before.

Agisoft Photoscan 3D reconstruction general workflow consists of four main steps: (1) photo alignment, (2) building dense point cloud, (3) building mesh and (4) generating texture.

During photo alignment the software automatically identifies keypoints which overlap in the pictures in order to determine camera position and orientation for each photo. Alignment having been completed, a sparse point cloud model is built and displayed. If any, incorrectly positioned photo can be removed and realigned setting markers over the pictures (at least 4 per photos).

Dense point cloud model is generated calculating depth information for each camera on the basis of the estimated camera positions. Dense point cloud can be edited and exported in several format for further analysis. Dense point cloud can be used to build 3D polygon mesh representing the object' surface and generate the texture.

Afterwards GCPs are used in order to both reference and scale the models in local coordinate system. This procedure allows us to measure area and volume of the scenes, assign the right orientation to the models and export DEMs in different formats (GeoTIFF elevation data, Arc/Info ASCII Grid, Band interleaved file format, XYZ file format and Sputnik KMZ) usable by other software for further analysis. GCPs are placed manually as markers in the corresponding locations of the scene and the x, y, z values are assigned to each GCP. Agisoft Photoscan automatically estimates the referencing total error and the error associated to each GCP.

Once referenced, the model has been edited to remove section of the seabed covered with Posidonia oceanica and other moving or floating objects and exported as DEM in both GeoTIFF elevation data (*.tiff) and XYZ file (*.xyz) formats (fig. 4.17).

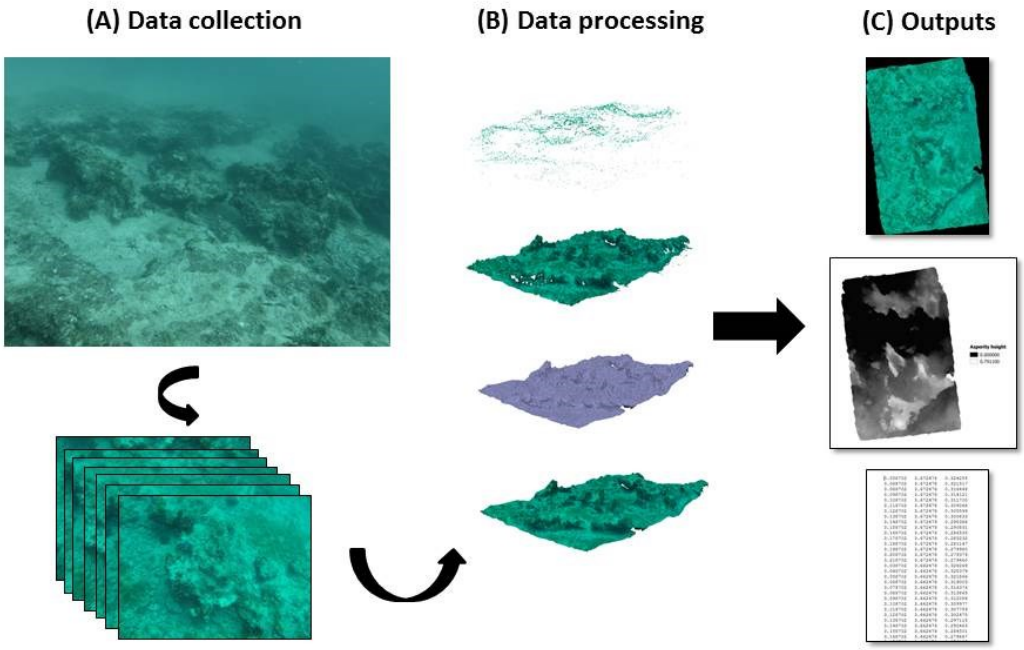

Figure 4.17 - Workflow from data collection to exporting results. A) Field survey and data/imagery collection. B) Processing procedure from sparse point cloud generation (top-center) to textured model (bottom-center). C) Exporting results and data mining in different formats: 3D models and ortho-mosaics (top-right); DEM (center-right); numerical data (bottom-right).

4.3.3 Benthic coverage and taxa abundance

In order to estimate the percentage cover of benthic organisms and abiotic elements of the seabed, 2D ortho-photo images of the DEMs were exported in GeoTiff format by means of Agisoft Photoscan and then imported in photoQuad, an open source software for image processing of 2D photographic samples developed by the Department of Marine Sciences of the University of the Aegean (Trygonis & Sini, 2012). This software allowed us to draw an outline around the specific image features such as species, substrates or categories, and successively quantify the percentage coverage of the different features (fig. 4.18).

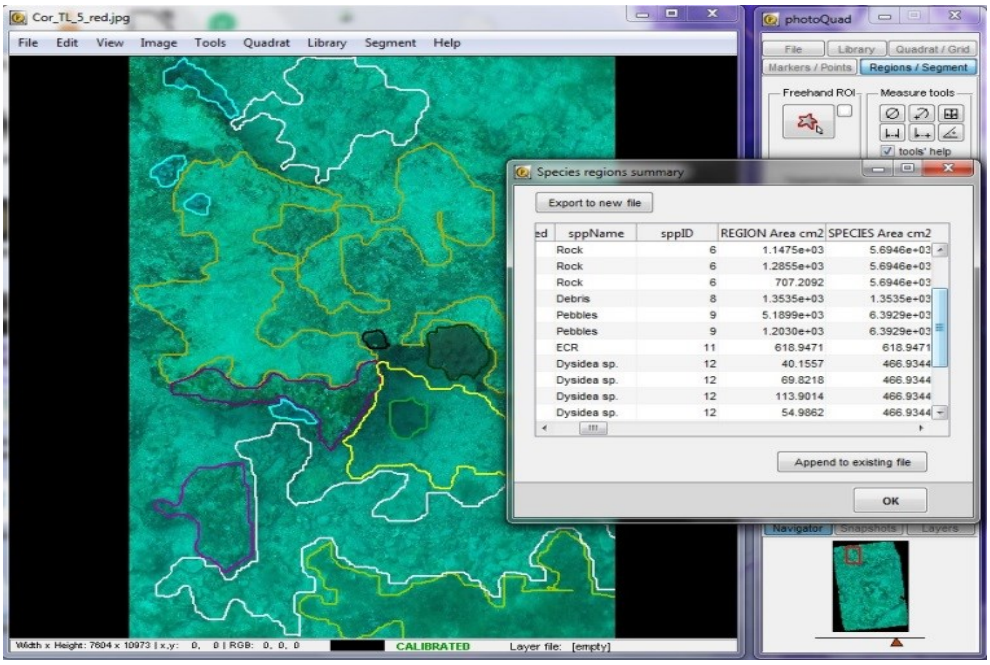

Figure 4.18 - An example of PhotoQuad's screenshot which shows the species regions outlined by different colors and the summary database.

All benthic living organisms were identified to the lowest possible taxonomic level and the associated substrates were included into the coverage estimation process. The coverage data were then used in comparison of the measures of roughness to examine the relationship between the complexity of the seabed and the richness in species of the different sites.

4.3.4 Seabed roughness estimation

Digital elevation models of the surveyed seabed can be processed for quantifying spatial properties of the modeled surfaces. DEMs resulting from the procedure above described allow us to easily obtain less than 0.5 cm cell size models. Spatial resolution and the level of detail should be set to values appropriately chosen for the purpose of the research. Nevertheless, a finer spatial resolution may be required in studies in which the characteristics of individual organism living in the habitat are investigated (sessile species growth rate assessment, damage assessment, morphometric, etc.).

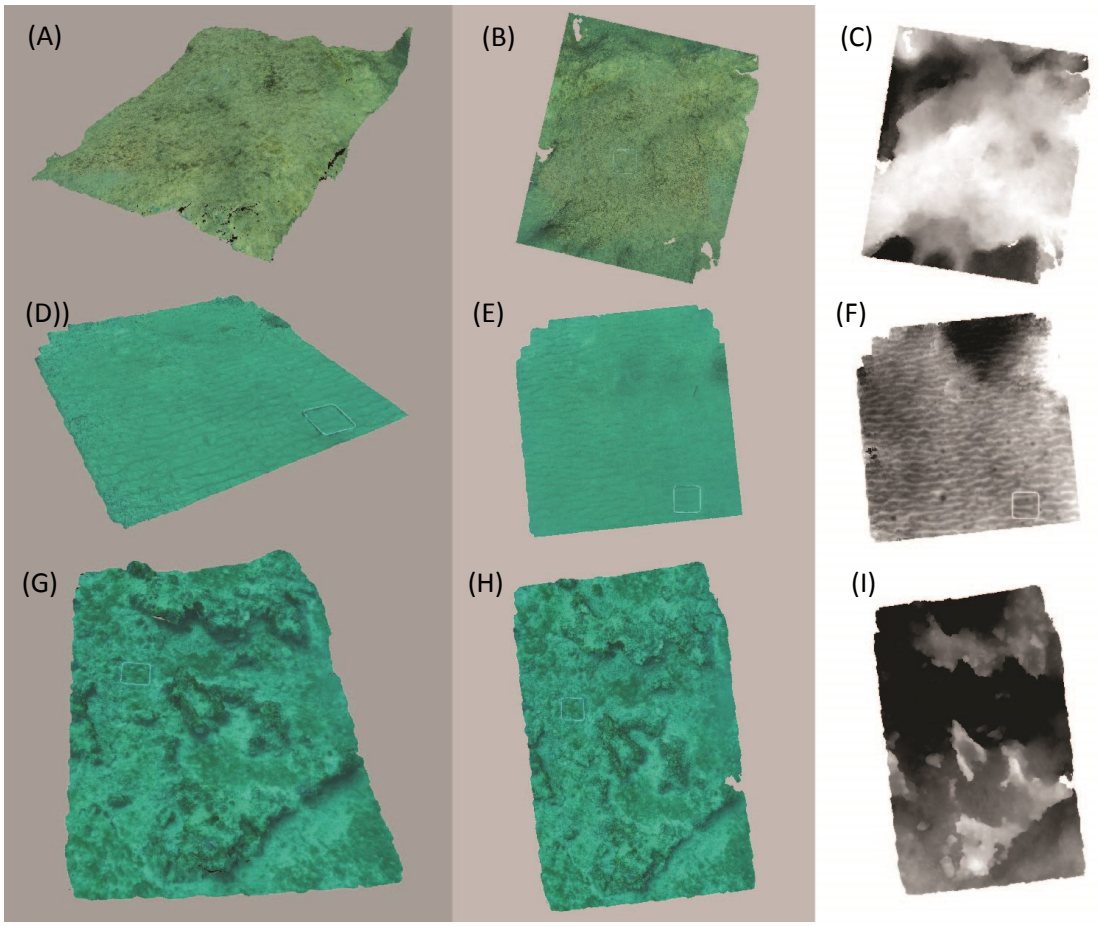

Figure 4.19 - Example of the main final outcomes used for roughness estimation. A, B and C represent respectively texturized mesh, ortomosaic and DEM of a seabed section hosting *IA;* D, E and F represent respectively texturized mesh, ortomosaic and DEM of a seabed section hosting *SB;* G, H and I represent respectively texturized mesh, ortomosaic and DEM of a seabed section hosting *CA.*

All 3D models have been exported as DEMs in both formats GeoTiff (*.tiff) and XYZ (*.xyz) with 1 cm cell size resolution. Topographic characteristics and metrics were obtained using different ArcMap (ArcMap 10.1; Environmental System Research Institute, Inc., Redlands, California) tools for GeoTiff data and MATLAB (Matrix Laboratory, numerical computing environment and programming language) for xyz data. Processing details are specified below.

Ratio Area 3D/2D. 3D and 2D surface area have been computed importing exported DEMs into ArcMap ESRI (Environmental System Research Institute, Inc., Redlands, California) software by using 3D analyst > Surface Volume tool. Additionally, 3D surface area for each full resolution 3D model was estimated through Agisoft Photoscan "Measure Area and Volume" tool.

In order to decouple roughness from the slope, because the quadrat identified by GCPs complies with the slope and the distance between GCP is steady, Z-coordinate of GCPs has been imposed as

a fixed value/depth (=0) so that all GCPs lie on the same plane. The result is a horizontalisation of 3D model and exported DEM.

Two different "Area-based rugosity index" have been estimated: (1) 3D_DEM_AREA/2D_DEM_AREA (here called *Simplified_DSM*) where 3D_DEM_AREA is the surface area of exported DEM calculated with ArcMap 3D Analyst tool; (2) 3D_MODEL_AREA/2D_DEM_AREA (here called *Full_DSM*) where 3D MODEL AREA is the surface area of full resolution model built with Photoscan. 2D_DEM_AREA is estimated taking into account exclusively non-null cells of digital ortho-photo extracted from 3D model.

The ratios AREA_3D/AREA_2D have been calculated for each modelled surface. The two "Area-based rugosity indexes" were then compared.

Statistical surface absolute roughness measure. Rugosity profiles are waveforms and could be analyzed through similar methods used to analyze the electromagnetic radiation. Usually roughness statistical parameters are amplitude, wavelength, slope and other more complex as power spectra parameters, stochastic methods and fractal dimension methods (Tesfamariam, 2007). In our research we focused on amplitude parameters since those provide a measure of absolute roughness (*R*) of surfaces that can be used for several purposes.

In particular for each model we have calculated:

(1) the central-line average ($\boldsymbol{R_a}$) is the deviation of the asperity heights with respect to reference plane:

$$\boldsymbol{R_a = \frac{1}{A}\int_0^A |z|\, dA}$$

(2) $\boldsymbol{R_q}$ or Root Mean Square (*RMS*) is the square root of the arithmetic mean of the square of asperity heights (vertical deviation) from the mean plane (reference plane):

$$\boldsymbol{R_q = RMS = \left[\frac{1}{A}\int_0^A z^2\, dA\right]^{0.5}}$$

(3) $\boldsymbol{\mu(z)}$ is the mean value of Z:

$$\boldsymbol{\mu(z) = \frac{1}{A}\int_0^A z\, dA}$$

(4) *max(z)* or $\boldsymbol{K_{max}}$ is the difference between the highest peak and the lowest valley of the asperities and could be define as an extreme-value height descriptor (Anonymous 1975, 1985; Bharat 2000):

$$\boldsymbol{max(z) = R_{max} = max[z(x,y)] - min[z(x,y)]}$$

where *A* is the area of the reference plane, and *z*-values are the asperity heights determined relative to this plane.

DEMs were exported as *XYZ* file format and all datasets were processed into MATLAB® (available from The MathWorks, Inc.) environment as *m*X3 matrix where each column represents respectively x, *y* and *z* point coordinates. The number of rows *m* is variable and depends from the spatial extension of the considered surface.

In order to decouple the roughness measurement by the slope, we chose the reference plane that minimizes the perpendicular distances between the points and the plane (best-fit plane with orthogonal distance regression). The best-fit plane to XYZ data has been found using Principal Component Analysis (PCA).

After combining X, Y and Z data into one array, the matrix is centered finding the column means and subtracting off these respectively to each column (*X, Y*, and *Z*). The planar regression is now accomplished by *Singular Value Decomposition* (*SVD*). *SVD* is a method (general matrix decomposition method) used to reduce an *n*-dimensional dataset into fewer dimension. For an *m-by-n* matrix XYZ with *m*>*n*, the SVD function of MATLAB® provides an *m-by-n* orthogonal matrix U, an *n-by-n* diagonal matrix S, and an *n-by-n* orthogonal matrix V so that XYZ=U*S*V', where V' is the complex conjugate of the transpose of V.

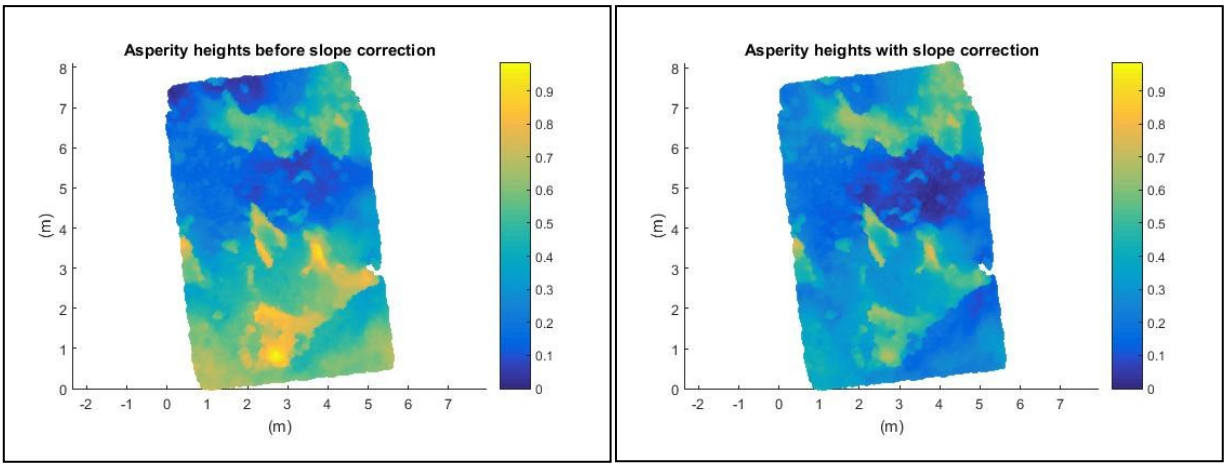

Figure 4.20 - Figures show how the slope can affect amplitude parameters. It seems evident that asperity heights after the rotation of XYZ- dataset (figure on the right) appear to be lower than those before slope correction (on the left). Not taking in consideration the slope, all amplitude parameters can be overestimated.

The coefficients for the first two principal components (first two columns of V) define vectors drawing the basis for the plane. The third principal component is orthogonal to the first two and its coefficients define the normal vector of the plane. So normal vector P of the best-fit plane is given by the third singular vector, thus the third column of V. The equation of the plane for any point lied on the plane is given by the dot product of the normal vector P with the difference of column means (cm) from our points that must be zero for the points onto the plane:

$$\boldsymbol{P} \cdot [(\boldsymbol{X}, \boldsymbol{Y}, \boldsymbol{Z}) - \boldsymbol{cm}] == \boldsymbol{0}$$

This means that any point *Z(mp)* on best-fit plane is given assuming the coefficient of Z is not zero:

$$\boldsymbol{Z_{mp}} = \frac{(\boldsymbol{P} \cdot \boldsymbol{cm}) - \boldsymbol{P(1)} \cdot \boldsymbol{X} - \boldsymbol{P(2)} \cdot \boldsymbol{Y}}{\boldsymbol{P(3)}}$$

where P(1), P(2) and P(3) are respectively the first, second and third component of the normal vector P.

Knowing the normal vector P of the best-fit plane, it is possible to rotate appropriately the original point cloud so that the new fitting plane is parallel to xy-plane (P_0=0, 0, 1). So the rotated XYZ-dataset was obtained using AxelRot function MatLab tool.

Now by removing the slope effect all amplitude roughness parameters can be easily calculated (fig. 4.20).

4.3.5 Statistical analysis

To examine the ability of roughness measures to discriminate among different habitats, statistical analysis were performed. Given the characteristics of the two locations, we considered Bogliasco as low- impacted location, while Porto Cesareo as altered location because of the historic human use of this area.

First of all, the differences among the structures of populations were analyzed by means of multivariate statistical technique. The percentage cover data were transformed using square root transformation to reduce the effect of most abundant species/categories and the resemblance between every pair of sampled surface was calculated using Bray-Curtis similarity coefficient. Principal Coordinates Analysis (PCoA) was then performed to represent the relationships between the populations of different sites and PERMANOVA (Anderson 2001a, Anderson 2001b, Anderson & Robinson, 2001) was used as statistical test to detect statistical significance among groups (benthic features).

Afterwards the multivariate correlation between benthic features (multivariate species abundance data) and different roughness measures was analyzed with DistLM (Distance-based Linear Model) in order to determine the measures that better represent the complexity of the surveyed surfaces. All statistical tests were performed by means of PRIMER v6 (Clarke & Gorley, 2006) software.

4.3.6 Relationship between physical and hydraulic roughness

Lowe and colleagues (2005) used the definition of $\boldsymbol{K_w}$ given by Nielsen (1992) in his friction formula. He elaborated this equation by performing empirical procedures using fixed beds where bottom roughness was measured. Nielsen found that $\boldsymbol{K_w = 2D}$, where $\boldsymbol{D}$ was the grain diameter. After having measured bottom roughness through profile gauge used by McCormick (1994), Lowe et al. (2005) characterized roughness at each survey location by the standard deviation $\boldsymbol{\sigma_r}$ of the asperity heights which is nothing else than the root mean square of roughness amplitude (among our

statistical measures $\boldsymbol{R_q = RMS}$). According to Nielsen's relationship and assuming as approximation $\boldsymbol{D \approx 2\,\sigma_r}$, hydraulic roughness becomes $\boldsymbol{K_w \approx 4\,\sigma_r}$, .($\boldsymbol{\approx 4\,R_q}$).

Then Lowe et al. (2005) compared $\boldsymbol{K_w}$ obtained from the wave friction estimates with $\boldsymbol{K_w}$ calculated from the in-situ measurements of bottom roughness and they found a great similarity between the average values of the two hydraulic roughness lengths, suggesting that it is reasonable to predict dissipation due to bottom friction by doing bottom roughness surveys.

4.4 Process-based numerical model

Once the roughness length has been estimated, we quantify the supply of protection services provided by the habitats on different slope seabed by modelling the evolution of waves' height and energy over the 1D bathymetric profiles from offshore toward the shoreline along straights transects. A simplified numerical model of wave propagation based on the formulation developed by Thornton and Guza (1983) has been implemented and integrated with the dissipation term due to bottom frictions.

We model the evolution of the wave field along the cross-shore profiles by solving the well-established equation of the conservation of wave energy already previously mentioned:

$$\frac{\partial(Ec_G \cos\theta)}{\partial x} = -\varepsilon_D = -(\varepsilon_B + \varepsilon_F)$$

Thus, in our model waves dissipate their energy via breaking ($\boldsymbol{\varepsilon_B}$) and via bottom friction ($\boldsymbol{\varepsilon_F}$).

Following the formulation of Thornton and Guza (1983) the dissipation term due to breaking phenomena is given by:

$$\varepsilon_B = \frac{3\sqrt{\pi}}{16}\rho g f B^3 \frac{H_{rms}}{h}\left(\frac{H_{rms}}{\gamma h}\right)^2 \left[1 - \frac{1}{\left(\left(\frac{H_{rms}}{\gamma h}\right)^2\right)^{\frac{5}{2}}}\right]$$

Where $\boldsymbol{\gamma}$ is a breaker index and controls the fraction of breaking waves ($\gamma = 0.50$); $\boldsymbol{B}$ is of order 1 and controls the level of energy dissipation during breaking.

The fraction of breaking or broken waves can be estimated using a full Rayleigh distribution.

Following the formulation of Kamphuis (1975) the dissipation term due to bottom friction is given by:

- Boundary layer turbulent:

$$\boldsymbol{\varepsilon_D = \frac{\rho f_w}{6\pi}\left[\frac{H}{2}\frac{\sigma}{\sinh(kh)}\right]^3}$$

- Boundary layer laminar:

$$\boldsymbol{\varepsilon_D = \rho\frac{\sqrt{\nu\sigma}}{2\sqrt{2}}\left[\frac{H}{2}\frac{\sigma}{\sinh(kh)}\right]^2}$$

Where $\boldsymbol{f_w}$ is evaluated solving

$$\boldsymbol{\frac{0.32}{f_w} = \left\{\log(6.36\, r\, f_w^{1/2}) - \log\left[1 - \exp\left(-0.0262\frac{R_e f_w^{1/2}}{r}\right)\right] + \frac{4.71\, r}{R_e f_w^{1/2}}\right\}^2 + 1.64}$$

Where

$$\boldsymbol{r = \frac{A}{k_w} = \frac{U_{1m}T}{2\pi k_s} = \frac{a}{\sinh(kh)}\frac{1}{k_w}}$$

Where $\boldsymbol{A}$ is the wave amplitude, $\boldsymbol{U_{1m}}$ is the first-order particle velocity at the bottom, and $\boldsymbol{k_w}$ is the bottom roughness.

$$\boldsymbol{R_e = \frac{U_{1m}A}{\nu} = \frac{{U_{1m}}^2 T}{2\nu\pi} = \frac{{U_{1m}}^2}{\nu\sigma} = \frac{a^2\sigma}{\sinh^2(kh)}\frac{1}{\nu}}$$

$\boldsymbol{R_e}$ is the Reynold number and it is a dimensionless quantity providing information on the fluid flow situation. Laminar flow occurs for $\boldsymbol{R_e < 5 * 10^4}$, while turbulent flow occurs for $\boldsymbol{R_e > 2 * 10^5}$.

Furthermore, the numerical model allows to activate and/or deactivate the contribution given by bottom friction to the dissipation, allowing to take it into account or not.

To run the model, the initial conditions of the wave in deep water (where the waves are not affected by the presence of the sea bottom) are required. So the input information needed for the use of the simulation model are the wave height $\boldsymbol{H_0}$, the wave period $\boldsymbol{T}$ and the wave angle relative to shore normal $\boldsymbol{\theta_0}$. In addition the bathymetric profile from the offshore section $\boldsymbol{x_0}$ to the breaking section $\boldsymbol{x_b}$, and the equivalent roughness value $\boldsymbol{K_w}$ associated with the seabed must be specified. Since for *P. oceanica* meadow it was not possible to directly derive the roughness measure through photogrammetric technique, we used K_w =0.4 m suggested by Infantes et al. (2012) corresponding to a meadow with a shoot density of 600 shoots/m^2 and mean shoot length of 0.8 m similar to our case studies.

To implement the simulations, the following initial conditions of two extreme events with similar frequency of occurrence within the 2 areas were chosen: 1) $\boldsymbol{H_0}$ = 3 m - $\boldsymbol{T}$ = 7.8 sec; 2) $\boldsymbol{H_0}$ = 5.8 m e $\boldsymbol{T}$ = 11.8 sec.

At Bogliasco, a clear predominance of the sea state coming between 200° and 240°N is outlined, while at Porto Cesareo between 130° and 175°N. In particular, for Bogliasco waves of greatest intensity originate from 220°N, while for Porto Cesareo from 150°N. Here below a summary of the input data used for the simulations.

Table 4.1 – Summary of input parameters used for the simulations.

	Bogliasco	**Porto Cesareo**
Wave angle - θ	220°	150°
Deep water wave height - H_0	3.0 – 5.8 m	3.0 – 5.8 m
Wave period - T	7.8 – 11.8 s	7.8 – 11.8 s
K_w sand	0.08832	0.07192
K_w photophylous algae	0.59944	0.27728
K_w *Posidonia oceanica*	0.4	0.4
K_w coralligenous	1.03552	0.62784

4.4.1 Wave attenuation due to bottom friction

Simulations were carried out along 10 cross-shore profiles for each of the case studies (fig. 4.21). The process-based study was performed first without taking into account the contribution provided by the bottom friction (*No-friction* simulation) and, subsequently, by activating the dissipation term due to friction (*Friction* simulation). The approach allowed to estimate the influence of seabed roughness on waves' height and energy reduction in real conditions during considered sea-states.

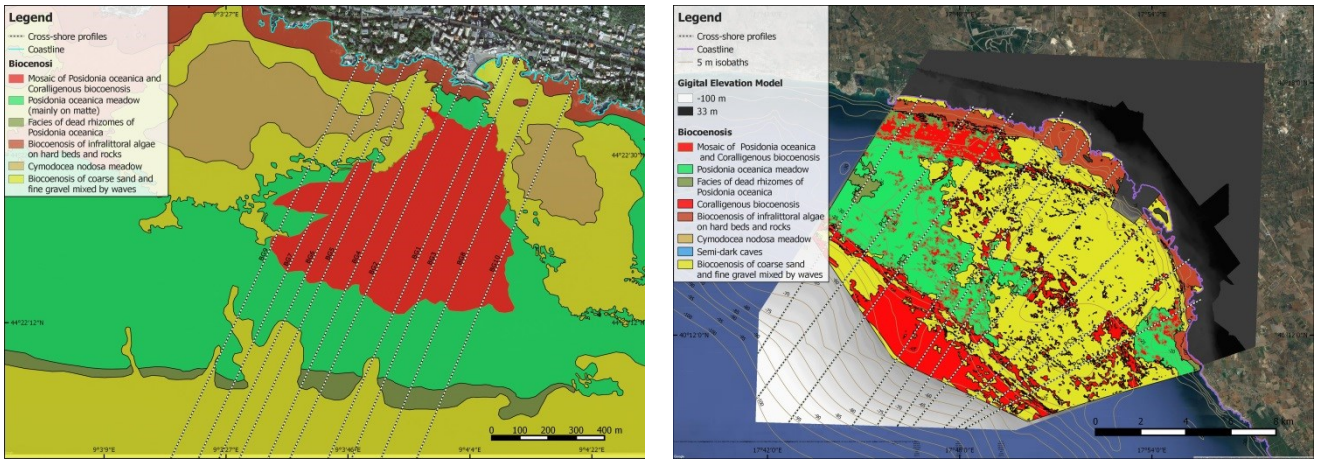

Figure 4.21 – Cross-shore transects at each location (Bogliasco on the left and Porto Cesareo on the right) used for the process-based numerical models.

According to statistics obtained from various simulations, wave parameters were extrapolated before the wave breaking phenomenon took place. Thus, the wave damping rate along the profiles between the offshore section x_0 of the simulation and the section x_b before breaking was estimated. By the difference between the estimated damping rates (without and with bottom friction contribution), the percentage of dissipation attributable solely to the friction with the seabed has been estimated.

Furthermore, data from simulations under different bottom roughness condition were used for investigating changes in wave run-up and inland inundation under two scenarios: present seabed roughness condition and smooth seabed (K_w =0) simulating completely degraded seabed.

4.4.2 Wave attenuation due to each habitat

Since results of the simulations in real conditions were very heterogeneous because of the number of the involved variables, to assess the effectiveness of each habitat in attenuating the wave motion

we attempted to reduce the effect of these variables by performing a further numerical simulation along one profile in each location. The additional simulation has been carried out on a real profile by dividing the transect in 3 sections: from offshore to 40 m depth, from 40 m to 12 m depth, from 12 m depth up to the shoreline. Simulations have been performed by substituting the roughness values related to a given habitat in the central section (fig. 4.22) and considering the wave front direction normal to the shoreline ($\theta_0 = 0°$).

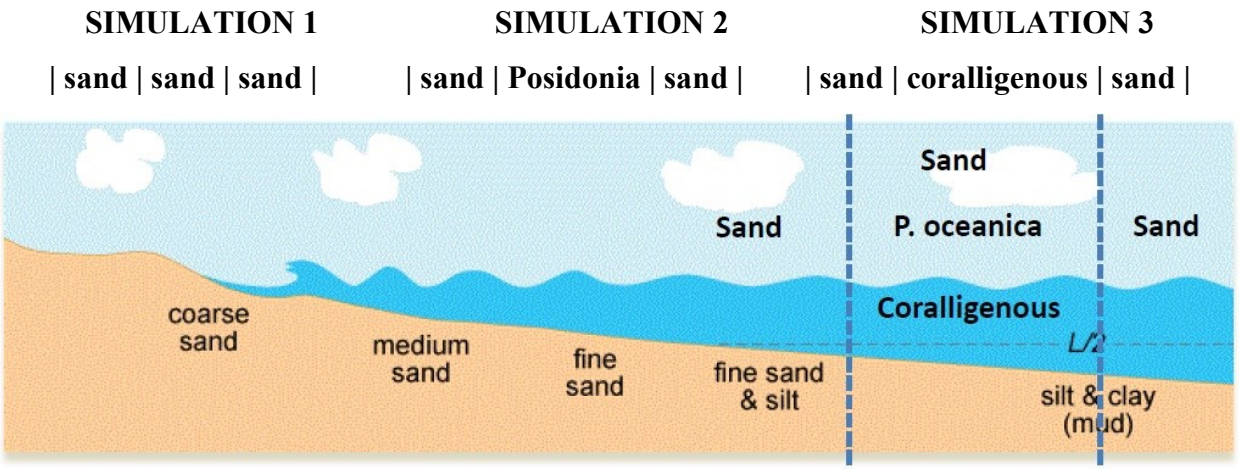

Figure 4.22 – Partition of cross-shore profiles in 3 sections. The equivalent roughness value is changed only in the central section.

The percentage of wave height reduction only along the central section between 40 m and 12 m depth was then estimated.

Comparison of results allowed us to evaluate the effectiveness of each habitat in wave attenuation excluding the contribution of other variables (seabed morphology, wave approach angle, habitat's distribution and extent) to dissipation.

4.4.3 Run-up and on land inundation

Among the possible applications, the study on the wave's propagation and evolution and on the hydrodynamic processes is used to predict the wave run-up and the subsequent flooding on the mainland. Prediction of wave run-up during extreme events, such as those here considered, is of

particular importance for defining and managing the coastal risk, for the design of coastal structures and the protection of natural features that can mitigate the risk.

Run-up and the subsequent flooding calculation has been carried out along each profile considered during the first group of simulations, highlighting the deviation between values calculated in presence of bottom friction and those that do not include this dissipation term. For this purpose we used the empirical relationship of Stockdon et al. (2006) for run-up ($\boldsymbol{R_{2\%}}$) calculation. They reported a large beach run-up data set consisting of data from nine full scale experiments conducted between 1982 and 1996. These authors decomposed the swash in frequency bands (incident and infragravitational) and provided the following formula:

$$\boldsymbol{R_{2\%} = 1.1\left(0.35\beta_f\left(H_{m0}L_{0p}\right)^{1/2} + \frac{1}{2}\left[H_{m0}L_{0p}\left(0.563\beta_f{}^2 + 0.004\right)\right]^{1/2}\right)}$$

Where β_f is the tangent of the angle β between the beach and the horizontal plane, and H_{m0} and L_{0p} are respectively the wave height in deep water and the wave length always in deep water. The first term in parentheses represents the contribution of the wave setup, the term β_f^2 represents the contribution of the incident waves and 0.0004 is the infragravitative contribution.

The Stockdon's equation does not take account of the wave's path over seabed with different roughness. To take into account this variable and to be able to compare the results, we used as H_{m0} and L_{0p} respectively the wave height and length before the breaking phenomenon took place. The formula works very well for dissipative beaches, while for steep beaches (reflective beaches) the results are not reliable. Therefore we decided to use the derived estimates only where $tan\beta \leq 0.25$.

For the inland flooding estimation we used the expression:

$$\boldsymbol{X_{max} = \frac{R_{2\%}}{\tan\beta}}$$

where $\boldsymbol{\beta}$ is the slope of the intertidal zone.

5 RESULTS

5.1 Three-dimensional digital models of the seabed

Totally, 10024 digital photos were collected and 30 three-dimensional digital models of seabed sections hosting 3 different habitats were built: 5 models for each habitat within the 2 locations. The resulting full resolution 3D models have a ground sample distance variable between 0.000416 and 0.000927 m/pix and a total error between a minimum value of 0.00252 m and a maximum of 0.00741 m. DEMs used to process roughness parameters and Area-based rugosity indexes had a cell size of 1cm.

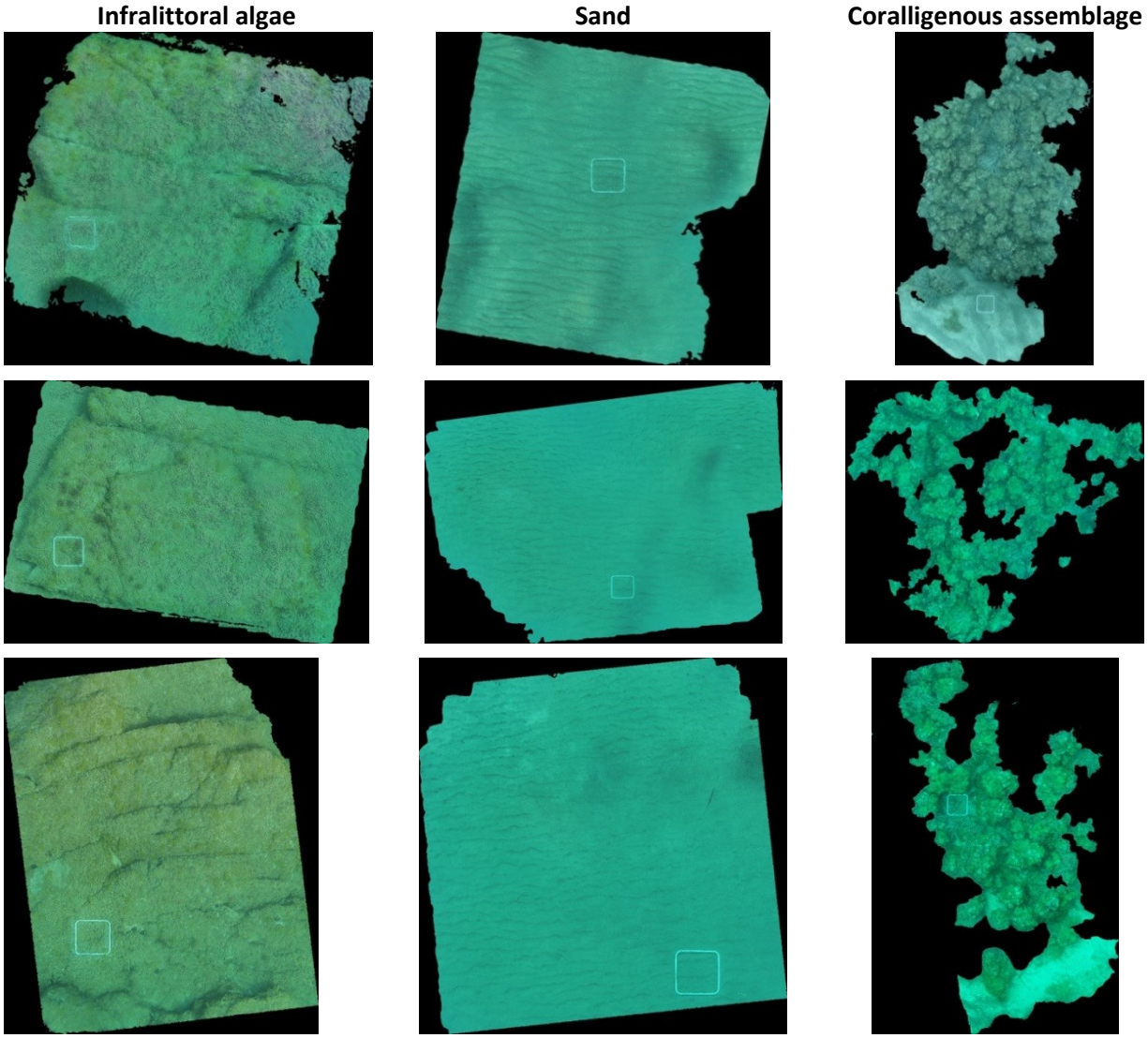

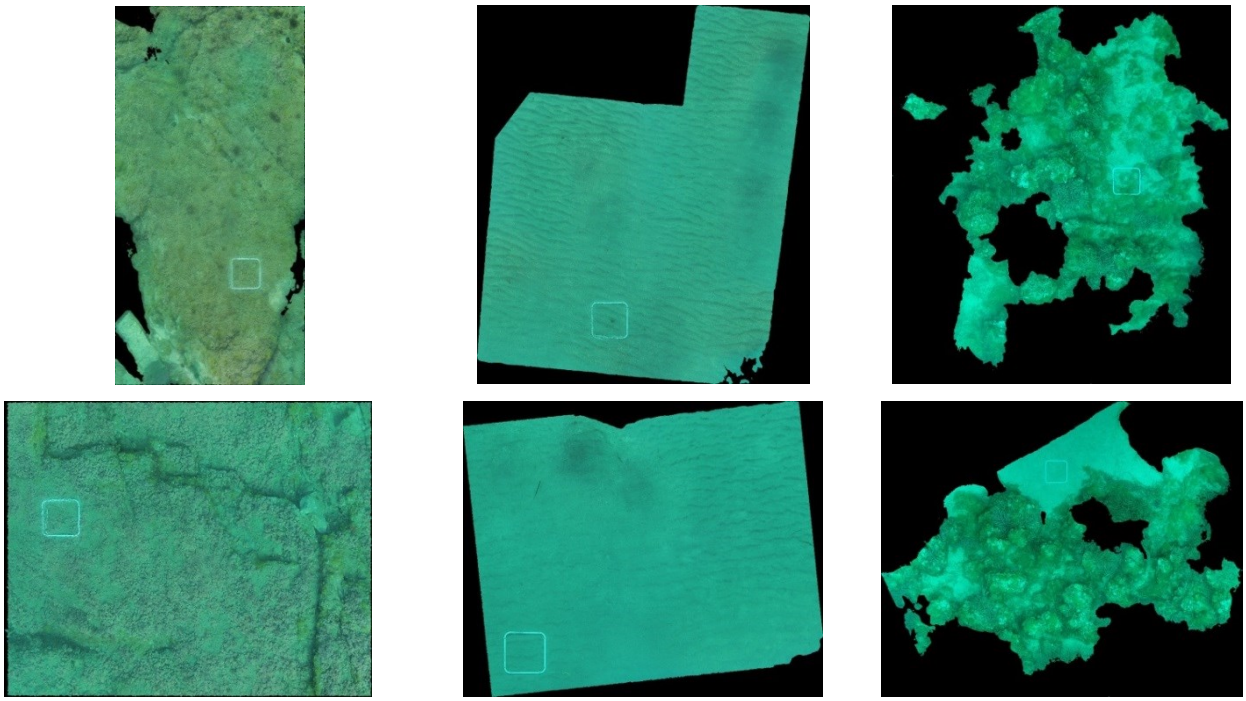

Figure 5.1 – Textured orthomosaic of the resulting three-dimensional models of the seabed at Bogliasco.

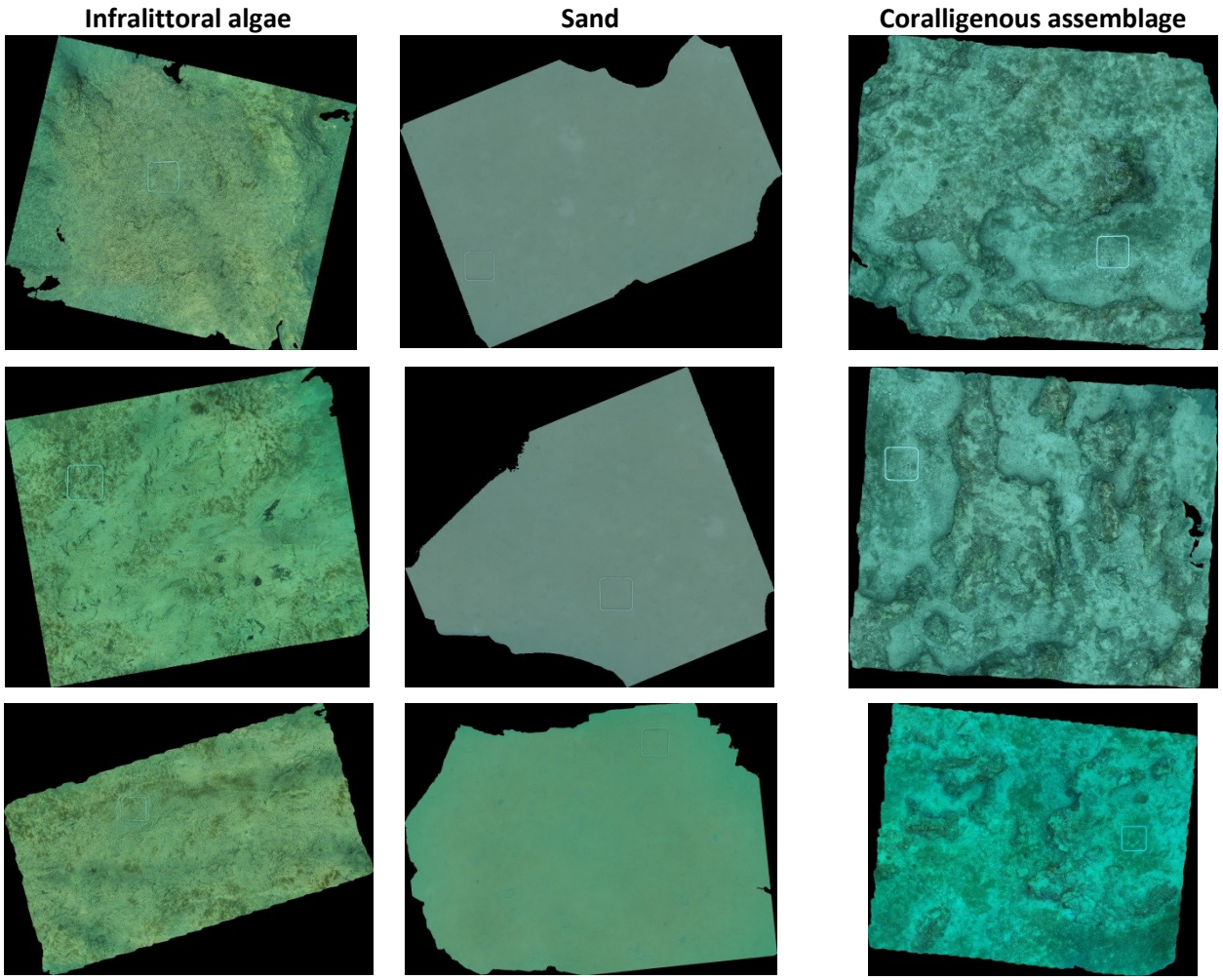

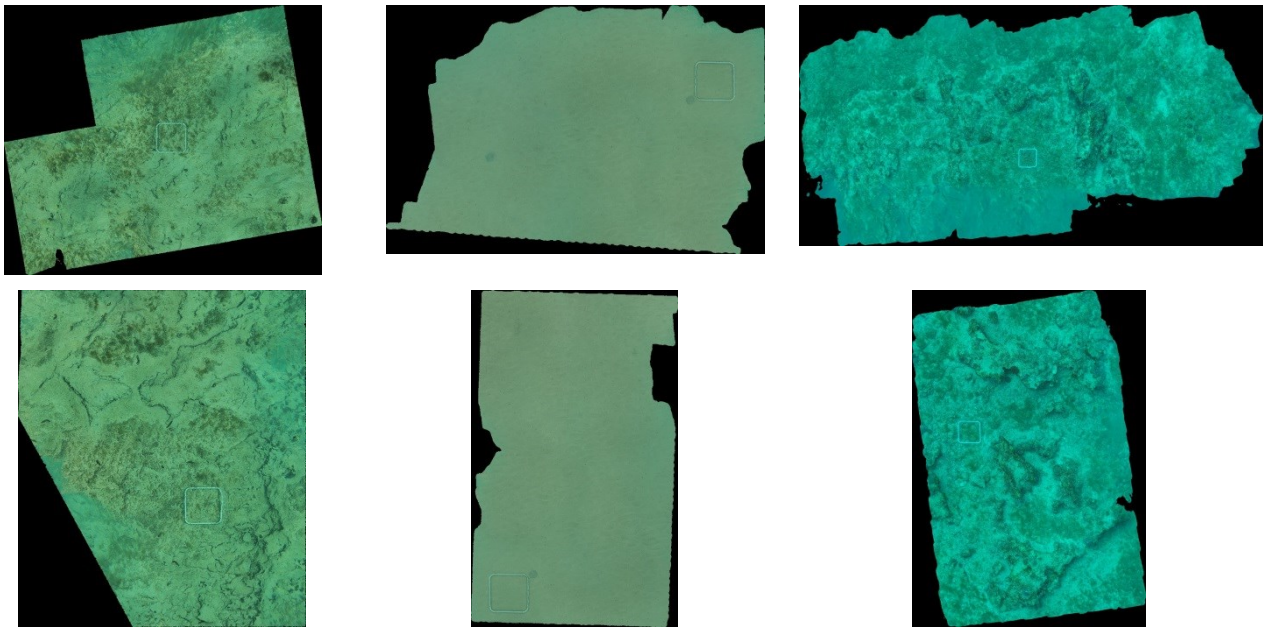

Figure 5.2 – Textured orthomosaic of the resulting three-dimensional models of the seabed at Porto Cesareo.

5.2 Benthic coverage and taxa abundance

The 2D textured ortho-mosaics exported from DEMs were used to estimate the percentage cover of benthic organisms and abiotic features of the seabed's portions.

All benthic living organisms were identified to the lowest possible taxonomic level and the associated substrates were included into the coverage estimation process (table 5.1). A list of 18 benthic categories has been compiled and includes: 6 algae groups (*Halopteris scoparia*, *Ellisolandia elongata*, *Codium bursa*, Encrusting Calcareous Rhodophyta, other bushy algae, algal felt and/or filamentous algae), 4 sponge groups (*Dysidea* sp., *Petrosia ficiformis*, massive sponges and encrusting sponges), 1 massive hard coral (*Cladocora coespitosa*), 3 echinoderm groups (sea urchins, sea stars and holothurians), 4 substrate types (rock, pebbles, sand, organogenic detritus).

Table 5.1 – Percentage coverage of benthic organisms and abiotic features estimated from orthomosaics (BG=Bogliasco, PC=Porto Cesareo).

Model Code	Algal felt / filamentous algae	Bushy algae	*Halopteris scoparia*	*Ellisolandia elongata*	*Codium bursa*	ECR	Encrusting sponges	Massive sponges	*Dysidea* sp.	*Petrosia ficiformis*	*Cladocora coespitosa*	Sea urchins	Holothurians	Sea stars	Rock	Pebbles	Sand	Organogenic detritus
IA_BG_1	0.00	0.00	54.52	5.78	0.00	0.00	0.54	0.00	0.00	0.00	0.00	0.00	0.00	0.00	13.12	0.00	0.00	0.00
IA_BG_2	28.37	0.00	39.38	4.19	0.00	0.00	0.00	0.00	0.00	0.00	0.00	0.00	0.00	0.00	16.18	0.00	0.00	0.00
IA_BG_3	21.10	14.64	18.04	0.00	0.00	0.00	0.00	0.00	0.00	0.00	0.00	0.00	0.00	0.00	18.64	0.00	0.00	0.00

IA_BG_4	20.23	3.34	47.60	0.00	0.00	0.00	0.00	0.00	0.00	0.00	0.00	3.61	0.00	0.00	14.27	0.00	0.00	0.00
IA_BG_5	9.07	0.38	65.02	0.00	0.00	0.00	0.19	0.00	0.00	0.00	0.00	1.52	0.00	0.00	6.08	0.00	0.00	0.00
CA_BG_1	0.00	4.32	0.00	0.00	0.50	46.21	0.80	0.00	0.00	0.00	0.00	0.00	0.00	0.00	0.00	0.00	23.05	0.00
CA_BG_2	0.00	4.18	0.00	0.00	0.26	54.16	0.00	0.00	0.00	0.00	0.00	0.00	0.00	0.00	0.00	0.00	4.06	0.00
CA_BG_3	0.00	4.01	0.00	0.00	0.74	48.27	2.04	0.00	0.00	0.00	0.00	0.00	0.00	0.00	0.00	0.00	22.70	0.00
CA_BG_4	0.00	4.57	0.00	0.00	1.03	48.58	1.11	0.00	0.00	0.00	0.00	0.00	0.00	0.00	0.00	0.00	26.95	0.00
CA_BG_5	0.00	3.71	0.00	0.00	0.92	40.41	2.27	0.00	0.00	0.00	0.00	0.00	0.00	0.00	0.00	0.00	24.04	0.00
IA_PC_1	4.53	88.46	0.00	0.00	0.00	0.00	0.00	0.00	0.00	0.00	0.00	0.00	1.14	0.00	3.99	0.00	0.00	0.00
IA_PC_2	22.29	45.24	0.00	0.00	0.00	0.00	0.00	0.00	0.00	0.00	0.00	0.85	6.53	0.00	4.67	0.00	0.00	0.00
IA_PC_3	26.18	18.58	0.00	0.00	0.00	0.00	0.00	0.00	0.00	0.00	0.00	1.80	6.16	0.00	23.97	0.00	0.00	0.00
IA_PC_4	5.10	43.99	0.00	0.00	0.00	0.00	0.00	0.00	0.00	0.00	0.00	0.98	4.89	0.00	43.87	0.00	0.00	0.00
IA_PC_5	20.82	49.92	0.00	0.00	0.00	0.00	0.00	0.00	0.00	0.00	0.00	1.79	3.20	0.00	5.85	0.00	0.00	0.00
CA_PC_1	2.63	11.30	0.00	0.00	0.53	11.97	0.54	0.00	1.65	0.40	0.27	0.54	0.00	0.12	16.77	2.24	0.00	24.51
CA_PC_2	2.46	7.13	0.00	0.00	0.34	20.61	0.60	0.60	1.19	0.17	0.27	0.52	0.00	0.17	10.38	6.45	0.00	25.88
CA_PC_3	1.24	17.76	5.74	0.00	0.44	10.91	0.20	0.92	0.96	0.20	0.00	0.10	0.00	0.07	4.98	7.12	0.00	10.22
CA_PC_4	1.28	6.35	25.13	0.00	1.58	7.47	0.27	1.19	1.58	0.00	0.00	0.12	0.12	0.06	1.95	11.89	0.00	14.80
CA_PC_5	1.80	7.34	11.29	0.00	0.36	12.12	0.18	0.48	1.47	0.18	0.00	0.18	0.00	0.06	7.38	6.63	0.00	12.34

We underline that in the table above the coverage of sandy bottoms does not appear as no living organism has been observed (only 100% sand).

The coverage data were then used in comparison of the measures of roughness to examine the relationship between the complexity of the seabed and the richness in species of the different sites.

5.3 Seabed roughness estimation and comparison of different roughness measures

All roughness measures show that surface complexity was significantly greater for bioconstructed seabed (CA) and significantly lower were no living organisms were found (SB) (table 5.2). Intermediate values were found for IA systems where bio-builders are uncommon. If we compare results for two different locations, we notice that structural complexity of IA habitat in Bogliasco (BG), although slightly lower, is similar to the values found for CA habitat in Porto Cesareo (PC). The reasons are to be found not only in the geological history and in the intrinsic complexity of the rocky basal layer characterizing these two regions, but also in the different degree of exploitation to which the seafloors within the two locations have been exposed in the past years.

PCoA plot (fig.5.3A), which generally shows 81.2% of total variation (cumulative value), highlights that benthic populations are clearly separated between habitat and sites, with the main

principal coordinate axis of variation representing differences between habitats (PCO1 58.3%). Coverage data for SB models were not included in the analysis because no living organisms were found on the modeled surfaces, so the chart shows only results for IA and CA habitats.

Table 5.2 - Values of roughness measures (2 Area-based Rugosity Indexes and 4 statistical measures) for modeled surfaces:

DEM_file	R_a (m)	R_q (m)	μ(z) (m)	Kmax (m)	Simplified DSM	Full DSM
IA_BG_1	0.0892	0.1132	0.7235	1.3748	1.6059	1.8351
IA_BG_2	0.0952	0.1245	0.4767	0.7369	1.3412	1.5071
IA_BG_3	0.1419	0.1826	0.7008	1.2339	1.4934	1.6423
IA_BG_4	0.1102	0.1435	0.8052	1.2613	1.6434	1.7592
IA_BG_5	0.1532	0.1855	0.5602	1.0249	1.5566	1.7636
CA_BG_1	0.2906	0.3316	0.8611	1.5562	2.1603	2.5729
CA_BG_2	0.2054	0.2476	0.6778	1.5115	2.5595	2.9898
CA_BG_3	0.191	0.226	0.7271	1.2833	2.5058	2.9476
CA_BG_4	0.1995	0.2438	0.5136	1.579	2.1721	2.4365
CA_BG_5	0.2037	0.2454	0.6646	1.3615	2.7644	2.9399
SB_BG_1	0.0191	0.0258	0.1012	0.2098	1.1515	1.3016
SB_BG_2	0.0114	0.015	0.0586	0.1754	1.1154	1.2513
SB_BG_3	0.0232	0.0296	0.0716	0.3064	1.1119	1.2294
SB_BG_4	0.0113	0.0166	0.0654	0.1826	1.0771	1.1788
SB_BG_5	0.0171	0.0234	0.0615	0.2505	1.1150	1.2343
IA_PC_1	0.1135	0.1399	0.4149	0.7286	1.2981	1.4215
IA_PC_2	0.0283	0.0386	0.194	0.3209	1.1632	1.2735
IA_PC_3	0.0285	0.0391	0.1845	0.3428	1.1536	1.2555
IA_PC_4	0.0554	0.0675	0.1602	0.3647	1.2311	1.3380
IA_PC_5	0.0492	0.0615	0.257	0.541	1.2409	1.3908
CA_PC_1	0.1192	0.1546	0.2713	0.885	1.5272	1.6859
CA_PC_2	0.1614	0.188	0.2824	0.8235	1.7543	1.8868
CA_PC_3	0.1332	0.1606	0.3099	0.8619	1.4967	1.6184
CA_PC_4	0.0888	0.123	0.3887	0.9812	1.3406	1.4321
CA_PC_5	0.1295	0.1586	0.3019	0.7911	1.4908	1.6122
SB_PC_1	0.0077	0.0125	0.0879	0.2128	1.0902	1.2086
SB_PC_2	0.014	0.0233	0.077	0.2875	1.1331	1.2821
SB_PC_3	0.0272	0.0351	0.0777	0.2728	1.1205	1.2760
SB_PC_4	0.0092	0.0132	0.0467	0.1208	1.0536	1.1626
SB_PC_5	0.0041	0.0058	0.039	0.0882	1.0290	1.0970

Statistical test of PERMANOVA (Anderson, 2001; McArdle & Anderson, 2001; table 5.3) suggests that there is a significant difference among habitats. Going on to analyze the differences between groups, populations always show a high degree of differentiation (table 5.4, $P<<0.05$).

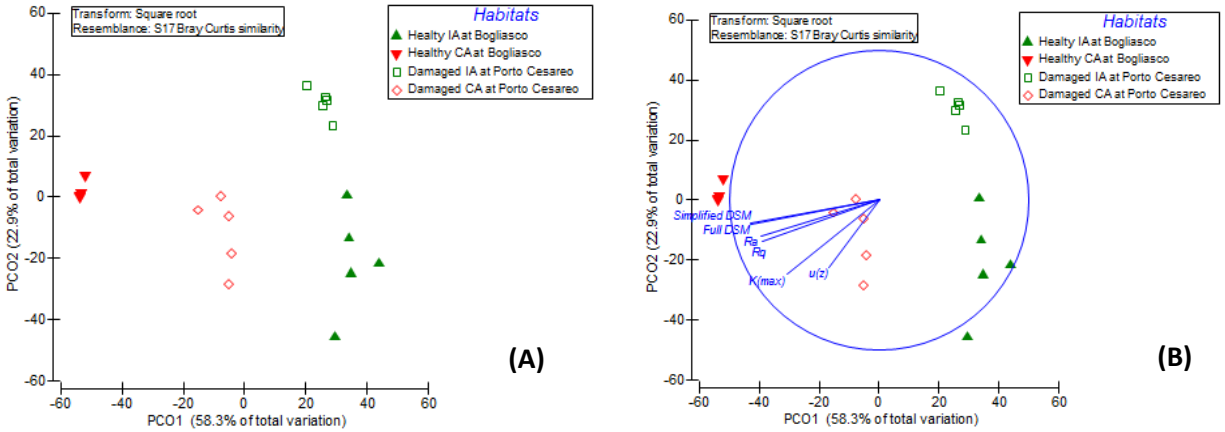

Figure 5.3 - (A) PCoA chart represents relationships between the populations of different habitats; (B) PCoA chart on the covering percentage data transformed with square root and using the similarity index of Bray-Curtis, with correlation vectors superimposed.

Table 5.3 - Results of PERMANOVA statistical test on composition and abundance of observed taxa/categories:

Source	df	SS	MS	Pseudo-F	P(perm)	perms	P(MC)
Habitat	3	37154	12385	49.954	0.0001	9937	0.0001
Res	16	3967	248				
Total	19	41121					

Table 5.4 - Paired comparison between populations of different sites (where A= *IA* at Bogliasco, B= *CA* at Bogliasco, C= *IA* at Porto Cesareo, D=*CA* at Porto Cesareo):

Groups	t	P(perm)	perms	P(MC)
A, B	9.1889	0.0090	126	0.0001
A, C	4.5753	0.0076	126	0.0007
A, D	5.3342	0.0082	126	0.0003
B, C	10.115	0.0099	126	0.0001
B, D	8.1732	0.0078	126	0.0001
C, D	6.0996	0.0069	126	0.0001

The comparison with the roughness parameters exhibits that all roughness measures are substantially correlated with the pattern of similarity of benthic populations and, specifically, their value increases in the direction of coralligenous population, which presents a greater physical complexity than other habitats. By analysing multivariate correlation using Distance-based Linear Model (DistLM), it appears evident that all roughness measures are significant (P<0.05), but the variables that exhibit the highest correlation are *Full DSM* and *Simplified DSM* (respectively 45.6% and 45.4% of the observed variability), followed by R_a, R_q and K_{max} (respectively 37.9%, 37.5% and 30.1%). Only $\mu(z)$ shows lower values of correlation but it is still significant (P=0.0261) (table 5.5).

Table 5.5- Results of correlation analysis using DistLM:

Variable	SS(trace)	Pseudo-F	P	Prop.
Full DSM	18771	15.117	0.0001	0.45647
Simplified DSM	18670	14.969	0.0001	0.45403
Ra	15594	10.995	0.0002	0.37921
Rq	15433	10.814	0.0001	0.37530
K(max)	12378	7.752	0.0007	0.30102
μ(z)	6918	3.641	0.0261	0.16823

5.4 Relationship between physical and hydraulic roughness for hard beds

Many authors working in the field of fluid mechanics attempted to describe the relationship between measured surface roughness parameters and equivalent hydraulic roughness, since those influence friction factor and drag coefficient useful for calculating bed share stress. Our literature search identified only few works describing the relationship between physical and hydraulic roughness on seafloors (Mathisen & Madsen ,1999; Nelson, 1996; Raudviki, 1988; Lowe et al., 2005; Nielsen, 1992) being most of studies focused on artificial and natural channels or pipes (Camenen et al., 2006; Camenen et al., 2009; Adams et al., 2012; Nikuradse, 1937; Kandlikar, 2005; Limerinos et al., 1970; Simoes, 2010; Moody, 1944; Wilson, 1987; Yalin, 1992; Van Rijn, 1993; Bayram et al., 2003; Kamphuis ,1974; Nnadi & Wilson, 1992).

Among consulted literature we found that only Lowe and colleagues in 2005 described a relationship useful to convert physical roughness of hard seabed obtained through bottom roughness surveys into hydraulic roughness length usable during numerical simulation of wave propagation with satisfactory results.

Table 5.6 reports the data of R_q physical roughness parameters and their corresponding hydraulic roughness length estimation K_w.

Table 5.6 - Calculated Physical roughness parameters R_q and corresponding hydraulic roughness length K_w for each habitat within each location (average values):

Site	Habitat	R_q	K_w
Bogliasco	Infralittoral Algae	0.14986	0.59944
	Coralligenous	0.25888	1.03552
	Sand	0.02208	0.08832
Porto Cesareo	Infralittoral Algae	0.06932	0.27728

	Coralligenous	0.15696	0.62784
	Sand	0.01798	0.07192

5.5 Process-based numerical models

We first examine how bottom friction due to the presence of different habitat can affect the wave propagation towards the coast quantifying its contribution to wave dissipation. Next, we examine the effectiveness of each considered habitat in wave attenuation and, thus, the protection benefits supplied by the habitats during two extreme conditions. All simulations were performed along real seafloor profiles at two sites with different slope: Bogliasco with steep seabed and Porto Cesareo characterized by mild slope seabed.

5.5.1 Wave attenuation due to bottom friction

We quantified the effect of seabed roughness in reducing wave height and energy by comparing results of the "*Friction"* simulation (activating bottom friction) with those "*No-friction"* (without taking into account bottom friction).

Most of the energy contained in the waves is dissipated by breaking. This phenomenon is beyond the scope of this work and, therefore, not considered here. The wave parameters before the wave breaking took place have been extracted from numerical data obtained through various simulations. Thus, the wave damping rate along the profiles between the beginning section x_0 of the simulation and the section x_f before breaking was estimated. By the difference between the estimated damping rates (without and with bottom friction contribution), the percentage of dissipation attributable solely to the friction with the seabed has been estimated. In the table 5.6 a summary of simulation results associated with both wave height and wave energy damping rates is shown.

Table 5.6 a, b, c, d - Wave length (L) and wave height (H) before breaking, wave height damping rate and wave energy damping rate along 10 profiles at each location. The abbreviations in the simulation titles indicate respectively the location (BG=Bogliasco, PC=Porto Cesareo, profile number, bottom friction contribution (NO=not considered, real=considered), wave height in deep water (H3=3m, H6=5.8m), wave period (T8=7.8sec, T12=11.8sec):

a) **Bogliasco H_0 = 3 m , T = 7.8 sec**

Simulation	L [m]	H [m]	Rate H	Rate E
out_BG_1_NO_H3_T8	70.0472	2.6733	10.89%	20.60%
out_BG_1_real_H3_T3	67.3749	2.6264	12.45%	23.36%
out_BG_2_NO_H3_T8	65.2911	2.6967	10.11%	19.20%
out_BG_2_real_H3_T8	62.9121	2.6364	12.12%	22.77%
out_BG_3_NO_H3_T8	60.6293	2.7171	9.43%	17.97%
out_BG_3_real_H3_t8	57.7732	2.6559	11.47%	21.63%
out_BG_4_NO_H3_T8	64.2371	2.6973	10.09%	19.16%
out_BG_4_real_H3_T8	64.2371	2.6532	11.56%	21.78%
out_BG_5_NO_H3_T8	64.5433	2.7041	9.86%	18.76%
out_BG_5_real_H3_T8	64.5433	2.6765	10.78%	20.41%
out_BG_6_NO_H3_T8	61.4018	2.6846	10.51%	19.92%
out_BG_6_real_H3_T8	61.4018	2.6521	11.60%	21.85%
out_BG_7_NO_H3_T8	62.8098	2.7071	9.76%	18.57%
out_BG_7_real_H3_T8	62.8098	2.6786	10.71%	20.28%
out_BG_8_NO_H3_T8	64.1694	2.7131	9.56%	18.21%
out_BG_8_real_H3_T8	64.1694	2.6727	10.91%	20.63%
out_BG_9_NO_H3_T8	71.2892	2.6681	11.06%	20.90%
out_BG_9_real_H3_T8	71.2892	2.6469	11.77%	22.16%
out_BG_10_NO_H3_T8	57.8102	2.7142	9.53%	18.15%
out_BG_10_real_H3_T8	57.8102	2.6842	10.53%	19.95%

b) **Bogliasco H_0 = 5.8 m , T = 11.8 sec**

Simulation	L [m]	H [m]	Rate H	Rate E
out_BG_1_NO_H6_T12	130.3231	5.3379	7.97%	15.30%
out_BG_1_real_H6_T12	125.2518	5.2186	10.02%	19.04%
out_BG_2_NO_H6_T12	131.4009	5.3203	8.27%	15.86%
out_BG_2_real_H6_T12	125.5279	5.2281	9.86%	18.75%
out_BG_3_NO_H6_T12	137.2851	5.3623	7.55%	14.52%
out_BG_3_real_H6_t12	133.3846	5.2798	8.97%	17.13%
out_BG_4_NO_H6_T12	133.6474	5.3326	8.06%	15.47%
out_BG_4_real_H6_T12	130.9803	5.2444	9.58%	18.24%
out_BG_5_NO_H6_T12	130.5970	5.3335	8.04%	15.44%
out_BG_5_real_H3_T8	129.4914	5.2373	9.70%	18.46%
out_BG_6_NO_H6_T12	136.5982	5.3232	8.22%	15.77%
out_BG_6_real_H6_T12	131.5223	5.2565	9.37%	17.86%
out_BG_7_NO_H6_T12	132.5327	5.3355	8.01%	15.37%
out_BG_7_real_H6_T12	132.5327	5.2432	9.60%	18.28%
out_BG_8_NO_H6_T12	132.9752	5.3186	8.30%	15.91%
out_BG_8_real_H6_T12	127.4491	5.2219	9.97%	18.94%
out_BG_9_NO_H6_T12	134.1777	5.3397	7.94%	15.24%
out_BG_9_real_H6_T12	134.1777	5.2647	9.23%	17.61%
out_BG_10_NO_H6_T12	131.4988	5.3250	8.19%	15.71%

out_BG_10_real_H6_T12	130.1719	5.2493	9.49%	18.09%

c) Porto Cesareo H_0 = 3 m , T = 7.8 sec

Simulation	L [m]	H [m]	Rate H	Rate E
out_PC_1_NO_H3_T8	68.5534	2.5910	13.63%	25.41%
out_PC_1_real_H3_T8	64.5366	2.4988	16.71%	30.62%
out_PC_2_NO_H3_T8	70.5900	2.4976	16.75%	30.69%
out_PC_2_real_H3_T8	69.0781	2.3661	21.13%	37.80%
out_PC_3_NO_H3_T8	68.2519	2.5622	14.59%	27.06%
out_PC_3_real_H3_T8	66.1427	2.4639	17.87%	32.55%
out_PC_4_NO_H3_T8	63.2380	2.6448	11.84%	22.28%
out_PC_4_real_H3_T8	63.2380	2.5920	13.60%	25.35%
out_PC_5_NO_H3_T8	65.9768	2.6521	11.60%	21.85%
out_PC_5_real_H3_T8	65.9768	2.6127	12.91%	24.15%
out_PC_6_NO_H3_T8	62.0303	2.4474	18.42%	33.45%
out_PC_6_real_H3_T8	62.0303	2.3675	21.08%	37.72%
out_PC_7_NO_H3_T8	66.3584	2.5281	15.73%	28.99%
out_PC_7_real_H3_T8	66.3584	2.4722	17.59%	32.09%
out_PC_8_NO_H3_T8	67.2922	2.5261	15.80%	29.10%
out_PC_8_real_H3_T8	67.2922	2.4982	16.73%	30.65%
out_PC_9_NO_H3_T8	63.2276	2.2420	25.27%	44.15%
out_PC_9_real_H3_T8	63.2276	2.1730	27.57%	47.54%
out_PC_10_NO_H3_T8	62.6149	1.9965	33.45%	55.71%
out_PC_10_real_H3_T8	61.1575	1.8264	39.12%	62.94%

d) Porto Cesareo H_0 = 5.8 m , T = 11.8 sec

Simulation	L [m]	H [m]	Rate H	Rate E
out_PC_1_NO_H6_T12	141.1066	4.4555	23.18%	40.99%
out_PC_1_real_H6_T12	136.3678	4.0927	29.44%	50.21%
out_PC_2_NO_H6_T12	140.8386	3.8512	33.60%	55.91%
out_PC_2_real_H6_T12	139.2336	3.3248	42.68%	67.14%
out_PC_3_NO_H6_T12	129.1246	3.6962	36.27%	59.39%
out_PC_3_real_H6_T12	126.2872	3.1137	46.32%	71.18%
out_PC_4_NO_H6_T12	132.9215	4.6716	19.46%	35.12%
out_PC_4_real_H6_T12	127.7749	4.3811	24.46%	42.94%
out_PC_5_NO_H6_T12	139.2688	4.8211	16.88%	30.91%
out_PC_5_real_H6_T12	139.2688	4.5839	20.97%	37.54%
out_PC_6_NO_H6_T12	137.8472	4.5669	21.26%	38.00%
out_PC_6_real_H6_T12	135.1787	4.2789	26.23%	45.57%
out_PC_7_NO_H6_T12	129.4833	4.0938	29.42%	50.18%
out_PC_7_real_H6_T12	128.3160	3.7591	35.19%	57.99%
out_PC_8_NO_H6_T12	134.3624	4.7062	18.86%	34.16%
out_PC_8_real_H6_T12	127.1634	4.5541	21.48%	38.35%
out_PC_9_NO_H6_T12	127.2463	4.0911	29.46%	50.25%
out_PC_9_real_H6_T12	126.1275	3.8132	34.26%	56.78%

out_PC_10_NO_H6_T12	134.0531	2.2118	61.87%	85.46%
out_PC_10_real_H6_T12	133.8145	1.3496	76.73%	94.59%

By comparing numerical data relating to wave propagation in presence and absence of bottom friction, a situation highly complicated is highlighted. Wave height and wave energy reduction is strongly influenced by variables such as the morpho-bathymetry, the distribution and the extent of habitats along the different profiles, the angle of attack of the wave front and the initial condition imposed.

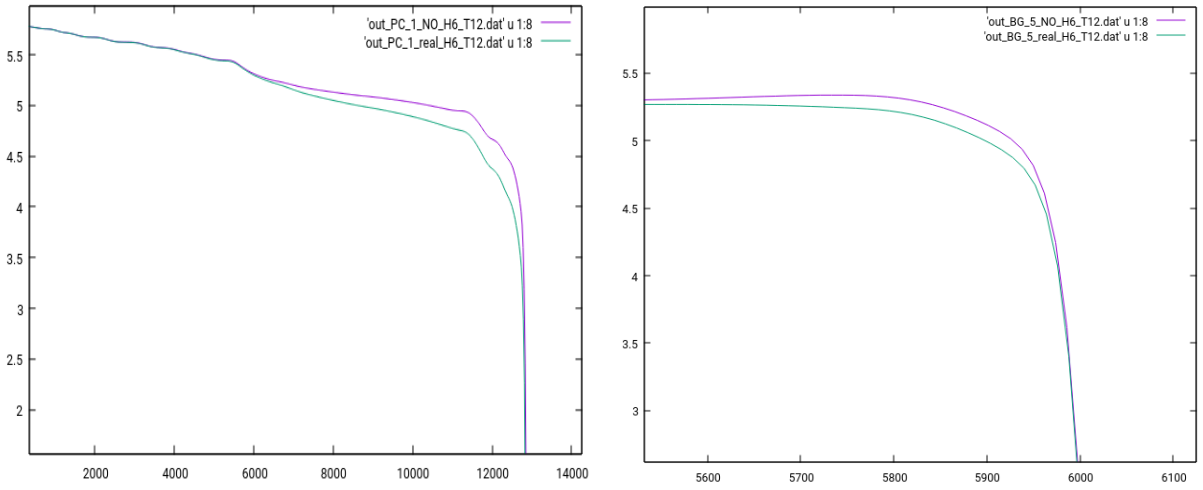

Figure 5.4 - Output examples of numerical simulations: profile of wave height from offshore to the shoreline along one transect in Bogliasco (right) and in Porto Cesareo (left). The red line shows simulation performed deactivating frictional dissipation, while the blue line represent simulation performed activating the contribution of the bottom friction.

In general, as expected, the highest values of damping rates were observed for simulations taking into account dissipation due to bottom friction.

In detail, for steep seafloors (e.g. Bogliasco) and considering initial condition H_0 = 3 m e T = 7.8 sec, the wave height reduction ranges between a minimum value of 28.3 cm and a maximum of 33.2 cm for *No-friction* simulations, while by activating the contribution of frictional dissipation the wave height reduction increases to values between 31.6 cm and 37.4 cm (table 5.6a).

Always for Bogliasco case study but considering as deep water conditions H_0 = 5.8 m e T = 11.8 sec, the decrease of the wave height varies in a range between 43.8 cm and 48.1 cm in *No-friction* simulations, and between 52.0 and 58.1 by activating the contribution of the bottom friction (table 5.6b).

For Porto Cesareo representing the mild-slope seafloors, taking into account initial condition H_0 = 3 m e T = 7.8 sec, the wave height in absence of bottom friction decreases of a value between 34.8 cm and 103.5 cm, while in presence of frictional dissipation the wave height decreases between a minimum of 38.7 cm and a maximum of 117.4 cm (table 5.6c).

Considering as initial conditions H_0 = 5.8 m e T = 11.8 sec, for mild-slope seabed the wave height reduction increases considerably to values between 97.9 cm and 358.8 cm, and between 121.6 cm and 445.0 cm for *No-friction* and *Friction* simulations (table 5.6d).

The high values recorded especially for Porto Cesareo case study are attributable even to the orientation of the coast, the direction of the wave motion in proximity of Porto Cesareo and the consequent transects arrangement along which the simulations are carried out.

The general results outlined above, in terms of wave heights damping rates, provide us information about wave height reduction excluding the dissipation due to the breaking phenomenon. If we analyze the damping rates of the wave heights before breaking, for Bogliasco and H_0 = 3 m e T = 7.8 sec, an average reduction in wave height of 11.39% due to phenomena other than wave breaking can be observed. This percentage includes the dissipation term due only to the friction, which represents the 11.49% of the total no-breaking phenomena. For Porto Cesareo instead, the attenuation rate during the same sea conditions reaches the 20.43%, with the 13.33% of the total dissipation (not due to wave breaking) is attributable only to friction with the seabed (fig. 5.5).

By considering the sea state H_0 = 5.8 m e T = 11.8 sec, for steep sea bottoms as those of Bogliasco, the attenuation not due to wave breaking phenomena appears to be less pronounced reaching the 9.58%, of which the 15.92% is represented solely by frictional dissipation. For Porto Cesareo, the total attenuation not due to breaking instead represents the 35.77%, of which 18.87% is attributable to bottom friction.

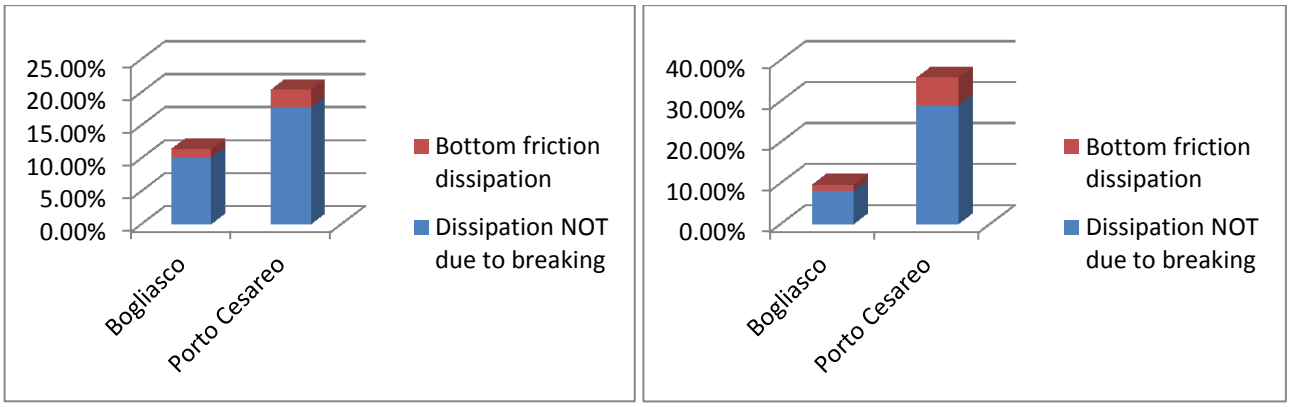

Figure 5.5 – Wave height attenuation rate up to breaking section x_f. The diagrams show the attenuation due to no-breaking phenomena. The red color indicates the attenuation attributable only to bottom friction. The blue color indicates the attenuation ascribable to other variables. The diagram on the left shows results for sea condition H_0 = 3 m T = 7.8 sec, the diagram on the right shows results considering H_0 = 5.8 m e T = 11.8 sec.

Being the results very heterogeneous due to the number of involved variables, it is complicated to assess the effectiveness of each habitat in attenuating wave motion. However important considerations can be made both regarding the combined effect of benthic habitats on waves at local scale and the usefulness and advantages arising from including also the frictional dissipation term in the wave simulation models. Furthermore, the data obtained can also be useful to highlight the consequences of habitat loss on the risk associated with extreme events and the vulnerability of coastal communities and infrastructures.

Therefore, the incident wave parameters obtained by each simulation before wave breaking have been used for calculating the values of relative run-up and flooding on land. Results were compared in order to demonstrate on the one hand the importance of considering the presence of different submerged habitat and their characteristics when assessing the coastal risk and quantifying the coastal protection services supplied by ecosystems, on the other hand the effect of the habitat loss on wave run-up and consequent increase of water propagation on land. Thus, the changes in wave run-up and inland inundation under two different seabed roughness scenarios were investigated: present seabed roughness condition and smooth seabed (roughness = 0) simulating completely degraded seabed.

5.5.2 Wave attenuation due to each habitat

To quantify the relative protective benefits of each considered ecosystem and to assess their effectiveness in mitigating swell, we performed an additional simulation by limiting the number of involved variables as described in the paragraph 4.4.2 above.

Thus the percentage reduction of wave height between 40 m and 12 m of depth was estimated.

Results show as the wave height reduction increases in presence of high-roughness ecosystems such as *P. oceanica* meadows and coralligenous assemblages (table 5.7).

Table 5.7 – Wave height attenuation rates induced by three considered ecosystems at two case studies during two extreme sea states.

	Sand	*P. oceanica*	Coralligenous
Bogliasco (H=3 ; T=7.8)	8.98%	9.41%	9.85%
Porto Cesareo (H=3 ; T=7.8)	11.12%	12.28%	12.77%
Bogliasco (H=5.8 ; T=11.8)	2.74%	3.54%	4.47%
Porto Cesareo (H=5.8 ; T=11.8)	11.82%	16.99%	18.35%

Observing the estimated values for steep seabed such as Bogliasco, in the case of H_0 = 3 m e T = 7.8 sec, the wave height reduction rate increases from 8.98% to 9.41% and up to 9.85% respectively for sand, *P. oceanica* and coralligenous (fig. 5.6). Thus, the damping rates increased by 0.44% from sand to *P. oceanica*, and by 0.87% from sand to coralligenous assemblages.

Taking into consideration H_0 = 5.8 m e T = 11.8 sec, the wave height reduction percentage seems generally to decrease (2.74%, 3.54% e 4.47% respectively for sand, *P. oceanica* and coralligenous) (fig. 5.6). But if we look at the differences induced by the different habitats, we realize that *P. oceanica* meadow entails a wave height reduction of 0.80% higher than sandy bottoms (about twice compared to the previously considered conditions), while the coralligenous entails a wave height reduction of 1.73% compared to sandy bottoms and 0.93% when compared with *P. oceanica*.

At Porto Cesareo characterized by mild-slope seabed, the attenuation due to the interaction with rugged seabed further increases and, considering the offshore conditions H_0 = 3 m e T = 7.8 sec, the wave height attenuation rate varies from 11.12% to 12.28%, up to 12.77% respectively for sandy bottoms, *P. oceanica* meadows and coralligenous (fig. 5.6). Thus the effectiveness of *P. oceanica* is

1.16% higher than sandy bottom, while for coralligenous the effectiveness is 1.65% higher than sand.

For the sea condition H_0 = 5.8 m e T = 11.8 sec, the attenuation rate increases from 11.82% for sand to 16.99% for *P. oceanica*, up to 18.35% for the coralligenous, with a difference of 5.17% between sand and *P. oceanica*, and 6.54% between sand and coralligenous (fig. 5.6 and 5.7). Therefore the effectiveness of coralligenous is 1.37% higher than *P. oceanica*.

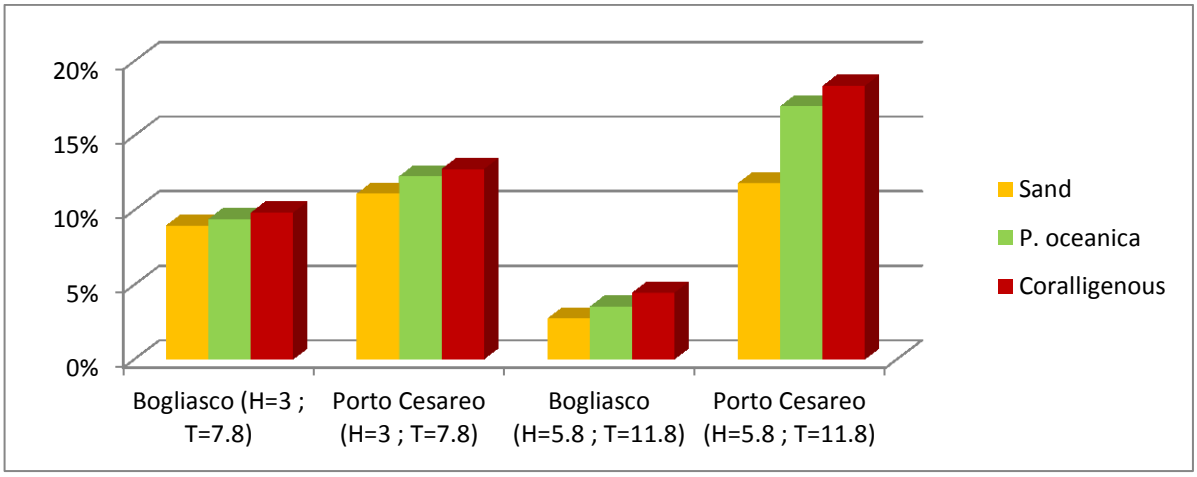

Figure 5.6 – Wave height attenuation rate attributable only to the central section of the considered profiles.

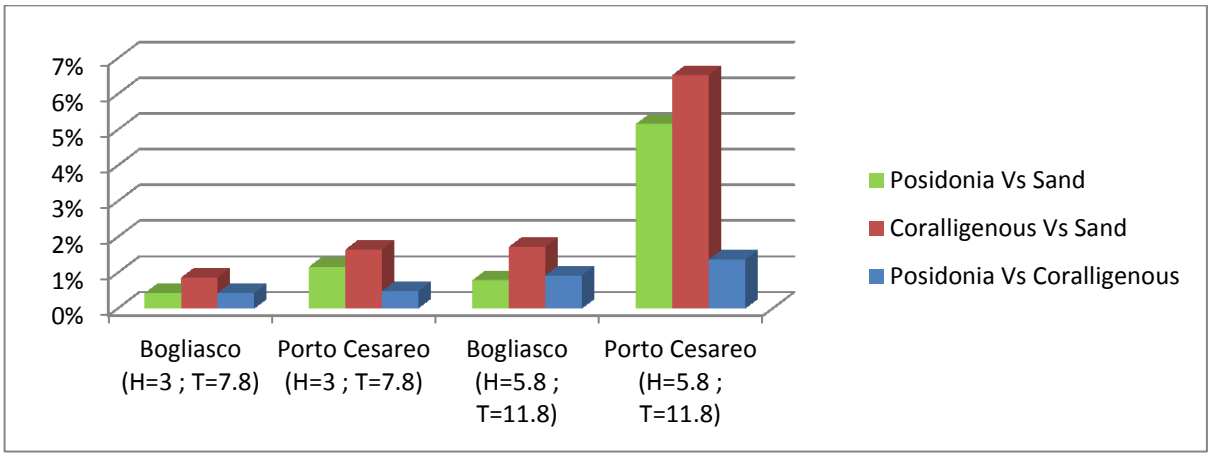

Figure 5.7 – Differences of attenuation rates among considered ecosystems during two considered sea states.

The comparison of the attenuation rate associated habitat allows to deduce a measure of the protective benefits of the biogenic ecosystems in dissipating waves through bottom friction. In fact, since the estimated roughness value of sand is close to zero (for Bogliasco K_w=0.08 and for Porto Cesareo K_w=0.07) it is admissible as approximation to consider close to zero also the contribution provided by its roughness to frictional dissipation. The difference between the dissipation rates can

therefore be seen as a measure of the relative effectiveness of the dissipation of biogenic habitats here considered.

In the specific case, for steeper seafloors such as those of Bogliasco, the effectiveness of the coralligenous is higher than *P. oceanica* between 0.44% and 0.93%, while for mild-slope seabed (such as Porto Cesareo) the coralligenous effectiveness is higher than *P. oceanica* between 0.48% and 1.37% (table 5.8).

Table 5.8 – Differences among dissipation rates of the considered habitats:

Initial parameters	Site	Posidonia Vs Sand	Coralligenous Vs Sand	Posidonia Vs Coralligenous
H=3 ; T=7.8	Bogliasco	0.44%	0.87%	0.44%
	Porto Cesareo	1.16%	1.65%	0.48%
H=5.8 ; T=11.8	Bogliasco	0.80%	1.73%	0.93%
	Porto Cesareo	5.17%	6.54%	1.37%

These statements can be very useful in terms of environmental accounting. Several recent studies attempt to evaluate the role that marine ecosystems have in mitigating the wave energy preventing coastal erosion, in order to quantify the value of specific ecosystem services provided by a given habitat, also in monetary terms. Regarding the seagrasses and in particular for *P. oceanica*, in literature there are several works that quantify in economic terms its value per square meter. Usually the portions attributable to each ecosystem service provided by the habitat are distinct (annual value of oxygen production, value of carbon fixation, coastal erosion prevention, shelter service for fishes and commercial species) in order to estimate the total value of natural capital.

For coralligenous however, despite the ecosystem services provided by this habitat are well-known and documented, the value of its role in the coastal erosion and risk prevention has never been contemplated and quantified.

By using data available in literature, the value of ecosystem services provided by *P. oceanica* meadows is rather easily obtainable. For example, in 2008 Blasi estimated the value of coastal erosion prevention of a *P. oceanica* meadow between 309 € and 39.000 € per m^2. By applying the approach just described, the value of one square meters of coralligenous bank type can be estimated by multiplying the value obtained from the difference in the dissipation rates between the two

biogenic habitats with the estimated value of coastal erosion prevention of the *P. oceanica* meadow, and summing the result to the value of the *P. oceanica*.

So in our study, for mild-slope seabed, the value of coastal erosion prevention service provided by coralligenous ranges between 310.48 €/m^2 (309€*0.48% + 309€) and 39534.3 €/m^2 (39.000 €*1.37% + 39.000 €).

For steeper seafloors, the value of coastal erosion prevention service provided by coralligenous ranges between 310.36 €/m^2 (309€*0.44% + 309€) and 39362.7 €/m^2 (39.000 €*0.93% + 39.000 €).

The elaborated bionomic mapping allows calculating the extent of biogenic habitats at two case studies.

In front of Bogliasco, the *P. oceanica* meadow covers about 72.8 hectares, while the coralligenous assemblage about 35 hectares. This means that the minimum value of coastal protection service supplied by the meadow is 224.952.000€, while the minimum coralligenous value is 108.998.432€.

At Porto Cesareo, where the *P. oceanica* meadow and the coralligenous assemblage cover respectively 3363.42 hectares and 1956.35 hectares, the minimum value of protection service provides by *P. oceanica* is estimated around 10.392.967.800€ , while the coralligenous has a minimum value of 6.074.075.480€.

The present work does not pretend to give a complete and absolute estimation, but it represents just an example by which we want to provide a rough estimate of the value of the coralligenous bank type in coastal protection. Consequently, results presented herein are an indication of the services supplied by the habitats in the two specific case studies under particular extreme sea states. Rather, we hope that this research constitutes a motivation to carry on and deepen further investigation in this field in order to provide new elements for the conservation of coralligenous concretions and other biogenic habitats.

5.5.3 Wave run-up and in land flooding

Among the possible applications, the study of the wave evolution and associated hydrodynamic processes is used to predict the wave run-up and the subsequent flooding on the mainland. The wave run-up calculation during extreme events such as those considered in the present work is of particular importance for the definition and the management of the coastal risk, for designing coastal structures and for the protection of natural features that mitigate the risk.

We performed the run-up and the flooding on land calculation considering the results of the simulations carried out along 10 transects in each case study. The derived estimates were then compared in order to highlight the deviation between values calculated in presence of bottom friction and those that do not include this dissipation term.

For considered sea states and steep seafloors (Bogliasco), the maximum deviation between the detected run-up is 13.7 cm which results in a maximum flooding decrease of 68.5 cm. In details, for sea state H_0 = 3 m T = 7.8 sec, the differences are much less marked than the most extreme situation (H_0 = 5.8 m and T = 11.8 sec) being observed a maximum run-up reduction of 6.5 cm in the presence of fiction and consequent decrease of flooding of 32.5 cm. Taking into account H_0 = 5.8 m and T = 11.8 sec, the differences are accentuated and reach the maximum at the profile 2. The estimate is considered reliable only for 4 of the 10 profiles because, as shown in the table 5.9 below, for beach slopes more than ¼, the Stockdon et al. formulation overestimates both the run-up and inundation values.

In case of dissipative beaches such as those of Porto Cesareo where the slope is less pronounced, a more complete picture is outlined. In detail, for sea state H_0 = 3 m T = 7.8 sec, values are consistent with those observed at Bogliasco and a maximum run-up deviation of 7.5 cm is recorded with a consequent difference in inundation level of 68.5 cm. Considering H_0 = 5.8 m and T = 11.8 sec, the decrease of the wave run-up becomes more accentuated with a maximum detected deviation of 38.7 cm and a consequent flood reduction greater than 3 m (table 5.10).

Table 5.9 – Summary of results of wave run-up and inland flooding calculations obtained by using numerical data of performed simulations at Bogliasco.

H = 3 m ; T = 7.8 sec							
Profile	Slope	No-friction R2%	Friction R2%	No-friction Xmax	Friction Xmax	Δ R2%	Δ Xmax
Bogliasco 1	0.20	2.28	2.22	11.40	11.08	0.064	0.318
Bogliasco 2	0.20	2.21	2.15	11.05	10.73	0.065	0.325
Bogliasco 3	0.40	4.14	4.00	10.35	9.99	0.145	0.361
Bogliasco 4	0.41	4.33	4.29	10.61	10.53	0.036	0.087
Bogliasco 5	0.45	4.81	4.79	10.63	10.58	0.025	0.054
Bogliasco 6	0.20	2.14	2.13	10.69	10.63	0.013	0.065
Bogliasco 7	0.91	9.47	9.42	10.42	10.37	0.050	0.055
Bogliasco 8	1.38	14.58	14.47	10.54	10.46	0.109	0.079
Bogliasco 9	0.23	2.58	2.57	11.38	11.34	0.010	0.045
Bogliasco 10	0.60	6.03	5.99	10.04	9.99	0.033	0.056

H = 5.8 m ; T = 11.8 sec							
Profile	Slope	No-friction R2%	Friction R2%	No-friction Xmax	Friction Xmax	Δ R2%	Δ Xmax
Bogliasco 1	0.20	4.39	4.26	21.97	21.29	0.135	0.674
Bogliasco 2	0.20	4.40	4.27	22.02	21.34	0.137	0.685
Bogliasco 3	0.40	8.76	8.56	21.89	21.41	0.192	0.480
Bogliasco 4	0.41	8.78	8.62	21.53	21.14	0.160	0.393
Bogliasco 5	0.45	9.62	9.49	21.24	20.96	0.128	0.282
Bogliasco 6	0.20	4.49	4.38	22.46	21.90	0.112	0.560
Bogliasco 7	0.91	19.30	19.14	21.26	21.07	0.168	0.185
Bogliasco 8	1.38	29.39	28.51	21.23	20.60	0.880	0.636
Bogliasco 9	0.23	5.01	4.97	22.09	21.94	0.035	0.156
Bogliasco 10	0.60	12.73	12.57	21.22	20.96	0.155	0.258

Table 5.10 – Summary of results of wave run-up and inland flooding calculations obtained by using numerical data of performed simulations at Porto Cesareo.

H = 3 m ; T = 7.8							
Profile	Slope	No-friction R2%	Friction R2%	No-friction Xmax	Friction Xmax	Δ R2%	Δ Xmax
Porto Cesareo 1	0.14	1.58	1.51	11.60	11.05	0.075	0.547
Porto Cesareo 2	0.06	0.86	0.83	14.73	14.19	0.032	0.548
Porto Cesareo 3	0.04	0.74	0.71	17.01	16.42	0.026	0.589
Porto Cesareo 4	0.15	1.63	1.61	11.14	11.03	0.016	0.112
Porto Cesareo 5	0.08	1.04	1.03	13.04	12.94	0.008	0.097
Porto Cesareo 6	0.06	0.80	0.78	13.69	13.47	0.013	0.225
Porto Cesareo 7	0.12	1.35	1.33	11.58	11.45	0.015	0.129

Porto Cesareo 8	0.06	0.88	0.87	14.08	14.00	0.005	0.078
Porto Cesareo 9	0.06	0.80	0.79	12.81	12.61	0.012	0.199
Porto Cesareo 10	0.11	1.15	1.08	10.04	9.49	0.063	0.550

H = 5.8 m; T = 11.8							
Profile	**Slope**	**No-friction R2%**	**Friction R2%**	**No-friction Xmax**	**Friction Xmax**	**Δ R2%**	**Δ Xmax**
Porto Cesareo 1	0.14	2.97	2.80	21.82	20.56	0.172	1.262
Porto Cesareo 2	0.06	1.51	1.39	25.84	23.87	0.115	1.968
Porto Cesareo 3	0.04	1.22	1.11	28.11	25.51	0.113	2.595
Porto Cesareo 4	0.15	3.13	2.98	21.47	20.38	0.158	1.085
Porto Cesareo 5	0.08	2.04	1.99	25.53	24.90	0.051	0.636
Porto Cesareo 6	0.06	1.62	1.56	27.88	26.73	0.067	1.156
Porto Cesareo 7	0.12	2.40	2.29	20.59	19.64	0.111	0.949
Porto Cesareo 8	0.06	1.69	1.62	27.16	25.99	0.073	1.168
Porto Cesareo 9	0.06	1.54	1.48	24.54	23.59	0.060	0.953
Porto Cesareo 10	0.11	1.76	1.38	15.47	12.07	0.387	3.395

In both sites, it is evident that the loss of natural elements capable of generating friction results in an increase in run-up and inundation, more or less pronounced depending on the bathymetric profile, the profile orientation and the extent of the various habitats along each profile.

The effects of this increase result in a potential increase of coastal risk and population and structures vulnerability. In addition to the particular shape of the coast line and the use of the coast, the extent of the potential damages is highly dependent on the degree of human settlement. To better clarify ideas, referring to the considered case studies, the effects of habitat loss on the inundation seem much more marked in Porto Cesareo (with the highest recorded increase in flooding of 3.39 m along the profile 10) than Bogliasco (with the highest recorded increase in flooding of 68.5 cm along the profile 2). But, if we analyze the position of the profiles along which the simulations were carried out and the corresponding inundation deviation between present scenario and degraded seabed scenario, at Bogliasco we note that the activities and building are much closer to the shoreline than Porto Cesareo. Consequently, at Bogliasco also a minimal increase of inundation due to habitat loss can significantly raise the risk of damages and the vulnerability of population.

In Porto Cesareo and along the considered profiles, most problems can be represented mainly by both beaches and dune erosion. In fact, the coast of Porto Cesareo is characterized by wide beaches landward bordered by a well-developed dune system. Near to town, however, the speculation in the past years caused the strong anthropization of the coastal zone and the construction of buildings in the immediate vicinity of the dune belt. This situation may cause an increase in coastal vulnerability as in the cases of the profiles 4 and 6 where the dune and the behind coastal vegetation were replaced by buildings thus causing a decrease in the beach amplitude. In this situation, the presence of submerged habitats, able to attenuate waves and consequently reduce the wave vertical growth and flooding, has an essential role in the mitigation of the coastal risk. In detail, analyzing results for the two scenarios along the profiles 4 and 6, we can observe how in the present scenario and in the strongest conditions considered, the presence of rugged habitats prevents the wave impact strikes streets and buildings. Where instead the dune system is almost intact, bathing facilities and the same dune system are subjected to greater risk. In particular along the profiles 5 and 2, an increase in flooding due to habitat loss, respectively of 64 cm and 197 cm, can cause the erosion of the base of the dune with consequent modification in the sedimentary budget of the beach.

6 DISCUSSIONS

The research can be divided into two main sections. Firstly, we illustrate a reliable and cost-effective method to measure seafloor roughness built up by both substrate and living organisms, as a proxy of the overall structural complexity, by means of underwater photogrammetry. This new alternative approach was able to overcome the main issues of traditional field techniques (e.g. resolution, slope effect, direct mechanical impact, etc.), while leading to an improved data quality. Results show that the new approach is able to characterize different features of the seafloor with higher resolution and accuracy at the same time reducing the effort during field activities. Furthermore, the method allows obtaining a measure in the metric system thus exploitable for several fields of application such as hydraulic engineering. We emphasize that adopting

standardized measures usable for several purposes can lead to advantages in terms of saving time and resources and, at the same time, allow the comparability of different datasets.

In the second section we highlighted the importance of including the term of bottom friction into wave propagation numerical model. Then, by using the calculated bottom roughness, we provide the first quantitative analysis of the role of different coastal habitats and in particular of coralligenous assemblages (infralittoral bank type) in reducing wave height and energy on the coastline in Mediterranean Sea.

6.1 Reconstruction of seabed morphology by using photogrammetry-based Structure from Motion techniques

The methodology here proposed make use of Structure from Motion (Sfm) photogrammetry for generating three-dimensional reconstructions of seafloor through which characterize small- and meso-scale topographic complexity and roughness of Mediterranean benthic seascapes. Usually in underwater environment structural complexity measurements were carried out through either traditional *in-situ* measurement techniques which require direct contact with the investigated surfaces (Risk, 1972; Mc Cormick, 1994; Carleton & Sammarco, 1987) or using extremely expensive instruments such as laser scan or micro-bathymetric sonar (Lefebvre et al., 2009; Friedman et al., 2012; Jaffe et al., 2001). Here we propose a completely free-contact method able to reduce time- cost- consumption during underwater activities while increasing safety for diving operators. This approach allows limiting field activities just to the acquisition of photographic samples and processing the acquired material in controlled environment by using a simple and automated workflow (fig. 4.17). Until few years ago the logistical advantages provided by SfM photogrammetry were overshadowed by both expensive equipment and long processing time. Today, the rapid technological development has made it possible to overcome the issues related to costs and computational demand, and speed up the modeling procedure.

Thus the results derived from SfM techniques, since exportable in several formats, can be used in combination with different tools (geospatial, statistical, graphics, etc.) to obtain increasingly precise and accurate estimates and/or to extract information (hardly be obtained by conventional techniques) which can be integrated into other research fields.

Despite the apparent simplicity of the workflow that allows the reconstruction of digital models, there are some aspects that need to be carefully considered. First, the choice of camera and lenses can greatly affect the final yield, especially in underwater environment where light conditions and visibility change daily and between different locations. Also it is important to define in advance the spatial scale at which the investigations have to be carried out. The spatial scale is closely dependent on the aim of the research and on the information that has to be highlighted. No less important is, during the processing phase, the choice of the mesh resolution. A coarse resolution can lead to an accuracy decrease, whereas a resolution that is too fine may generate noise in real-world surface reconstruction. 1-cm cell size resolution provides robust results and at the same time is enough versatile for small-, meso- and broad-scale surveys (Friedman et al., 2012). In the latter case, extra-computational effort could be required but, in the last years, the advances in technology made the process feasible. For micro-scale surveys it is recommended to use a smaller window size and a finer mesh resolution to avoid information loss.

This paper focus on structural complexity and roughness assessment of different seascapes, but the approach here concerted allows us to obtain information about a wide range of spatial properties of the surveyed seabed (slope, curvature, exposure, etc.) by using open-source tools or geospatial software usually purchased on the market. In addition, this methodology allows the extraction of third-generation photo-mosaics of surveyed seabed that could be used for the coverage estimation of benthic feature overcoming issues due to data collection during monitoring surveys. In our case the textured models allowed the recognition of features smaller than 5 cm on a total modeled area up to 90 m^2.

6.2 Effect of slope on roughness estimation

Slope has a strong effect on the calculation of seabed rugosity leading to overstate its value. For the two Area-based Rugosity indexes here contemplated, the larger the slope the smaller is the surface area obtained by projecting 3D surface into xy-plane, thus overstating the Area-based Rugosity index values. This issue can be avoided/overtaken by using some tricks on the field (as enunciated in the Methods).

The same behavior can be observed for all statistical absolute roughness measures. In this case, essential factor to take into account is the correct choice of the plane to which the measures have to be related. Simply considering the plane passing through the z-mean value, all amplitude parameters are affected by the slope effect. This means that the lower the slope is, the more estimated roughness values are closest to the real ones. This leads to an overestimation of roughness amplitude parameters that are larger the higher the slope. By using as reference the best-fit plane obtained through Principal Component Analysis (PCA) and rotating appropriately the original point cloud so that the new fitting plane is parallel to xy-plane, the slope effect can be easily removed. Unlike Area-based Rugosity Index, this procedure can be performed for any scaled surface regardless of its actual inclination. In light of above, we conclude that the roughness estimation by using statistical absolute measure approach leads to an homogenization of calculated values while reducing errors and time-consumption intrinsically linked to sampling activities.

6.3 Roughness as seabed structural complexity measure

We tested different methods for quantifying structural complexity of the substrates and we compared them with each other to understand the ability in distinguishing between various seascapes. The comparison of the six measures of surface complexity here considered shows that all methods were able to discriminate between surfaces with different structural reliefs (topography). These are strongly dependent on both geological setting of the surveyed location and the presence of both abiotic (natural or artificial) and biotic features (benthic living organisms). In this respect,

the roughness measures here contemplated can provide a description of the habitats complexity inhabiting the seabed and information about their health status. Hence, we expected that habitats hosting benthic living organisms able to increase the substrate heterogeneity through their own physical structure, such as biogenic habitats, also show higher values of roughness. Effectively, in our study we found that coralligenous assemblage ever exhibited the greatest value of surface roughness/complexity followed by respectively infralittoral photophylous algae and sandy bottom. Correlation analysis between benthic coverage and roughness measures for different locations shows an increase structural complexity in the direction of coralligenous habitat, providing a further confirmation of what previously stated. Furthermore, precious information concerning the health conditions and the importance of the impacts affecting different benthic habitat can be gathered. Comparing results for different sites it is clear that, for equal habitat, the rugosity value is greater where a lower impact is recorded and, consequently, where it is assumed that the habitat is in better conditions. This evidence suggests that stress factors can inhibit bio-builder forces or reduce structural complexity leading to loss of microhabitat and ecological niches, and thus decreasing diversity, specific richness and abundance of living organisms.

In our opinion and as a consequence of the obtained results, all techniques showed results very similar to each other with the exception of z-mean value $\mu(z)$ which would fail to distinguish between two surfaces where one is smooth but characterized by few large peaks and the other is composed by corrugations of the same amplitude. However it is important to emphasize that even the application of K_{max} can easily lead to an overestimation of the roughness parameter if used for not particularly homogenous surfaces, being simply the difference between the highest peak and the lowest valley of the asperities. Nevertheless it can be useful to highlight areas within the sampled surface whose complexity value significantly deviates. Both Area-Based Rugosity Index methods (*Full DSM* and *Simplified DSM*) performed consistently well, scoring the highest correlation values, but *Full DSM* provides the best results. This evidence could be considered a confirmation that photogrammetric techniques and a more accurate reconstruction of the substrates, taking into

account even holes and caves not included in DEMs, further refine and improve the estimate values thus approaching more closely the reality. However, the latter two measures are no more than a ratio of areas and therefore, by the nature of their calculation, the result is a dimensionless quantity difficult to compare with other measures and/or unlikely usable for different tasks and fields of application. Also the remaining two indices here considered, R_q and R_a, are significant and both exhibit high correlation value, each one explaining more than 37% of the observed variability. The latter are metric measurements and therefore usable for various purpose in several field of application and can be integrated in different engineering or mathematical models. In addition, once obtained the 3D model and extrapolated the information in the numerical format, statistical surface roughness approach provides the possibility to easily perform a broad range of calculation and statistical analysis useful to deepen the characteristics/properties of the surface. With respect to statistical surface roughness measures, in our opinion square root of the arithmetic mean of the square of asperity heights from the mean plane (R_q) would be preferable to the others because of its capability to provide robust results regarding the characterization of seabed complexity and because it is a widely recognized roughness length already employed in several studies. The example previously presented is just one of many applications for which an accurate estimation of structural complexity of the substrate is useful. The integration of different techniques and tools provides the means for a more accurate and precise characterization of topographic complexity at different spatial scales and broadens the perspectives for a wider use of this length. The inclusion of parameters referring to seabed topography in the models, whether they are environmental or engineering, as factors that affect events and natural processes can lead to an improvement of the model's results and to a deeper understanding of phenomena at the basis of those processes. For instance, predictive modeling for the distribution of living organism, habitats, biomass or biodiversity recently developed often requires geophysical substrate properties information (among them even rugosity) for running the calculation (Zapata et. al. 2014, Martin et al. 2015).

Given the heterogeneity of the disciplines in which roughness and complexity estimation is requested, the SfM photogrammetry and the analytical method described in this paper can provide the basis for the development of a standardized and shared procedure for roughness calculation. Sharing and exchange of data between different disciplines can be an advantage for future research by reducing time and cost consumption and allowing further comparisons.

6.4 Relationship with equivalent hydraulic roughness

Many hydrodynamic processes that occur in the coastal region are examined by process-based numerical modelling techniques being able to reproduce the main phenomena involved in the wave propagation toward the coastline. Wave modeling attempts to depict the sea state and predict the evolution of waves' energy (and/or waves' changes) using numerical simulation. These numerical methods are useful to obtain solutions within the continuous spatio-temporal domain and are increasingly being used in place of traditional physical models because of their versatility, reliability and cheapness. The most of the research effort in this field has the purpose of merely studying wave transformation and sediment transport processes, taking into account morphological characteristics of the seabed (usually only bathymetry) and including forcing by winds, waves or currents. Furthermore, most of these works assess the dissipation effect due to the turbulence associated with breaking waves. During the last years, several authors highlighted the relevance of considering dissipation due to bottom friction. The latter can be a relevant term even in relatively deep water where the presence of natural structures that rise from the seabed greatly increases the hydraulic roughness value, and consequently the wave friction factor and the drag coefficient on the bottom. In this context, coastal ecosystem and biogenic habitat could play crucial role in coastal protection reducing vulnerability of coastal communities to natural hazards and climate change (Spalding et al., 2014). This contribution rises the importance of coastal ecosystems already largely recognize (UNEP, 2011), and could be useful for quantifying the economic value of services

provided in terms of coastal protection in order to integrate these values into socio-economic analyses (Barbier et al. 2008; Koch et al. 2009; Guannel et al., 2011).

Recent works highlight the utility of using the bottom roughness for better calculating the friction factor and the drag coefficient (e.g. Infantes et al., 2012; Lowe et al., 2005). The main issue is that for those hydrodynamic models that consider dissipation term due to bottom friction, a hydraulic roughness K_w must be specified and it depends on particular characteristics of surveyed sites, besides it could be different also within the same site being made up of a mosaic of several habitats. Theoretically, K_w can be calculated indirectly from wave attenuation measurement as typical approach, but it would be preferable specify hydraulic roughness length based on physical roughness of the seabed (Lowe et al. 2005).

6.5 Process-based numerical models and run-up calculation

Comparing results from several process-based numerical models at two case studies we show that during extreme events dissipation effects due to phenomena other than breaking waves range between 9.6% and 11.5% for steep seafloors and between 20.4% and 35.8% for mild-slope seafloors. The attenuation due to bottom friction alone represents approximately 11-16% of no-breaking dissipation forces at steep case study and 13-19% at mild-slope one.

An in-deep analysis specific on considered habitat shows that sections of seafloors with higher values of bottom roughness attenuate wave height before breaking more effectively than low-rugged seafloors reducing more the energy reaching the coastline. In particular, during the simulations we used the highest equivalent roughness value found in the literature for *P. oceanica* meadows and we compared results with those obtained by using *in-situ* roughness values of coralligenous assemblages. Results show that during extreme events, at the same depth range, the effectiveness of coralligenous assemblages in wave attenuation within no-breaking zone is increased between 0.44% and 0.93% compared to *P. oceanica* meadows for steep seabed and

between 0.93% and 1.37% for mild-slope seabed. This means that even and especially coralligenous assemblages, in certain conditions, contribute to wave attenuation mostly within no-breaking zone where usually are located. This remark can be useful in terms of provision of ecosystem services and environmental accounting computations.

The wave attenuation benefits provided by the coralligenous assemblages are here considered for the first time. On the contrary there are many studies concerning *P. oceanica* beds that quantify also in monetary terms the value of this ecosystem service provided by seagrass meadows and the consequences that their loss may cause. This little interest towards coralligenous is due to its typical deeper range depth. Anyway, peculiar coralligenous outcrops can be found also at shallow depths. Likewise for coralligenous assemblages, the approach here described can lead to the estimation of the value of the role that it assumes in coastal erosion prevention and reduction of risks associated to extreme events.

Furthermore habitat degradation has significant impacts on bottom roughness which influences bottom friction. Through run-up calculation and resulting inland flooding for both no-friction and with-friction wave propagation models we want to highlight some of the consequences that habitat degradation and/or loss may have on coastal dynamics. These aspects should be taken into account by coastal managers and serve as incentive to promote new tools to improve resource use planning and risk assessment associated with the coastal region. Understanding the role of coastal habitats in coastal defense is an essential step for well defining benefits associated to ecosystem services provided, understand conservation priorities and investments, and implement appropriate actions targeted to the preservation/restoration of these seascapes. The definition of these services and of how and when to restore them needs to be addressed in greater details and in an integrated way. This requires an inter-disciplinary approach and therefore a greater collaboration between several professionals such as ecologists, geologists, engineers and cartographers.

7 CONCLUSIONS

The research work attempts to fill some of the gaps concerning coastal biogenic habitats in the Mediterranean area, with particular regard to coralligenous assemblages. Besides the gap in the amount of research on biogenic habitats carried out in tropical and Mediterranean areas, a lack of knowledge exists on the effect of Mediterranean coastal habitat in influencing wave propagation and the sedimentary dynamics (except for *P. oceanica* meadows).

In the first part of the research, we described an innovative method based on photogrammetry by which to characterize the structural complexity and roughness of hard seabed. The method is able to solve practical issues related to traditional techniques reducing time- and cost-consumption during field activities and thus increasing safety of diving operators, while increasing resolution and accuracy of the collected data and eliminating the error due to the slope of the sampled surfaces. We emphasize how statistical absolute roughness measures can have wide applications in several fields, as well as providing a good estimate of the structural complexity of the seabed.

Furthermore, the tested roughness measures not only can provide a description of the habitat complexity but also information about habitat health status, especially for habitat sensitive to mechanical impacts such as coralligenous. Among the different roughness measurements we chose the root mean square of roughness amplitude (R_q) as it allowed to be converted into equivalent hydraulic roughness which can be embedded into wave propagation numerical models.

In the second part, by integrating the seabed roughness in the numerical models, we showed as different benthic habitats characterized by different structural complexity can influence the wave propagation and the amount of energy reaching the shoreline. For mild slope seabed and dissipative beaches, the effects of bottom roughness appear more evident and the presence of highly rugged habitats (such as coralligenous and *Posidonia oceanica*) decreases the susceptibility of the coastal areas to be affected by either inundation or erosion. For steeper seabed and reflective beaches, the protective function of biogenic habitat seems to be less pronounced but still significant compared to the previous case study. Beyond these observations, we emphasize that the obtained findings need

to be contextualized with respect of territorial setting of the considered coastal zone. In this regard, we showed as the seabed degradation will lead to a reduction of mitigation properties of habitats thus affecting the vulnerability of coastal communities. Our results also demonstrated the usefulness of characterizing in detail the structural complexity of coastal habitats as critical factor conditioning also abiotic processes.

Despite the significant findings, the performed process-based numerical models allowed obtaining wave parameters only along 1-Dimensional directional profiles. Further research is needed for including frictional dissipation factor into 2D and/or 3D hydrodynamic models able to provide results in a continuous spatial domain. This will allow the integration of numerical results into GIS environment for modelling run-up and inundation processes along the entire coastline. Despite this limitation, even just the visualization of results can help to better identify possible hazards, their causes and the best solutions to be undertaken.

Moreover, for the first time we demonstrated the role played by the coralligenous concretions in coastal zone protection. Our results provide the first estimation the coralligenous value in coastal protection and give us a more complete picture of the ecosystem services provided by this Mediterranean habitat. During storms and/or extreme conditions and under certain circumstances, coralligenous assemblages can dissipate more wave energy via bottom friction than *P. oceanica* meadow. Especially during winter, when the seagrass loses its leaves, coralligenous can act more effectively on wave dissipation, being a permanent hard substrate.

Our research also demonstrates the importance of taking integrated and placed-based approaches when quantifying the services supplied by ecosystems. In fact, especially coastal protection services vary as a function of local environmental setting and forcing conditions (Kock et al. 2009; Guannel et al. 2016) and no generalizations should be made.

In conclusion, the definition of ecosystem services and their benefits requires an interdisciplinary approach for a better understanding of the interactions between physical and biological processes

that characterize the coastal marine environment. This can lead to a better understanding of action priorities resulting in an improvement in the management of available financial resources.

8 AKNOWLEDGEMENTS

The work and the field activities were partially supported and financed by UBICA srl (Genoa, IT). Thanks to Liguria Region for cartographic data. We would also like to express our gratitude to "Porto Cesareo" Marine Protected Area Director Paolo D'Ambrosio (Lecce, IT) for supporting field activities within the MPA and for sharing multibeam bathymetric data, habitat distribution maps and LIDAR data. The multibeam bathymetric data and habitat distribution data of "Porto Cesareo" MPA were collected within BIOMAP Project ("BIOcostruzioni Marine in Puglia" in the framework of P.O. FESR 2007/2013 Program – ASSE IV. Linea 4.4 – Interventi per la rete ecologica) and COCONET Project ("Coast to Coast NETworks of marine protected areas -from the shore to the high and deep sea-, coupled with sea-based wind energy potential" within 7th Framework Progamme (FP7/2007-2013) under grant agreement No 287844). We are also very grateful to "Porto Cesareo" MPA's Staff for their logistical support during field activities and in particular Sergio Fai and Ilario (Lecce, IT). We are also grateful to Massimo Ponti (Ravenna, IT) for his suggestions in statistical analysis and his inputs. Special thanks to Ilaria dalle Mura (Genoa, IT) for her support during field activities and her contribution in collecting data and reviewing the manuscript.

9 REFERENCES

Adams, T., Grant, C., & Watson, H. (2012). A simple algorithm to relate measured surface roughness to equivalent sand-grain roughness. Journal ISSN, 2929, 2724.

Agisoft, L. L. C. (2014). Agisoft PhotoScan User Manual: Professional Edition.

Agnesi, S., Annunziatellis, A., Cassese, M. L., La Mesa, G., Mo, G., & Tunesi, L. (2009, June). State of knowledge of the geographical distribution of the coralligenous and other calcareous bio-concretions in the Mediterranean. In Mediterranean Action Plan. 9th Meeting of Focal Points for SPAs. Floriana, Malta (pp. 3-6).

Alexander, L. V., Hope, P., Collins, D., Trewin, B., Lynch, A., & Nicholls, N. (2007). Trends in Australia's climate means and extremes: a global context. Australian Meteorological Magazine, 56(1), 1-18.

Alexander, L. V., & Arblaster, J. M. (2009). Assessing trends in observed and modelled climate extremes over Australia in relation to future projections. International Journal of Climatology, 29(3), 417-435.

Allison, I., Bindoff, N. L., Bindschadler, R. A., Cox, P. M., de Noblet, N., England, M. H., Francis, J.E., Gruber, N., Haywood, A.M., Karoly, D.J., Kaser, G., Le Quéré, C., Lenton, T.M., Mann, M.E., Mc Neil, B.I., Pitman, A.J., Rahmstorf, S., Rignot, E.,Schellnhuber, H.J., Schneider, S.H., Sherwood, S.C., Somerville, R.C.J., Steffen, K., Steigh, E.J., Visbeck, M., Weaver, A.J. (2009). The Copenhagen Diagnosis: Updating the world on the latest climate science. The University of New South Wales Climate Change Research Centre (CCRC), Sydney, Australia, 60pp.

Alongi, D. M. (2008). Mangrove forests: resilience, protection from tsunamis, and responses to global climate change. Estuarine, Coastal and Shelf Science, 76(1), 1-13.

Altinok, Y., & Ersoy, Ş. (2000). Tsunamis observed on and near the Turkish coast. Natural Hazards, 21(2-3), 185-205.

Anderson, M. J. (2001). Permutation tests for univariate or multivariate analysis of variance and regression. Canadian journal of fisheries and aquatic sciences, 58(3), 626-639.

Anonymous (1975). Instrument for the measurement of surface roughness by profile methods. ISO3274, International Standardization Organization.

Anonymous (1985). Surface texture (Surface Roughness, Waviness and lay). ANSI/ASME B46.1, ASME, New York.

Asano, T., Tsutsui, S., & Sakai, T. (1988). Wave damping characteristics due to seaweed. In Procceedings of 25th Coastal Engineering Conference in Japan (pp. 138-142).

Ballesteros, E. (2006). Mediterranean coralligenous assemblages: a synthesis of present knowledge. Oceanogr. Mar. Biol. Annu. Rev. 44, 123-195.

Barbier, E. B., Koch, E. W., Silliman, B. R., Hacker, S. D., Wolanski, E., Primavera, J., Granek, E.F., Polasky, S., Aswani, S., Cramer, L.A., Stoms, D.M., Kennedy, C.J., Bael, D., Kappel, C.V., Perillo, G.M.E., & Reed, D.J. (2008). Coastal ecosystem-based management with nonlinear ecological functions and values. science, 319(5861), 321-323.

Bayram, A., Camenen, B., & Larson, M. (2003). Equivalent roughness under sheet flow conditions. In Proc. Coastal Sediment (Vol. 3).

Bellan-Santini, D., Bellan, G., Bitar, G., Harmelin, J., & Pergent, G. (2002). Handbook for interpreting types of marine habitat for the national inventories of natural sites of conservation interest. UNEP Action Plan for the Mediterranean, 1-216.

Bellan-Santini, D., Bellan, G., Bitar, G., Harmelin, J. G., & Pergent, G. (2007). Handbook for interpreting types of marine habitat for the selection of sites to be included in the national inventories of natural sites of conservation interest.

Bender, M. A., Knutson, T. R., Tuleya, R. E., Sirutis, J. J., Vecchi, G. A., Garner, S. T., & Held, I. M. (2010). Modeled impact of anthropogenic warming on the frequency of intense Atlantic hurricanes. Science, 327(5964), 454-458.

Bharat, B. (2000). Surface Roughness Analysis and Measurement Techniques. Modern Tribology Handbook, Two Volume Set.

Blasi, F. (2009). The economic value of the Posidonia oceanica meadows. Biologia Marina Mediterranea, 16(1), 130-131.

Borsje, B. W., van Wesenbeeck, B. K., Dekker, F., Paalvast, P., Bouma, T. J., van Katwijk, M. M., & de Vries, M. B. (2011). How ecological engineering can serve in coastal protection. Ecological Engineering, 37(2), 113-122.

Bosello, F., Nicholls, R. J., Richards, J., Roson, R., & Tol, R. S. (2012). Economic impacts of climate change in Europe: sea-level rise. Climatic Change, 112(1), 63-81.

Boström, C., Pittman, S. J., Simenstad, C., & Kneib, R. T. (2011). Seascape ecology of coastal biogenic habitats: advances, gaps, and challenges. Marine Ecology Progress Series, 427, 191-217.

Bouma, T. J., De Vries, M. B., Low, E., Peralta, G., Tánczos, I. V., van de Koppel, J., & Herman, P. J. (2005). Trade-offs related to ecosystem engineering: A case study on stiffness of emerging macrophytes. Ecology, 86(8), 2187-2199.

Bradley, K., & Houser, C. (2009). Relative velocity of seagrass blades: Implications for wave attenuation in low-energy environments. Journal of Geophysical Research: Earth Surface, 114(F1).

Brown, S., Barton, M., & Nicholls, R. (2011). Coastal retreat and/or advance adjacent to defences in England and Wales. Journal of Coastal Conservation, 15(4), 659-670.

Camenen, B., Bayram, A., & Larson, M. (2006). Equivalent roughness height for plane bed under steady flow. Journal of Hydraulic Engineering, 132(11), 1146-1158.

Camenen, B., Larson, M., & Bayram, A. (2009). Equivalent roughness height for plane bed under oscillatory flow. Estuarine, Coastal and Shelf Science, 81(3), 409-422.

Canals, M., & Ballesteros, E. (1997). Production of carbonate particles by phytobenthic communities on the Mallorca-Menorca shelf, northwestern Mediterranean Sea. Deep Sea Research Part II: Topical Studies in Oceanography, 44(3), 611-629.

Carleton, J. H., & Sammarco, P. W. (1987). Effects of substratum irregularity on success of coral settlement: quantification by comparative geomorphological techniques. Bulletin of Marine Science, 40(1), 85-98.

Cazenave, A., & Llovel, W. (2010). Contemporary sea level rise. Annual review of marine science, 2, 145-173.

Cerrano, C., Bavestrello, G., Bianchi, C. N., Cattaneo-Vietti, R., Bava, S., Morganti, C., ... & Siccardi, A. (2000). A catastrophic mass-mortality episode of gorgonians and other organisms in the Ligurian Sea (North-western Mediterranean), summer 1999. Ecology letters, 3(4), 284-293.

Cerrano, C., Bavestrello, G., Bianchi, C. N., Calcinai, B., Cattaneo-Vietti, R., Morri, C., & Sarà, M. (2001). The role of sponge bioerosion in Mediterranean coralligenous accretion. In Mediterranean Ecosystems (pp. 235-240). Springer Milan.

Cerrano, C., Cardini, U., Bianchelli, S., Corinaldesi, C., Pusceddu, A., & Danovaro, R. (2013). Red coral extinction risk enhanced by ocean acidification. Scientific reports, 3, 1457.

Cerrano, C., Bertolotto, R., Coppo, S., Palma, M., Pantaleo, U., Valisano, L., Bavestrello, G., Ponti, M. (2014). Assessment of coralligenous assemblages status in the Ligurian sea. 2nd Mediterranean Symposium on the conservation of Coralligenous & other Calcareous Bio-Concretions (Portorož, Slovenia, 29-30 October 2014).

Church, J. A., White, N. J., Coleman, R., Lambeck, K., & Mitrovica, J. X. (2004). Estimates of the regional distribution of sea level rise over the 1950-2000 period. Journal of climate, 17(13), 2609-2625.

Church, J. A., & White, N. J. (2006). A 20th century acceleration in global sea-level rise. Geophysical research letters, 33(1).

Clarke, K. R., & Gorley, R. N. (2006). User manual/tutorial. Primer-E Ltd., Plymouth, 93.

Clarke, T. A., & Fryer, J. G. (1998). The development of camera calibration methods and models. The Photogrammetric Record, 16(91), 51-66.

Cokelet, E. D. (1977). Steep gravity waves in water of arbitrary uniform depth. Philosophical Transactions of the Royal Society of London A: Mathematical, Physical and Engineering Sciences, 286(1335), 183-230.

Creel, L. (2003). Ripple effects: population and coastal regions (pp. 1-7). Washington, DC: Population Reference Bureau.

Crowder, L. B., & Cooper, W. E. (1982). Habitat structural complexity and the interaction between bluegills and their prey. Ecology, 63(6), 1802-1813.

Dahdouh-Guebas, F., Jayatissa, L. P., Di Nitto, D., Bosire, J. O., Seen, D. L., & Koedam, N. (2005). How effective were mangroves as a defence against the recent tsunami?. Current biology, 15(12), R443-R447.

Diviacco, G., & Coppo, S. (2006). Atlante degli habitat marini della Liguria: descrizione e cartografia delle praterie di Posidonia oceanica e dei principali popolamenti marini costieri. Regione Liguria. Servizio Parchi e Aree protette. Settore Ecosistema Costiero.

Domingues, C. M., Church, J. A., White, N. J., Gleckler, P. J., Wijffels, S. E., Barker, P. M., & Dunn, J. R. (2008). Improved estimates of upper-ocean warming and multi-decadal sea-level rise. Nature, 453(7198), 1090-1093.

Drap, P., Merad, D., Mahiddine, A., Seinturier, J., Gerenton, P., Peloso, D., ... & Garrabou, J. (2013). Automating the measurement of red coral in situ using underwater photogrammetry and coded targets. In XXIV International CIPA Symposium, Strasbourg, France. Pierre Grussenmeyer (Ed.) (Vol. 5, p. W2).

Elgar, S., & Raubenheimer, B. (2008). Wave dissipation by muddy seafloors. Geophysical Research Letters, 35(7).

Elginoz, N., Kabdasli, M. S., & Tanik, A. (2011). Effects of Posidonia oceanica seagrass meadows on storm waves. Journal of Coastal Research, 64, 373-377.

Elsner, J. B., Kossin, J. P., & Jagger, T. H. (2008). The increasing intensity of the strongest tropical cyclones. Nature, 455(7209), 92-95.

Elwany, M. H. S., O'Reilly, W. C., Guza, R. T., & Flick, R. E. (1995). Effects of Southern California kelp beds on waves. Journal of waterway, port, coastal, and ocean engineering, 121(2), 143-150.

Eriksson, B. K., Rubach, A., & Hillebrand, H. (2006). Biotic habitat complexity controls species diversity and nutrient effects on net biomass production. Ecology, 87(1), 246-254.

European Commission (2007). Report to the European Parliament and the Council: An evaluation of Integrated Coastal Zone Management (ICZM) in Europe. COM(2007) 308 final.

Fang, J., Sun, S., & Shi, P. (2014). Assessment and mapping of potential storm surge impacts on global population and economy. International Journal of Disaster Risk Science, 5(4), 323-331.

Faulkner, B. (2001). Towards a framework for tourism disaster management. Tourism management, 22(2), 135-147.

Ferrario, F., Beck, M. W., Storlazzi, C. D., Micheli, F., Shepard, C. C., & Airoldi, L. (2014). The effectiveness of coral reefs for coastal hazard risk reduction and adaptation. Nature communications, 5, 3794.

Folkard, A. M. (2005). Hydrodynamics of model Posidonia oceanica patches in shallow water. Limnology and Oceanography, 50(5), 1592.

Fredsøe, J., Andersen, K. H., & Sumer, B. M. (1999). Wave plus current over a ripple-covered bed. Coastal Engineering, 38(4), 177-221.

Friedman, A., Pizarro, O., Williams, S. B., & Johnson-Roberson, M. (2012). Multi-scale measures of rugosity, slope and aspect from benthic stereo image reconstructions. PloS one, 7(12), e50440.

Gacia, E., & Duarte, C. M. (2001). Sediment retention by a Mediterranean Posidonia oceanica meadow: the balance between deposition and resuspension. Estuarine, coastal and shelf science, 52(4), 505-514.

Garrabou, J., & Ballesteros, E. (2000). Growth of Mesophyllum alternans and Lithophyllum frondosum (Corallinales, Rhodophyta) in the northwestern Mediterranean. European Journal of Phycology, 35(1), 1-10.

Geeraerts, J., Kortenhaus, A., González-Escrivá, J. A., De Rouck, J., & Troch, P. (2009). Effects of new variables on the overtopping discharge at steep rubble mound breakwaters—The Zeebrugge case. Coastal Engineering, 56(2), 141-153.

Ghisalberti, M., & Nepf, H. M. (2002). Mixing layers and coherent structures in vegetated aquatic flows. Journal of Geophysical Research: Oceans, 107(C2).

Gintert, B., Gleason, A. C. R., Cantwell, K., Gracias, N., Gonzalez, M., & Reid, R. P. (2012). Third-generation underwater landscape mosaics for coral reef mapping and monitoring. In Proceedings of the 12th international coral reef symposium, Cairns, Australia.

Gleason, K. L., Lawrimore, J. H., Levinson, D. H., Karl, T. R., & Karoly, D. J. (2008). A revised US climate extremes index. Journal of Climate, 21(10), 2124-2137.

Goda, Y., 1974. A new wave pressure formulae for composite breakwaters. In: Proceedings of 14th International Conference on Coastal Engineering, Copenhagen, Denmark, pp. 1702–1720.

Graham, N. A. J., & Nash, K. L. (2013). The importance of structural complexity in coral reef ecosystems. Coral Reefs, 32(2), 315-326.

Granata, T. C., Serra, T., Colomer, J., Casamitjana, X., Duarte, C. M., & Gacia, E. (2001). Flow and particle distributions in a nearshore seagrass meadow before and after a storm. Marine ecology progress series, 218, 95-106.

Grant, W. D., & Madsen, O. S. (1982). Movable bed roughness in unsteady oscillatory flow. Journal of Geophysical Research: Oceans, 87(C1), 469-481.

Gratwicke, B., & Speight, M. R. (2005). Effects of habitat complexity on Caribbean marine fish assemblages. Marine Ecology Progress Series, 292, 301-310.

Grilli, S. T., Voropayev, S. I., Testik, F. Y., & Fernando, H. J. S. (2003, January). Numerical Modeling And Experiments Of Wave Shoaling Over Semi-buried Cylinders In Sandy Bottom. In

The Thirteenth International Offshore and Polar Engineering Conference. International Society of Offshore and Polar Engineers.

Grinsted, A., Moore, J. C., & Jevrejeva, S. (2010). Reconstructing sea level from paleo and projected temperatures 200 to 2100 AD. Climate Dynamics, 34(4), 461-472.

Guannel, G., Arkema, K., Verutes, G., Guerry, A., Kim, C. K., Papenfus, M., Ruckelshaus, M., & Toft, J. (2011). Using Natural Habitats to Mitigate the Impact of Coastal Hazards and Inform Management Decisions. In Solutions to Coastal Disasters 2011 (pp. 233-245).

Guannel, G., Ruggiero, P., Faries, J., Arkema, K., Pinsky, M., Gelfenbaum, G., Guerry, G., & Kim, C. K. (2015). Integrated modeling framework to quantify the coastal protection services supplied by vegetation. Journal of Geophysical Research: Oceans, 120(1), 324-345.

Guannel, G., Arkema, K., Ruggiero, P., & Verutes, G. (2016). The power of three: coral reefs, seagrasses and mangroves protect coastal regions and increase their resilience. PloS one, 11(7), e0158094.

Harris, J. C., & Grilli, S. T. (2014). Large eddy simulation of sediment transport over rippled beds. Nonlinear Processes in Geophysics, 21(6), 1169-1184.

Harris, D. L., & Vila-Concejo, A. (2013). Wave transformation on a coral reef rubble platform. Journal of Coastal Research, 65(sp1), 506-510.

Hauser, A., Attrill, M. J., & Cotton, P. A. (2006). Effects of habitat complexity on the diversity and abundance of macrofauna colonising artificial kelp holdfasts. Marine Ecology Progress Series, 325, 93-100.

He, H., Ferrari, R., McKinnon, D., Roff, G., Mumby, P., Smith, R., & Upcroft, B. (2012, July). Measuring reef complexity and rugosity from monocular video bathymetric reconstruction. In Proceedings of the 12th International Coral Reef Symposium (pp. 1-5). James Cook University.

Hendriks, I. E., Sintes, T., Bouma, T. J., & Duarte, C. M. (2008). Experimental assessment and modeling evaluation of the effects of the seagrass Posidonia oceanica on flow and particle trapping. Marine Ecology Progress Series.

Hinrichsen, D. (1999, January). The coastal population explosion. In Trends and Future Challenges for US National Ocean and Coastal Policy: Proceedings of a Workshop (Vol. 22, pp. 27-29). Washington, DC: NOAA, January 22, 1999.

Hoyos, C. D., Agudelo, P. A., Webster, P. J., & Curry, J. A. (2006). Deconvolution of the factors contributing to the increase in global hurricane intensity. Science, 312(5770), 94-97

Hov, Ø., Cubasch, U., Fischer, E., Höppe, P., Iversen, T., Gunnar Kvamstø, N.,Kundzewicz W., Z, Rezacova, D., Rios, D., Duarte Santos, F., Schadler, B., Veisz, O. B.,Zerefos, C., Benestad, R., Murlis, J., Donat, M., Leckebusch C., G. & Ulbrich, U. (2013). Extreme weather events in Europe: Preparing for climate change adaptation. Oslo: Norwegian Meteorological Institute.

Hurther, D., & Chassagneux, F. X. (2013). Turbulence and bed shear stress estimations below irregular breaking waves over a mobile sediment bed.

Infantes, E., Orfila, A., Simarro, G., Terrados, J., Luhar, M., & Nepf, H. (2012). Effect of a seagrass (Posidonia oceanica) meadow on wave propagation. Marine Ecology Progress Series, 456, 63-72.

Ingebritsen, S. E., & Galloway, D. L. (2014). Coastal subsidence and relative sea level rise. Environmental Research Letters, 9(9), 091002.

Intergovernmental Oceanographic Commission of UNESCO, (2012). Coastal Management Approaches for Sea-level Related Hazards: Case Studies and Good Practices. (IOC Manuals and Guides, 61) 46 pp. (English.) (IOC/2012/MG/61Rev.).

IPCC, (2001). Climate Change 2001: the Scientific Basis.Contribution of Working Group I to the Third Assessment Report of the Intergovernmental Panel on Climate Change. Cambridge University Press, Cambridge, United Kingdom and New York, NY, USA, 881 pp.

IPCC. 2007. Fourth Assessment Report (AR4), Climate Change 2007: The Physical Science Basis, Contribution of Working Group I to the Fourth Assessment Report of the Intergovernmental Panel on Climate Change, ed. S Solomon et al. Cambridge, UK: Cambridge Univ. Press.

Ishii, M., & Kimoto, M. (2009). Reevaluation of historical ocean heat content variations with time-varying XBT and MBT depth bias corrections. Journal of Oceanography, 65(3), 287-299.

Jackson, G. A. (1984). Internal wave attenuation by coastal kelp stands. Journal of Physical Oceanography, 14(8), 1300-1306.

Jaffe, J. S., Moore, K. D., McLean, J., & Strand, M. P. (2001). Underwater optical imaging: status and prospects. Oceanography, 14(3), 66-76.

Jevrejeva, S., Grinsted, A., & Moore, J. C. (2009). Anthropogenic forcing dominates sea level rise since 1850. Geophysical Research Letters, 36(20).

Jevrejeva, S., Moore, J. C., & Grinsted, A. (2010). How will sea level respond to changes in natural and anthropogenic forcings by 2100?. Geophysical research letters, 37(7).

Jevrejeva, S., Moore, J. C., & Grinsted, A. (2012). Sea level projections to AD2500 with a new generation of climate change scenarios. Global and Planetary Change, 80, 14-20.

Jones, C. G., Lawton, J. H., & Shachak, M. (1994). Organisms as ecosystem engineers. In Ecosystem management (pp. 130-147). Springer New York.

Kamphuis, J. W. (1974). Determination of sand roughness for fixed beds. Journal of Hydraulic Research, 12(2), 193-203.

Kamphuis, J. W. (1975). Friction factor under oscillatory waves. Journal of the Waterways, Harbors and Coastal Engineering Division, 101(2), 135-144.

Kandlikar, S. G. (2005). Roughness effects at microscale–reassessing Nikuradse's experiments on liquid flow in rough tubes. Bull Acad Sci, 53.

Kim, J. H., Pyeon, M. W., Eo, Y. D., & Jang, I. W. (1920). An experiment of three-dimensional point clouds using GoPro. Screen, 2704(1440).

Koch, E. W., Barbier, E. B., Silliman, B. R., Reed, D. J., Perillo, G. M., Hacker, S. D., Granek, E. F., Primavera, J. H., Muthiga, N., Polasky, S., Halpern, B. S., Kennedy, C. J., Kappel, C. V. & Wolanski, E. (2009). Non-linearity in ecosystem services: temporal and spatial variability in coastal protection. Frontiers in Ecology and the Environment, 7(1), 29-37.

Kofoed, J. P. (2002). Wave Overtopping of Marine Structures: utilization of wave energy (Doctoral dissertation, Videnbasen for Aalborg UniversitetVBN, Aalborg UniversitetAalborg University, Det Teknisk-Naturvidenskabelige FakultetThe Faculty of Engineering and Science, Institut for Vand, Jord og MiljøteknikDepartment of Civil Engineering).

Koftis, T., Prinos, P., & Stratigaki, V. (2013). Wave damping over artificial Posidonia oceanica meadow: A large-scale experimental study. Coastal Engineering, 73, 71-83.

Komen, G. J., Cavaleri, L., Donelan, M., Hasselmann, K., Hasselmann, S., & Janssen, P., A., E., M. (1994). Dynamics and Modelling of Ocean Waves. Cambridge University Press, 532 pp.

Kunkel, C. M., Hallberg, R. W., & Oppenheimer, M. (2006). Coral reefs reduce tsunami impact in model simulations. Geophysical Research Letters, 33(23).

Laborel, J. (1987). Marine biogenic constructions in the Mediterranean: a review. Sci Rep Port-Cros Natl Park, 13, 97-126.

Lavy, A., Eyal, G., Neal, B., Keren, R., Loya, Y., & Ilan, M. (2015). A quick, easy and non-intrusive method for underwater volume and surface area evaluation of benthic organisms by 3D computer modelling. Methods in Ecology and Evolution, 6(5), 521-531.

Lefebvre, A., Lyons, A. P., Thompson, C. E., & Amos, C. L. (2009). A new system for seafloor characterisation: BRAD, the Benthic Roughness Acoustic Device. Underwater Acoustic Measurements: Technology and Results, 8.

Lemke, P., Ren, J., Alley, R. B., Allison, I., Carrasco, J., Flato, G., Fujii, Y., Kaser, G., Mote, P., Thomas, R.H. & Zhang, T. (2007). Observations: changes in snow, ice and frozen ground. In Fourth Assessment Report [AR4] Climate Change 2007: The Physical Science Basis, Contribution of Working Group I to the Fourth Assessment report of the Intergovernmental Panel on Climate Change, ed. S Solomon, et al. Cambridge, UK: Cambridge Univ. Press.

Le Quéré, C., Raupach, M. R., Canadell, J. G., Marland, G., Bopp, L., Ciais, P., ... & Friedlingstein, P. (2009). Trends in the sources and sinks of carbon dioxide. Nature Geoscience, 2(12), 831-836.

Levitus, S., Antonov, J. I., Boyer, T. P., Locarnini, R. A., Garcia, H. E., & Mishonov, A. V. (2009). Global ocean heat content 1955–2008 in light of recently revealed instrumentation problems. Geophysical Research Letters, 36(7).

Limerinos, J. T., & California. Dept. of Water Resources. (1970). Determination of the Manning coefficient from measured bed roughness in natural channels.

Liu, P. L. F., & Losada, I. J. (2002). Wave propagation modeling in coastal engineering. Journal of Hydraulic Research, 40(3), 229-240.

Lombard, A., Cazenave, A., Le Traon, P. Y., & Ishii, M. (2005). Contribution of thermal expansion to present-day sea-level change revisited. Global and Planetary Change, 47(1), 1-16.

Lombard A, Garric G, Penduff T, Molines JM. 2009. Regional variability of sea level change using a global ocean model at 1/4 resolution. Ocean Dyn, doi: 10.1007/s10236-009-0161-6.

Lowe, R. J., Falter, J. L., Bandet, M. D., Pawlak, G., Atkinson, M. J., Monismith, S. G., & Koseff, J. R. (2005). Spectral wave dissipation over a barrier reef. Journal of Geophysical Research: Oceans, 110(C4).

Mann, M. E., Bradley, R. S., & Hughes, M. K. (1998). Global-scale temperature patterns and climate forcing over the past six centuries. Nature, 392(6678), 779-787.

Marin, F. (2004). Eddy viscosity and Eulerian drift over rippled beds in waves. Coastal Engineering, 50(3), 139-159.

Martin, C.S., Fletcher, R., Jones, M.C., Kaschner, K., Sullivan, E., Tittensor, D.P., Mcowen, C., Geffert, J.L., van Bochove, J.W., Thomas, H., Blyth, S., Ravillious, C., Tolley, M., & Stanwell-Smith, D. (2014). Manual of marine and coastal datasets of biodiversity importance. May 2014 release. Cambridge (UK): UNEP World Conservation Monitoring Centre. 28 pp. (+ 4 annexes totalling 174 pp. and one e-supplement).

Martin, C. S., Giannoulaki, M., De Leo, F., Scardi, M., Salomidi, M., Knittweis, L., ... & Bavestrello, G. (2014). Coralligenous and maërl habitats: predictive modelling to identify their spatial distributions across the Mediterranean Sea. Scientific Reports, 4, 5073.

Massel, S. R., & Brinkman, R. M. (2001). Wave-induced set-up and flow over shoals and coral reefs. Part 1. A simplified bottom geometry case. Oceanologia, 43(4).

Mathisen, P. P., & Madsen, O. S. (1996). Waves and currents over a fixed rippled bed: 1. Bottom roughness experienced by waves in the presence and absence of currents. Journal of Geophysical Research: Oceans, 101(C7), 16533-16542.

Mathisen, P. P., & Madsen, O. S. (1999). Waves and currents over a fixed rippled bed: 3. Bottom and apparent roughness for spectral waves and currents. Journal of Geophysical Research: Oceans, 104(C8), 18447-18461.

McArdle, B. H., & Anderson, M. J. (2001). Fitting multivariate models to community data: a comment on distance-based redundancy analysis. Ecology, 82(1), 290-297.

McCormick, M. I. (1994). Comparison of field methods for measuring surface topography and their associations with a tropical reef fish assemblage. Marine ecology progress series. Oldendorf, 112(1), 87-96.

Mendez, F. J., & Losada, I. J. (2004). An empirical model to estimate the propagation of random breaking and nonbreaking waves over vegetation fields. Coastal Engineering, 51(2), 103-118.

Meyer, D. L., Townsend, E. C., & Thayer, G. W. (1997). Stabilization and erosion control value of oyster cultch for intertidal marsh. Restoration Ecology, 5(1), 93-99.

Michell, J. H. (1893). XLIV. The highest waves in water. The London, Edinburgh, and Dublin Philosophical Magazine and Journal of Science, 36(222), 430-437.

Möller, I. (2006). Quantifying saltmarsh vegetation and its effect on wave height dissipation: Results from a UK East coast saltmarsh. Estuarine, Coastal and Shelf Science, 69(3), 337-351.

Möller, I., Kudella, M., Rupprecht, F., Spencer, T., Paul, M., Van Wesenbeeck, B. K., Wolters, G., Jensen, K., Bouma, T.J., Miranda-Lange, M., & Schimmels, S. (2014). Wave attenuation over coastal salt marshes under storm surge conditions. Nature Geoscience, 7(10), 727-731.

Möller, I., Spencer, T., French, J. R., Leggett, D. J., & Dixon, M. (1999). Wave transformation over salt marshes: a field and numerical modelling study from North Norfolk, England. Estuarine, Coastal and Shelf Science, 49(3), 411-426.

Möller, I., & Spencer, T. (2002). Wave dissipation over macro-tidal saltmarshes: Effects of marsh edge typology and vegetation change. Journal of Coastal Research, 36(1), 506-521.

Moody, L. F. (1944). Friction factors for pipe flow. Trans. Asme, 66(8), 671-684.

Morrison, M. A., Jones, E. G., Consalvey, M., & Berkenbusch, K. (2014). Linking marine fisheries species to biogenic habitats in New Zealand: a review and synthesis of knowledge. New Zealand Aquatic Environment and Biodiversity Report, 130, 1-160.

Myrhaug, D., Holmedal, L. E., & Ong, M. C. (2009). Nonlinear random wave-induced drag force on a vegetation field. Coastal Engineering, 56(3), 371-376.

Nnadi, F. N., & Wilson, K. C. (1992). Motion of contact-load particles at high shear stress. Journal of Hydraulic Engineering, 118(12), 1670-1684.

Nelson, R. C. (1996). Hydraulic roughness of coral reef platforms. Applied Ocean Research, 18(5), 265-274.

Neumeier, U., & Ciavola, P. (2004). Flow resistance and associated sedimentary processes in a Spartina maritima salt-marsh. Journal of Coastal Research, 435-447.

Nielsen, P. (1992). Coastal bottom boundary layers and sediment transport (Vol. 4). World Scientific Publishing Co Inc.

Nikuradse, J. (1937). Laws of flow in rough pipes. Translation of Stromungsgesetze in rauhen Rohren, Nikuradse, Forschung auf dem Gebiete des Ingenieurwesens, 1933. NACA Technical Memorandum, 1292.

Pansini, M., & Pronzato, R. (1973). Il coralligeno di Bogliasco ed il suo popolamento di Poriferi. Bollettino dei Musei e degli Istituti Biologici dell'Università di Genova, 41, 5-34.

Papadopoulos, G. A., & Fokaefs, A. (2005). Strong tsunamis in the Mediterranean Sea: a re-evaluation. ISET Journal of Earthquake Technology, 42(4), 159-170.

Pardaens, A. K., Lowe, J. A., Brown, S., Nicholls, R. J., & De Gusmâo, D. (2011). Sea-level rise and impacts projections under a future scenario with large greenhouse gas emission reductions. Geophysical Research Letters, 38(12).

Paul, M., & Amos, C. L. (2011). Spatial and seasonal variation in wave attenuation over Zostera noltii. Journal of Geophysical Research: Oceans, 116(C8).

Pérès, J. M., & Picard, J. (1952). Les corniches calcaires d'origine biologique en Méditerranée occidentale. Recueil des Travaux de la Station Marine d'Endoume, 4, 2-33.

Pfeffer, W. T., Harper, J. T., & O'Neel, S. (2008). Kinematic constraints on glacier contributions to 21st-century sea-level rise. Science, 321(5894), 1340-1343.

Piazza, B. P., Banks, P. D., & La Peyre, M. K. (2005). The potential for created oyster shell reefs as a sustainable shoreline protection strategy in Louisiana. Restoration Ecology, 13(3), 499-506.

Ponti, M., Perlini, R. A., Ventra, V., Grech, D., Abbiati, M., & Cerrano, C. (2014). Ecological shifts in Mediterranean coralligenous assemblages related to gorgonian forest loss. PloS one, 9(7), e102782.

Prinos, P., Stratigaki, V., Manca, E., Losada, I., López Lara, J., Sclavo, M., Càceres Rabionet, I., & Sánchez-Arcilla Conejo, A. (2010). Wave propagation over Posidonia oceanica: large scale experiments. In 7th HYDRALAB III Joint Transnational Access User Meeting (pp. 57-60).

Quiroga, P. D., & Cheung, K. F. (2013). Laboratory study of solitary-wave transformation over bed-form roughness on fringing reefs. Coastal Engineering, 80, 35-48

Rahmstorf, S. (2007). A semi-empirical approach to projecting future sea-level rise. Science, 315(5810), 368-370.

Raudkivi, A. J. (1988). The roughness height under waves. Journal of Hydraulic Research, 26(5), 569-584.

Reed, D. (2010). Understanding the Effects of Sea-Level Rise on Coastal Wetlands: The Human Dimension. In EGU General Assembly Conference Abstracts (Vol. 12, p. 5480).

REGION, L. (2009). Atlante degli Habitat Marini della Liguria (sc. 1: 10000).

Rende, F. S., Irving, A. D., Lagudi, A., Bruno, F., Scalise, S., Cappa, P., ... & Di Mento, R. (2015). Pilot Application of 3D Underwater Imaging Techniques for Mapping Posidonia Oceanica (L.) Delile Meadows. The International Archives of Photogrammetry, Remote Sensing and Spatial Information Sciences, 40(5), 177.

Reiss, H., Birchenough, S., Borja, A., Buhl-Mortensen, L., Craeymeersch, J., Dannheim, J., Darr, A., Galparsoro, I., Gogina, M., Neumann, H., Populus, J., Rengstorf, A., M., Valle, M., van Hoey, G., Zettler, M., L., & Degraer, S. (2014). Benthos distribution modelling and its relevance for marine ecosystem management. ICES Journal of Marine Science: Journal du Conseil, fsu107.

Rignot, E., Velicogna, I., Van den Broeke, M. R., Monaghan, A., & Lenaerts, J. T. M. (2011). Acceleration of the contribution of the Greenland and Antarctic ice sheets to sea level rise. Geophysical Research Letters, 38(5).

Risk, M. J. (1972). Fish diversity on a coral reef in the Virgin Islands. Smithsonian Institution.

Rockel, B., & Woth, K. (2007). Extremes of near-surface wind speed over Europe and their future changes as estimated from an ensemble of RCM simulations. Climatic Change, 81(1), 267-280.

Rosman, J. H., Koseff, J. R., Monismith, S. G., & Grover, J. (2007). A field investigation into the effects of a kelp forest (Macrocystis pyrifera) on coastal hydrodynamics and transport. Journal of Geophysical Research: Oceans, 112(C2).

Sarà, M. (1968). Un coralligeno di piattaforma (coralligène de plateau) lung oil litorale pugliese. Arch. Oceanogr. Limnol., 15 (Suppl.): 139-150.

Sarà, M. (1969). Research on coralligenous formations: problems and perspectives. Pubbl. Staz. Zool. Napoli, 37(suppl), 124-134.

Sarà, M. (1971). Un biotope da proteggere: il coralligeno pugliese. 1st National Symposium for nature conservation. Istit. Zool. Univ. Bari.

Sarà, M. (1973). Sponge population of the Apulian coralligenous formations. Rapp Comm Int Mar Mediterr, 21, 613-615.

Sartoretto, S., Verlaque, M., & Laborel, J. (1996). Age of settlement and accumulation rate of submarine "coralligène"(− 10 to− 60 m) of the northwestern Mediterranean Sea; relation to Holocene rise in sea level. Marine Geology, 130(3-4), 317-331.

Scarsi, G., & Stura, S. (1972). Actual and mean energies of cylindrical waves at the third order of approximation. Meccanica, 7(1), 72-72.

Scarsi, G., & Stura, S. (1980). Il frangimento delle onde su profondita molto basse. Istituto Lombardo, Rend Se. B, 114, 52-60.

Schmidt, V. E., & Rzhanov, Y. (2012). Measurement of micro-bathymetry with a GOPRO underwater stereo camera pair. In Oceans, 2012 (pp. 1-6). IEEE.

Schmidt-Thomé, P., & Kallio, H. (2006). Natural and technological hazard maps of Europe. Special paper-geological survey of finland, 42, 17.

Sillmann, J., & Roeckner, E. (2008). Indices for extreme events in projections of anthropogenic climate change. Climatic Change, 86(1-2), 83-104.

Simoes, F. J. (2010). Flow resistance in open channels with fixed and movable bed. In 2nd Joint Federal Interagency Conference.

Skarlatos, D., Demestiha, S., & Kiparissi, S. (2012). An 'open'method for 3D modelling and mapping in underwater archaeological sites. International Journal of Heritage in the digital era, 1(1), 1-24.

Sørensen, M. B., Spada, M., Babeyko, A., Wiemer, S., & Grünthal, G. (2012). Probabilistic tsunami hazard in the Mediterranean Sea. Journal of Geophysical Research: Solid Earth, 117(B1).

Soukissian, T. H., Ntoumas, M. C., Anagnostou, C., & Kiriakidou, C. (2010, January). Coastal Vulnerability of Eastern Saronikos Gulf to intense natural events. In The Twentieth International Offshore and Polar Engineering Conference. International Society of Offshore and Polar Engineers.

Spalding, M. D., Ruffo, S., Lacambra, C., Meliane, I., Hale, L. Z., Shepard, C. C., & Beck, M. W. (2014). The role of ecosystems in coastal protection: Adapting to climate change and coastal hazards. Ocean & Coastal Management, 90, 50-57.

Stancheva, M., Rangel-Buitrago, N., Anfuso, G., Palazov, A., Stanchev, H., & Correa, I. (2011). Expanding level of coastal armouring: case studies from different countries. Journal of Coastal Research, (64), 1815.

Stockdon, H. F., Holman, R. A., Howd, P. A., & Sallenger, A. H. (2006). Empirical parameterization of setup, swash, and runup. Coastal engineering, 53(7), 573-588.

Sutherland, J., & Barfuss, S. L. (2012). Composite Modelling, combining physical and numerical models. 34th IAHR World Congress. Brisbane, Australia.

Teo, T. (2015). Video-Based Point Cloud Generation Using Multiple Action Cameras. The International Archives of Photogrammetry, Remote Sensing and Spatial Information Sciences, 40(4), 55.

Tesfamariam, E. K. (2007). Comparing discontinuity surface roughness derived from 3D terrestrial laser scan data with traditional field-based methods. Unpublished Dissertation/Thesis, International Institute for Geo-information Science and Earth Observation, The Netherlands.

Thornton, E. B., & Guza, R. T. (1983). Transformation of wave height distribution. Journal of Geophysical Research: Oceans, 88(C10), 5925-5938.

Tolman, H. L. (2009). User manual and system documentation of WAVEWATCH III TM version 3.14. Technical note, MMAB Contribution, 276, 220.

Trygonis, V., & Sini, M. (2012). photoQuad: a dedicated seabed image processing software, and a comparative error analysis of four photoquadrat methods. Journal of Experimental Marine Biology and Ecology, 424, 99-108.

Tusinski, A. (2012). The role of mangroves in the design of coastal dikes: Hydrodynamic and cost related aspects. Delft (MSc thesis report).

UN, D. (2013). World population prospects: The 2012 revision.

UNEP-MAP-RAC, S. P. A. (2008). Action plan for the conservation of the coralligenous and other calcareous bio-concretions in the Mediterranean Sea. UNEP MAP RAC-SPA publ., Tunis.

UNEP (2011). Taking Steps toward Marine and Coastal Ecosystem-Based Management - An Introductory Guide. United Nations, Department of Economic and Social Affairs, Population

Division (2013). World Population Prospects: The 2012 Revision, Highlights and Advance Tables. Working Paper No. ESA/P/WP.228.

UNEP (2011a). Adoption of the Action Plan for the implementation of the ICZM Protocol for the Mediterranean (2012-2019).

Utter, B., & Denny, M. (1996). Wave-induced forces on the giant kelp Macrocystis pyrifera (Agardh): field test of a computational model. Journal of Experimental Biology, 199(12), 2645-2654.

van Keulen, M., & Borowitzka, M. A. (2003). Seasonal variability in sediment distribution along an exposure gradient in a seagrass meadow in Shoalwater Bay, Western Australia. Estuarine, Coastal and Shelf Science, 57(4), 587-592.

van Leeuwen, B., Augustijn, D. C. M., Van Wesenbeeck, B. K., Hulscher, S. J. M. H., & De Vries, M. B. (2010). Modeling the influence of a young mussel bed on fine sediment dynamics on an intertidal flat in the Wadden Sea. Ecological Engineering, 36(2), 145-153.

Van Rijn, L. C. (1993). Principles of sediment transport in rivers, estuaries and coastal seas (Vol. 1006). Amsterdam: Aqua publications.

Vellinga P, Katsman CA, Sterl A, Beersma JJ, Church JA, Hazeleger W, Kopp RE, Kroon D, Kwadijk J, Lammersen R, Lowe J, Marinova N, Oppenheimer M, Plag HP, Rahmstorf S, Ridley J, von Storch H, Vaughan DG, van der Wal RSW, Weisse R (2008) Exploring high-end climate change scenarios for flood protection of The Netherlands. International scientific assessment carried out at request of the delta committee. Scientific Report WR-2009-05. KNMI/Alterra, The Netherlands.

WBGU - German Advisory Council on Global Change, (2006) The Future Oceans - Warming Up, Rising High, Turning Sour. (WBGU, Berlin).

Webster, P. J., Holland, G. J., Curry, J. A., & Chang, H. R. (2005). Changes in tropical cyclone number, duration, and intensity in a warming environment. Science, 309(5742), 1844-1846.

Wiberg, P. L., & Harris, C. K. (1994). Ripple geometry in wave-dominated environments. JOURNAL OF GEOPHYSICAL RESEARCH-ALL SERIES-, 99, 775-775.

Wilson, K. C. (1987). Analysis of bed-load motion at high shear stress. Journal of Hydraulic Engineering, 113(1), 97-103.

Wingham, D. J., Wallis, D. W., & Shepherd, A. (2009). Spatial and temporal evolution of Pine Island Glacier thinning, 1995–2006. Geophysical Research Letters, 36(17).

Wöppelmann, G., Le Cozannet, G., Michele, M., Raucoules, D., Cazenave, A., Garcin, M., Hanson, S., Marcos, M. & Santamaría-Gómez, A. (2013). Is land subsidence increasing the exposure to sea level rise in Alexandria, Egypt?. Geophysical Research Letters, 40(12), 2953-2957.

Yalin, M. S. (1992). River Mechanics. Pergamon, Tarrytown, N. Y., 219 pp.

Yamada, H. (1957). On the highest solitary wave. Rep. Res. Inst. Appl. Mech. Kyushu Univ, 5, 53-67.

Zapata-Ramírez, P. A., Scaradozzi, D., Sorbi, L., Palma, M., Pantaleo, U., Ponti, M., & Cerrano, C. (2013). Innovative study methods for the Mediterranean coralligenous habitats. Advances in Oceanography and Limnology, 4(2), 102-119.

Zapata-Ramirez, P. A., Huete-Stauffer, C., Coppo, S., & Cerrano, C. (2014, October). Using Maxent to understand and predict the distribution of coralligenous environments. In Proceedings 2nd Mediterranean Symposium on the Conservation of Coralligenous and Other Calcareous Bio-concretions, Portoroz (pp. 183-188).

Zeppilli, D., Pusceddu, A., Trincardi, F., & Danovaro, R. (2016). Seafloor heterogeneity influences the biodiversity–ecosystem functioning relationships in the deep sea. Scientific reports, 6.

Zhao, H., & Chen, Q. (2013). Modeling attenuation of storm surge over deformable vegetation: Methodology and verification. Journal of Engineering Mechanics, 140(12), 04014090.

Zhao, H., & Chen, Q. (2016). Modeling Attenuation of Storm Surge over Deformable Vegetation: Parametric Study. Journal of Engineering Mechanics, 142(8), 06016006.

Zhuang, F., & Lee, J. J. (1997). A viscous rotational model for wave overtopping over marine structure. In Coastal Engineering 1996 (pp. 2178-2191).